ANALYSIS OF FORCES ON CORE STRUCTURES
DURING A LOSS-OF-COOLANT ACCIDENT
by
D.P. Griggs, R.B. Vilim, C.H. Wang and J.E. Meyer

Energy Laboratory Report No. MIT-EL 80-029

August 1980

ANALYSIS OF FORCES ON CORE

STRUCTURES DURING A

LOSS-OF-COOLANT-ACCIDENT

D.P. Griggs, R.B. Vilim, C.H. Wang and J.E. Meyer

Energy Laboratory and
Department of Nuclear Engineering
Massachusetts Institute of Technology
Cambridge MA 02139

Table of Contents

List of Figures

LIST OF TABLES

Nomenclature

kg	kilogram
m	meter
mm	millimeter
ms	millisecond
Mg	megagram
MN	meganewton
MPa	megapascal
N	newton
s,sec	second

1. INTRODUCTION

1.1 Objectives

There are several design requirements related to the emergency core cooling which would follow a hypothetical loss-of-coolant accident (LOCA). One of these requirements is that the core must retain a coolable geometry throughout the accident. A possible cause of core damage leading to an uncoolable geometry is the action of forces on the core and associated support structures during the very early (blowdown) stage of the LOCA. An equally unsatisfactory design result would occur if calculated deformations and failures were so extensive that the geometry used for calculating the next stages of the LOCA (refill and reflood) could not be known reasonably well. Subsidiary questions involve damage preventing the operation of control assemblies and loss of integrity of other needed safety systems. A reliable method of calculating these forces is therefore an important part of LOCA analysis.

These concerns provided the motivation for this study. The general objective of the study was to review the state-of-the-art in LOCA force determination. Specific objectives were:

(a) determine state-of-the-art by reviewing current (and projected near future) techniques for LOCA force determination.

(b) consider each of the major assumptions involved in force determination and make a qualitative assessment of their validity.

(c) use a small number of illustrative problems to obtain

quantitative information concerning these assumptions.

This report will attempt to address each of the stated objectives.

1.2 Description of LOCA Forces Problem

The analysis of LOCA forces is a complex problem involving the marriage of fluid dynamics and structural mechanics techniques to calculate a very severe transient response. Following the initiation of a LOCA, hydraulic pressure waves result which reverberate within the reactor loop and core for a short interval of about 50 ms. Flows in the system experience high amplitude oscillations for a few seconds, resulting in large magnitude, short duration mechanical loads on structural elements. Both single phase and two-phase flow conditions occur during the accident. The character of the flows in the annular downcomer and in plenum regions is multi-dimensional and the problem is asymmetric as a whole. Loads are induced on structures by the action of interface stresses (both pressure and shear) at the surfaces in contact with the fluid. Pressure differentials in the fluid cause net forces on the structures and may originate in a number of ways, including:

- wall shears, expansion/contraction losses, and form losses;

- forces needed to turn fluid jets which are directed toward (or away from) the structure surface;

- fluid acceleration both from velocity changes with position (spatial acceleration) and velocity changes with time (temporal acceleration); and

- depressurization of different regions around the structure at different rates during the blowdown.

The forces arising from temporal acceleration-induced pressure differentials can give "water-hammer" effects, taking the form of pressure waves propagating through the system at sonic velocity (and being reflected, transmitted, attenuated, etc.). Wall shears not only cause pressure differentials in the coolant but also are direct forces on the structure.

The relation between forces on the structures and resulting stresses is, of course, a dynamic one. Recoil of previously stressed structures from which applied loads have been reduced is one dynamic effect. Another dynamic effect is the overshoot to larger than "static stresses" when a new load is applied rapidly but is sustained for a fairly long time. A third effect is the undershoot to smaller than static stresses when the new load is applied for only a short time (with respect to a natural period of vibration of the structure). This interaction between structural motions and loads may be very important in calculating the stresses during the accident. Loads calculated on the basis of a rigid structure (no wall motion) can, in certain cases, be shown to be quite different than loads calculated with structural flexibility and resultant wall motion accounted for. Finally, for a complete description of LOCA forces, a determination of peak magnitude is not enough. The time-dependent history of the structural loadings may be necessary in some cases, so methods are needed for recognizing those cases for which peak magnitudes are sufficient.

1.3 Organization

In order to address the goals of the project, this report has been organized as follows: Chapter 2 presents the illustrative problem which was considered the basis of the analytical work; Chapter 3 is a review of state-of-the-art methods of LOCA forces analysis; Chapter 4 contains an examination of the major assumptions made in LOCA forces analysis; Chapter 5 summarizes the conclusions of the study and gives suggestions for future work. Appendices and references conclude the report.

2. BASE CASE ILLUSTRATIVE PROBLEM

One of the objectives of the project is to identify the
underlying assumptions of present and projected methods of LOCA force
analysis and to determine the applicability of these assumptions to
Boston Edison and Yankee Atomic reactors. To this end, it was decided
that a base case problem representative of the reactors owned/purchased
by the sponsoring utilities would be identified and examined for the
applicability of such assumptions. Discussions with utility engineers
led to the selection of an instantaneous double-ended guillotine
break of a Maine Yankee primary coolant pipe (pump discharge leg) as
the base case problem.

This chapter describes the geometry and steady-state operating
conditions of the base case. A description of blowdown based on a
one-dimensional fluid representation is also given.

2.1 Major Flow Paths and Components

The Maine Yankee plant is a three loop pressurized water reactor
owned and operated by Maine Yankee Atomic Power Company. Figures
showing major core structures and flowpaths may be found in Appendix A.
A nodal diagram combining reactor details with the calculational
coolant representative is shown in Fig. 2.1. This coolant representa-
tion given in this chapter was taken from a WREM (Water Reactor Evalu-
ation Model) model of the Maine Yankee Reactor (1). This model uses a
version of the code RELAP (2) to solve the one-dimensional conservation
equations. The RELAP codes provide for describing a thermal-hydraulic
system as a series of interconnecting control volumes, as in Fig. 2.1.
Mass and energy balances are solved for the volumes and momentum

balances are solved for the connecting junctions. The solution assumes one-dimensional homogeneous fluid with the vapor and liquid phases in thermodynamic equilibrium. The importance of these assumptions to calculating LOCA forces will be addressed in Chapter 3. The intent in using the model here is to provide a first order description of the steady-state and blowdown phases of a cold leg pipe break accident.

In the WREM representation of the Maine Yankee reactor, twenty control volumes are used for coolant in and near the reactor core. The in-vessel volumes are indicated in Fig. 2.1, while the corresponding geometric information is given in Table 2.1. Referring to the table, the volume column gives the coolant content of each control volume. The "flow path" column gives the length a typical fluid particle would traverse in passing through the control volume. These lengths were either obtained from reference (1) or were estimated from figures in the Maine Yankee safety analysis report (30).

Flow path operating conditions (pre-transient steady state) are supplied in Table 2.2. These conditions were combined with the geometric information of Table 2.1 to produce two sets of time constants that characterize physical processes of interest. The first of these is the "enthalpy transport time constant" which was defined for a particular control volume as:

$$\tau_h = \frac{\rho V}{W}$$

where ρ = coolant density (kg/m^3);

V = coolant volume (m^3); and

W = mass flow rate (kg/s).

Physically, this time constant is the "fluid transport time" or "transport delay time" for a pipe-like component. The second time constant is the "sonic time", the time required for a sonic wave to travel the length L:

$$\tau_s = (L/c)$$

where L = flow path length (m); and

c = sonic velocity (m/s).

The time constants are given in Table 2.1, giving a basis for comparing the speeds of fluid transport and sonic/water hammer effects. The constants indicate, for example, that in steady-state it takes 0.33 seconds for fluid to be transported from the break location to the reactor inlet nozzle, 1.86 seconds from there to the core inlet (by summing numbers for volumes 27, 28, 29 and 47), and 0.75 seconds to pass through the core. The corresponding numbers for sonic propagation are 4.4 ms, 120 ms, and 3.8 ms. Therefore, break occurrence "information" is transmitted by sonic pressure wave through the usual coolant path to the core exit in a very short time (20.2 ms). Short-cuts through structure can cause information transmittal in even shorter times.

2.2 Description of Transient

The base case transient occurs as a result of a pipe break to the left of control volume 26 in Fig. 2.1 at time t=0. As liquid

rushes toward the break a decompression wave advances through the system displayed in Fig. 2.1. The actual pressure wave transmission is complicated by reflections at area changes and by interactions with coolant volumes not shown in Fig. 2.1, such as pumps and steam generators. Figure 2.2 shows the calculated flow rate from the vessel to the broken loop during the early blowdown portion of the accident. The magnitude of the flow out the break increases rapidly to a maximum value (at t=60 ms) or approximately five times the pre-transient steady-state value. The flow slowly decreases during the next two seconds. Figure 2.3 shows the pressures in volumes 28 (downcomer) and 31 (middle core volume), for the first two seconds of the blowdown. By comparing these two pressure curves, the pressure differential across the core barrel can be inferred. Although this pressure difference is actually asymmetric (as multi-dimensional calculation reveal), Fig. 2.3 correctly shows it to be greatest in the first forty milliseconds of the decompression. During this period, the pressures have not yet reached the saturation values shown in Table 2.2, so pressures drop very rapidly. Following this subcooled blowdown portion of the transient, saturation pressures are reached in the hotter portions of the system resulting in flashing to steam and a slowdown in the rate of decompression. Examination of the plots from the WREM model indicate that the first flashing occurs at t=60 ms in the upper plenum and hot leg regions, taking place at a pressure of approximately 11.0 MPa. Figure 2.4 shows the decompression of the outlet plenum during the first two seconds, demonstrating the abrupt change in decompression rate when the pressure fell below the 11.0 MPa saturation value given

in Table 2.2. However, the control volumes (27, 28, 36) that are most important in influencing core structural behavior remain single phase liquid for more than two seconds. At t=20 sec the system pressure has dropped to about 8.3 MPa and these control volumes begin flashing (at approximately 7.1 MPa) soon thereafter.

2.3 Additional Details

The advance of the decompression wave through the downcomer (control volumes 27 and 28) supplies the first large forces on the barrel and the first opportunity for significant structural damage. An "unwrapped" Maine Yankee downcomer is shown, approximately to scale, in Fig. 2.5. The nozzle that connects to the broken cold leg is at Z=0, θ=0 in the figure. The decompression wave that spreads out from this position soon encounters reflections from the top of the downcomer and from the hot leg pipes which penetrate the downcomer. The wave also reaches the open pipes leading to the other cold legs before reaching the bottom of the downcomer. These interactions of pressure wave and structural features are obviously of a multi-dimensional nature, a complication whose importance must be assessed.

A thermal shield (see Fig. A.1) is located between the core barrel and pressure vessel at the same elevation as the active section of the fuel elements. The purpose of the shield is to reduce the level of gamma heating in the pressure vessel wall. It is secured at the top and bottom by seven circumferentially spaced studs anchored to the outside of the core barrel. These studs present neglible resistance to flow. The impact of the thermal shield on hydrodynamic response to a LOCA is not clear and may need to be addressed.

There are six bumpers at the bottom of the core support barrel that prevent excessive motion of the barrel with respect to the reactor vessel. Each bumper consists of a snubber block and a core restraining lug. The snubber block is mounted on the bottom of the outside surface of the core barrel, having a vertical slot in its outside face that runs the length of the block. The core restraining lug is fastened to the reactor vessel at the same elevation and azimuthal angle as the snubber block. The lug is machined in the field to fit snugly (azimuthally) into the snubber block slot. A clearance of 13.5 mm exists in the radial direction between the face of the lug and the face of the snubber block slot. The bottom of the core barrel is therefore restrained with respect to rotation about its axis but un-restrained in the axial direction. Local deformations of 13.5 mm are permitted in the radial direction at each snubber block location. These movement inhibitors could have an important impact on core barrel response to asymmetric pressure wave loadings.

The core support barrel is hung from a lip on the inside of the pressure vessel (see Fig. A.2). An alignment key locates the core barrel in the azimuthal direction in the pressure vessel. An expansion ring (Bellevelle spring type) sits on top of the barrel flange and is compressed by a force of approximately 4 MN when the reactor vessel head is bolted down. It may be that sufficiently large asymmetric forces could be applied to the core barrel to result in the flange being unseated. Since LOCA force analyses consider the core barrel flange to be properly seated at all times, this effect is not taken into consideration. The importance of this simplification is not known.

The response of the core shroud to different rates of decompression in the core bypass and core regions may also be important in maintaining a coolable geometry. The shroud is an open-ended stainless steel can that covers the outside faces of the peripheral fuel assemblies. The core bypass region is located between the core shroud and core barrel. The bypass region is characterized by relatively small inlet/outlet flow area to volume ratio and hence may decompress at a slower rate than the core region. This could lead to net inward forces on the core shroud with possible damage to peripheral fuel elements.

2.4 Summary

For the purpose of performing a one-dimensional thermal-hydraulic analysis of the Maine Yankee plant during a LOCA, a volume and flow path representation of the core, reactor vessel and other primary components is used. In addition to the assumption of one-dimensionality, the fluid within a control volume is assumed to be at equilibrium and structures are rigid. Analyses performed on this basis indicate that the largest pressure differential across the core barrel occurs during the subcooled portion of the blowdown. The calculational volumes most crucial to determining core barrel response do not experience flashing until about two seconds after the break, well into the saturated blowdown phase. A multitude of important structural details pose complications in determining core response to the hydraulic forces created by the rapid decompression.

Table 2.1 Base Case Geometric Information and Characteristic Times
(Pre-Transient Steady State)

Control Volume Identity (Circles in Fig. 3.1)	Volume (m^3)	Flow Path (m)	Fluid Transport (s)	Sonic Time (ms)
Ruptured Loop Cold Leg (26)	2.5	4.38	0.33	4.4
Upper Downcomer (27)	10.0	1.7	0.44	1.7
Lower Downcomer (28)	14.0	5.58	0.62	5.6
Flowing Lower Plenum (29)	7.8	2.3	0.34	2.3
Below Core (47)	10.4	2.43	0.46	2.4
216 "Avg" Core Assy's (30-32)	17.1	3.48	0.75	3.8
Above Core (2)	3.4	0.44	0.14	0.5
"Flowing" Upper Plenum (41)	24.2	1.29	0.98	1.5
Ruptured Loop Hot Leg (15)	5.4		0.65	
Intact Loops Cold Legs (14)	5.0		0.33	
"Static" Lower Plenum (46)	5.5		--	
1 "Hot" Assy (33-35)	0.1		0.75	
Core Bypass (36)	6.0		10.5	
"Static" Upper Plenum (1)	16.0		23.0	
Control Element Assy Shrouds (42)	11.8		17.0	
Intact Loops Hot Legs (3)	10.8		0.65	

Table 2.2 Base Case Flow Path Operating Conditions
(Pre-Transient Steady State)

Flow Path Identity (Squares in Fig. 3.1)	Flow (Mg/s)	Pressure (MPa)	Temperature (°C)	/	Saturation Pressure (MPa)
Ruptured Loop Cold Leg (27)	5.65	15.64	290	/	7.44
Downcomer (28)	16.93	15.70	290	/	7.44
"Avg" Core Exit (37)	16.42	15.56	319	/	11.12
Ruptured Loop Hot Leg (15)	5.65	15.50	318	/	10.98
Intact Loops Cold Leg (14)	11.30	15.64	290	/	7.44
Hot Assy Exit (33)	0.08	15.56	332	/	13.18
Core Bypass (39)	0.43	15.56	290	/	7.44
Intact Loops Hot Leg (2)	11.30	15.50	318	/	10.98
"Leakage" Paths (1) and (47)	0.48	15.50	318	/	10.98
"Leakage" Path (48)	0.03	15.70	290	/	7.44

Notes

(a) Leakage paths (1) and (47) pass into and out of the "static" upper plenum (1).

(b) Leakage path (48) passes from the upper downcomer (27) to the "flowing" upper plenum (41).

(c) Pressure and temperature values are given on a "donor cell" basis (i.e., for the control volume providing flow to the flow path).
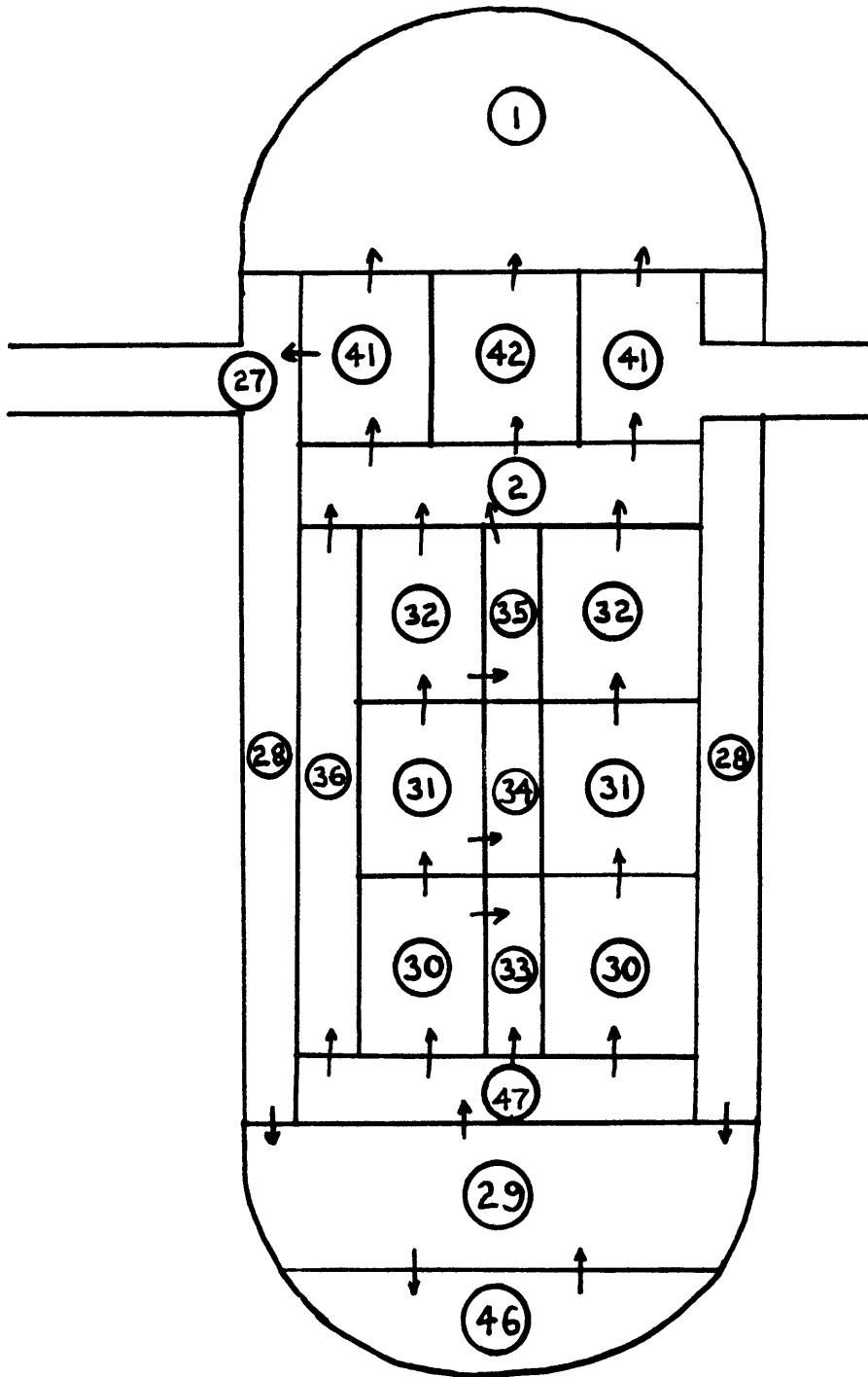
Figure 2.1 Core Control Volumes, Base Case Problem.

MAINE YANKEE RELAP4/EM BLOWDOWN ** SAMPLE PROBLEM **
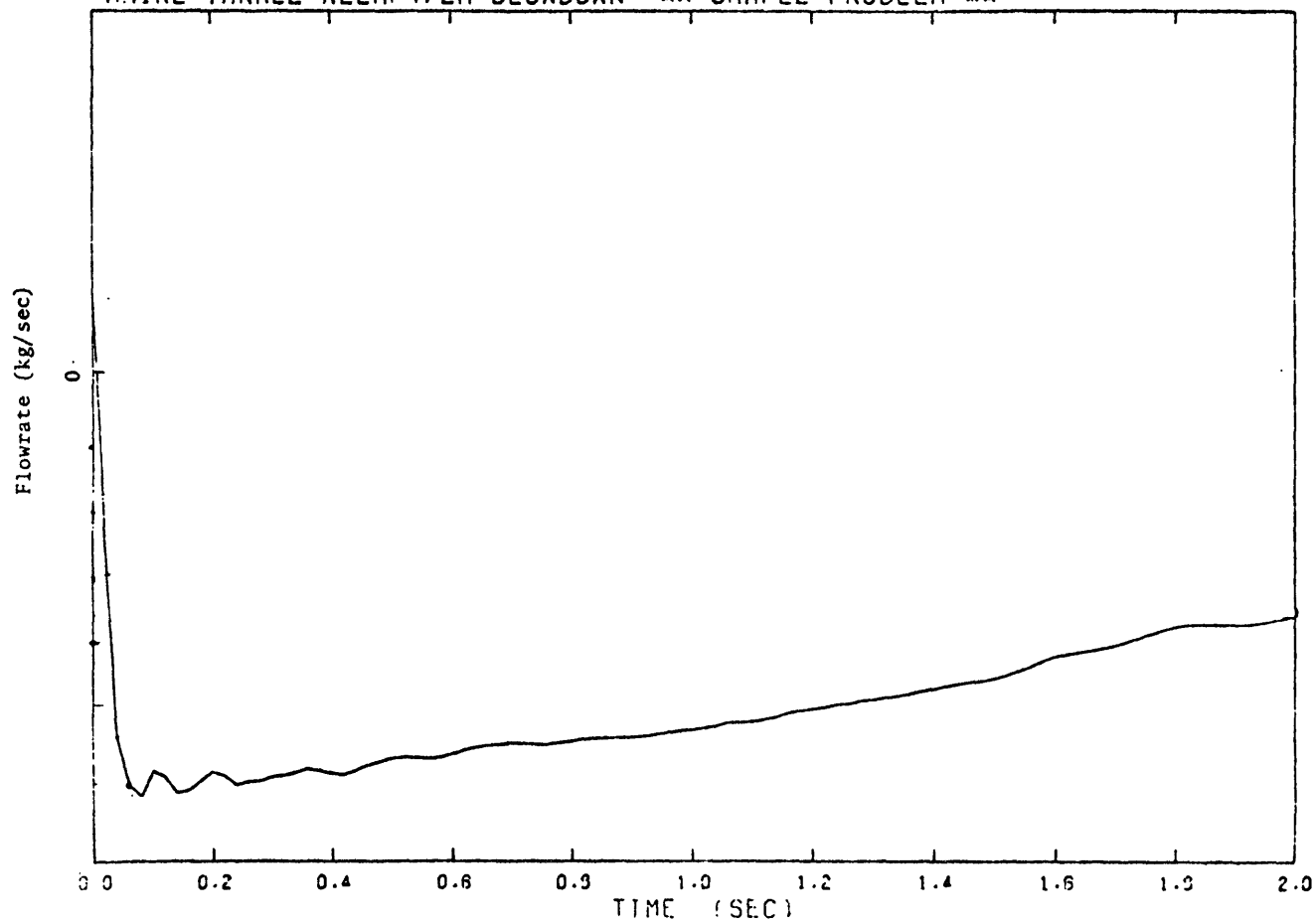
Fig. 2.2 Flowpath 27 Flowrate Following Cold Leg Double Ended Guillotine (Ref. 1)
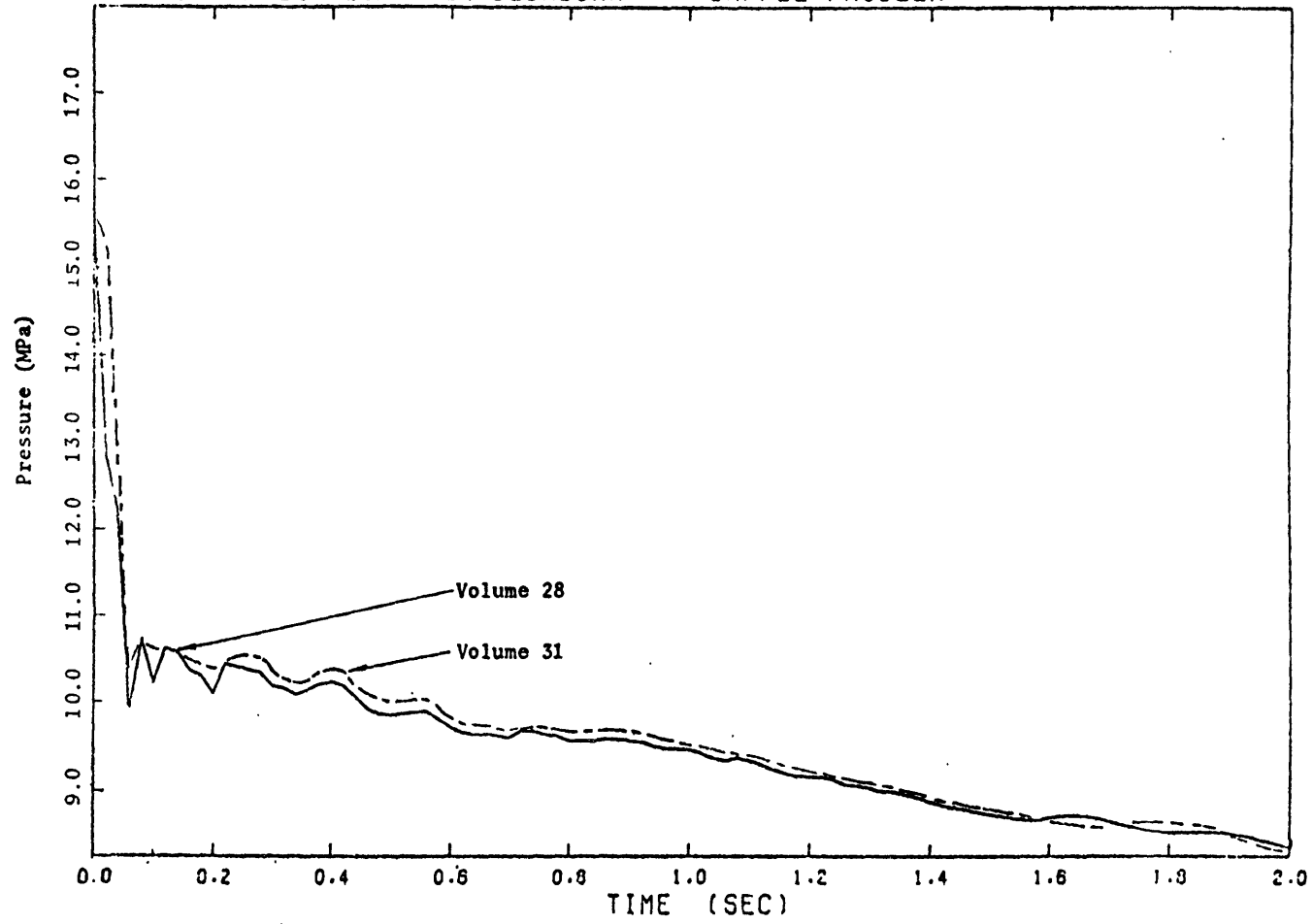
Fig. 2.3 Volume 28 and 31 Pressures Following Cold Leg Double Ended Guillotine (Ref. 1)

MAINE YANKEE RELAP4/EM BLOWDOWN ** SAMPLE PROBLEM **
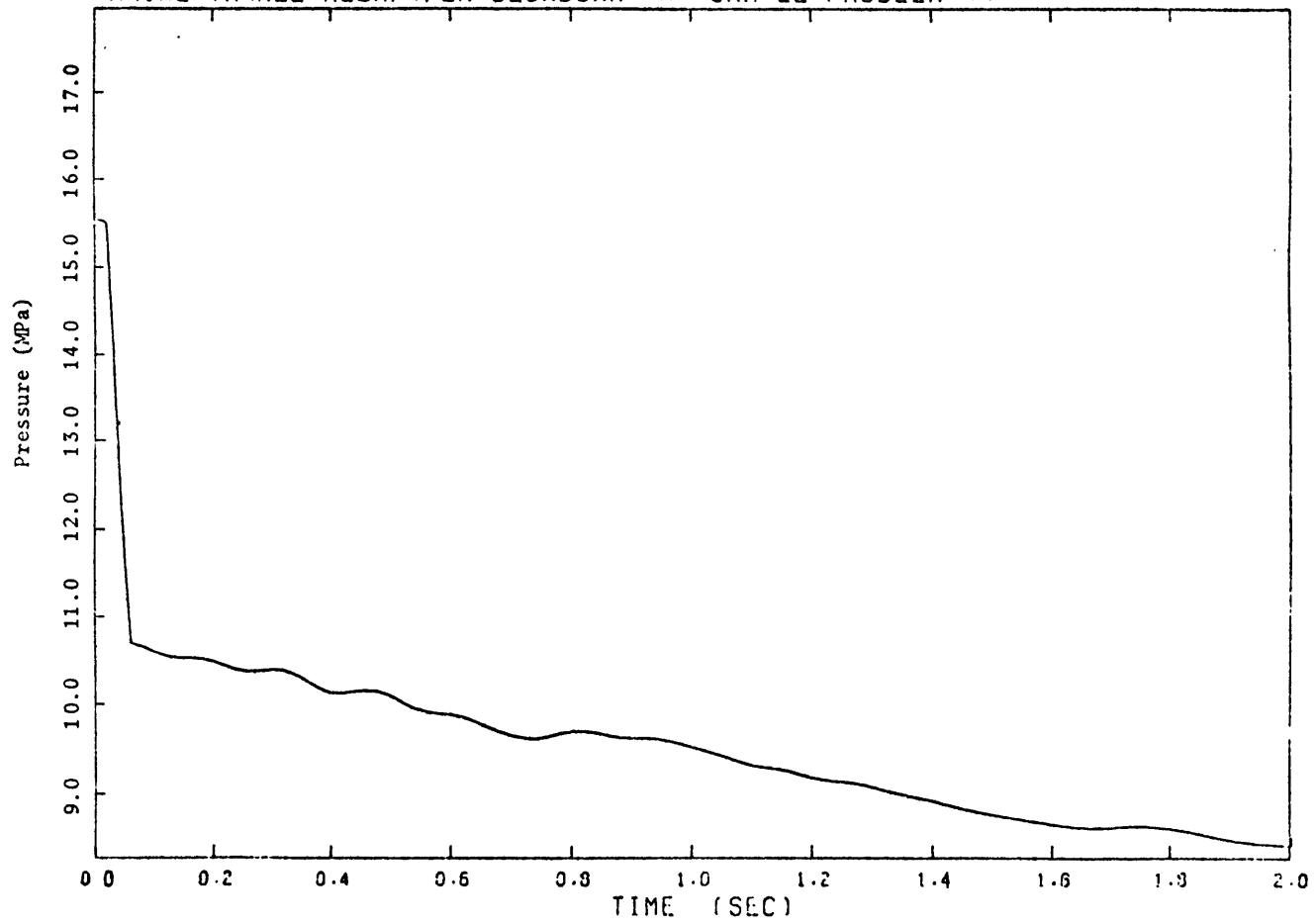
Fig. 2.4 Volume 41 Pressure Following Cold Leg Double Ended Guillotine (Ref. 1)
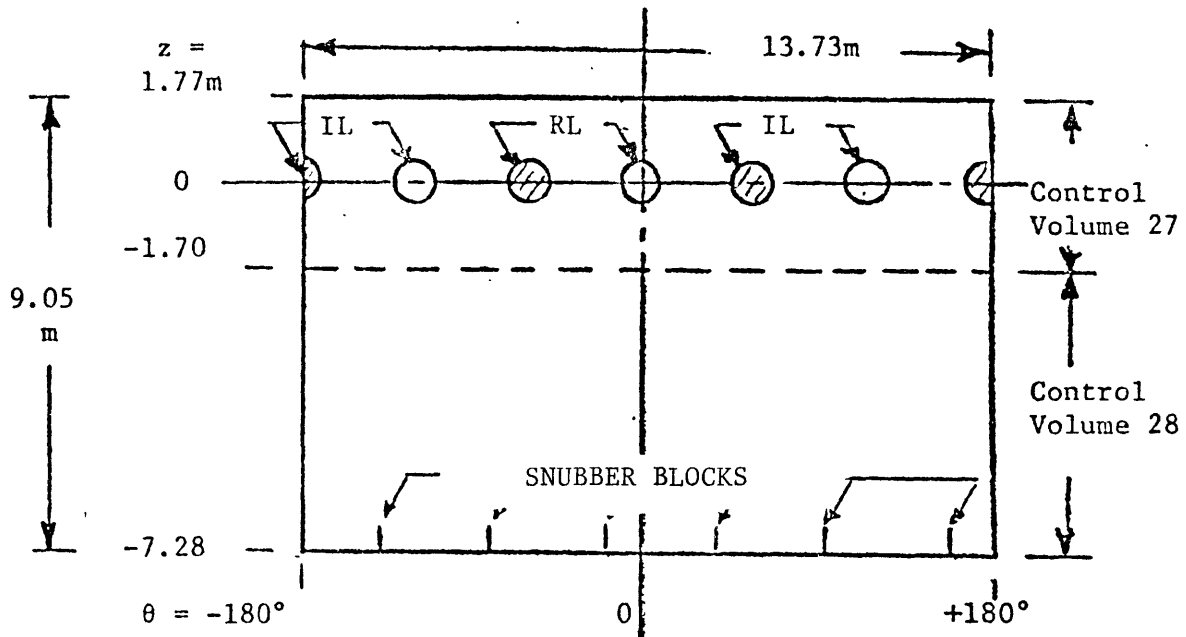
Figure 2.5 Base Case Problem Unwrapped Downcomer

- z = vertical position above nozzle centerline

- θ = angular position relative to cold leg of ruptured loop

- RL = ruptured loop

- IL = intact loop

- ◯ = cold leg nozzle

- ⊘ = hot leg nozzle

- View is from reactor vessel (inside diameter = 4.37 m) toward core support barrel

- Total coolant thickness = 182 mm

3. STATE-OF-THE-ART

This chapter describes the existing state-of-the-art for the calculation of forces on core structures during blowdown. The state-of-the-art consists of those methods which are currently being used commercially as well as those methods which are being developed. The chapter begins with a presentation of methods that are representative of those used by vendors. Unfortunately, the proprietary nature of this work has made it impossible to obtain details on some of the more interesting aspects of these methods. Research efforts aimed at the investigation of certain key assumptions used in current blowdown forces analyses are then described. These studies have centered on the coupling of fluid and structural interactions, utilizing both new analytical methods and experiments. To date, most of the work done in assessing the conservatism of an uncoupled analysis has been part of a cooperative program between the Los Alamos Scientific Laboratory and the Karlsruhe Laboratory in Germany. Therefore, a presentation of the work done at Los Alamos is followed by a description of the related Karlsruhe results.

3.1 Description of Design Methods

Several vendors perform blowdown calculations as an integral part of their safety analysis. Understandably each vendor is interested in protecting the investment required to develop such calculational methods and hence classifies some of the information as proprietary. Unfortunately, much of this proprietary information concerns the selection of the appropriate model to adequately describe a key aspect of the blowdown process. Where the information was unavailable, an attempt was made to provide the background upon which a selection should be based.

This section consists of a description of the problem, followed by a discussion of aspects of calculating the blowdown induced forces. This is followed by a discussion of three aspects of the blowdown process which require special attention. These are nonequilibrium thermodynamics, critical flow and multidimensional flow.

3.1.1 Problem Description

A postulated LOCA can impose large magnitude, short duration loads on core structures during the blowdown phase of the accident. These loads result from the rapid depressurization of the reactor vessel cavity. Failure of reactor vessel internals under such loads can lead to improper functioning of the control rods or loss of coolable core geometry. Therefore, to ensure the structural integrity of core structures, several vendors (4,5) perform dynamic analysis to define the transient forces that act during the blowdown phase of a LOCA.

3.1.2 Calculation of Blowdown Induced Hydraulic Forces

The worst case for adverse loads on core and core supports is identified as an instantaneous (less than 20 ms) double-ended shear in the cold (pump discharge) leg pipe (6). Resulting hydraulic pressure waves reverberate within various regions of the core for a short interval (about 50 ms). Flows experience high amplitude oscillations for a few seconds. Such an event causes large magnitude, short duration mechanical loads on structural elements.

The loads induced on components within the reactor vessel result from the action of interface stresses (both pressure and shear) at the structural surfaces in contact with the coolant. These stresses arise from the following fluid-dynamic mechanisms:

- momentum transfer;

- spatial acceleration of fluid (caused by change in flow
direction or flow area); and

- temporal acceleration of fluid.

These mechanisms appear as terms in the hydraulic model. From
the hydraulic model one determines the interface stresses and hence
the loads induced on components.

In practice it is necessary to model the thermal-hydraulics of
the entire primary system in order to estimate the forces imposed on
the core and core supports. In principle these forces could also be
obtained by studying the reactor pressure vessel as an isolated com-
ponent with boundary conditions specified at the inlet and outlet legs.
The difficulty with this approach is that these boundary conditions
are dependent on the depressurization process in the entire primary
system and hence can be determined accurately only if the total loop
thermal-hydraulics are examined.

With the possible exception of a few key components (to be
mentioned shortly), the primary system thermal-hydraulics are modeled
in one dimension. The Water Reactor Evaluation Model (WREM) used by
Yankee Atomic Electric Company for simulation of its Maine Yankee
plant (7) serves as an example. Control volumes designated as nodes
are connected via flow paths to other nodes. The conservation equa-
tions for mass and energy are applied in the nodes while the one
dimensional conservation equation for momentum is applied in the flow-
paths. A solution is obtained by numerically integrating the conser-
vation equations over a node-flowpath network set up to model the

primary system. Other one-dimensional schemes are described in Refs. 4, 5 and 8.

In components where the flow is complex, a more detailed model may be required for an accurate prediction of system blowdown. The downcomer [5,8,27] and broken inlet leg [29] are two cases. Flow here is usually modeled in two dimensions with the equations for mass, momentum and energy solved over a finite difference mesh. A detailed discussion is given later.

Independent of the flow models used, the thermal-hydraulic analysis of primary system blowdown is carried through with all structures assumed static. As a result, local volume or pressure changes that may occur due to structural displacements in the actual system are not represented in the thermal-hydraulic model. The exclusion of fluid-structure effects is believed to give conservative estimates of blowdown loads on core structures. This however, has not been proven in general.

Three different methods for evaluating the fluid forces acting on the surface of a structure during blowdown have been identified. Each is suited to a particular characterization of flow in the vicinity of the structure. For flow described with the use of an Eulerian mesh, the shear and normal forces acting on the structure are available directly from the fluid computational cells adjacent to the fluid-structure interface. In Ref. 6, the forces exerted by the fluid in the downcomer region on the core support barrel are determined using this method. For flow given in terms of an average flow rate, empirical correlations based on the geometry and the Reynolds number yield the

forces acting on the structure. Reference 5 describes the use of this method for the computation of the drag forces exerted on a control element shroud subjected to a large transverse flow component during blowdown. Finally, when flow is characterized by the node-flowpath method, the forces on structures such as orifice plates can be determined from the momentum control volume concept. In this approach the fluid around the structure is enclosed in a control volume and the linear momentum equation applied. The control volume is drawn such that node pressures are the known external forces acting on it while the forces exerted by the structure on the control volume are the unknown external forces (5).

3.1.3 Nonequilibrium Thermodynamics

Recall that a two-phase system is in thermodynamic equilibrium when both phases are at the same pressure and their temperatures are at the corresponding saturation value. Under any other conditions the system is in a state of thermodynamic nonequilibrium.

The possible occurrence of nonequilibrium thermodynamic effects during blowdown has been investigated by several groups (5,9,10). Their findings indicate that these effects are negligible for the coolant not immediately adjacent to the break. The fluid here can be considered to be in a state of thermodynamic equilibrium. The fluid escaping through the break, however, is in a nonequilibrium state.

The evidence supporting the use of equilibrium thermodynamics throughout the primary system, excluding the break, is as follows. Non-equilibrium behavior has been found only in small scale experiments. Hirt et al. (9) describe a blowdown experiment conducted with a 1/25

scale model of a reactor pressure vessel and downcomer. They found that experimental-analytical agreement could be obtained only by incorporating a thermodynamic nonequilibrium model of vapor bubble growth in their analysis. Other cases of nonequilibrium behavior in small scale experiments are given in Ref. 5. This reference points out that the above experiments differ from a typical PWR blowdown in the following respects: fluid volume is small and break area to system volume ratio is large. Further, two large scale experiments (LOFT and CSE) typical of a PWR blowdown in these respects showed no nonequilibrium effects inside the vessel. Reference 5 points out that local decompression rates in the small scale experiments were two orders of magnitude greater than in the large scale experiments. Hence, the nonequilibrium effects observed in the small scale experiments cannot necessarily be expected to occur in the blowdown of a typical PWR.

The break thermodynamics are nonequilibrium in nature. A discussion is given below.

3.1.4 Critical Flow

An important part of modeling primary system blowdown is the prediction of the discharge flow rate from the broken coolant pipe. This flow is critical during the subcooled and saturated phases of blowdown and hence is independent of containment pressure.

Experiments reported in Ref. 10 indicate that during the subcooled phase of decompression, the break flow thermodynamics are nonequilibrium. At least one vendor (5) uses a nonequilibrium critical flow model. Comparison of the model with experiment gave good agreement.

This same model, along with the Moody and homogeneous equilibrum critical flow models was used to predict pressures for blowdown of a typical PWR. With all input parameters but the critical flow model made equal, the nonequilibrium flow model gave a more rapid decompression and higher pressure loads than either of the other two models. Unfortunately the model is unavailable for proprietary reasons.

3.1.5 Multi-dimensional Effects

The methods for blowdown analysis described in the literature contain largely one dimensional flow models (4,5,9). However, in components where the detail of spatial representation has a profound effect on the calculation of loads, the flow is modeled in higher dimensions and with fine nodalization.

The depressuraization of the downcomer following a cold leg nozzle break is highly asymmetric and hence a case for multi-dimensional flow modeling. In the standard representation (6), pressure changes in the fluid due to structural motion are neglected. The region is then treated as a thin two-dimensional layer of fluid of constant thickness.

One vendor has investigated the effect of downcomer spatial representation (dimensionality and nodalization) on the predicted space-time decompression of the region (5). In this study, two full representations of the primary system were examined. The models differed only in the degree of spatial representation in the downcomer region. Unfortunately, the exact models and results have been deleted from the text of the report for proprietary reasons.

3.2 Los Alamos Laboratory Research

The major thrust of the Los Alamos research in methods for the calculation of LOCA forces has been in investigating the effect of uncoupled fluid-structural analysis. That is, the blowdown induced forces acting on the reactor vessel internals have been calculated using an uncoupled fluid-structure procedure. In this approach, the fluid pressures and shears are first computed from a hydrodynamic model that considers the walls of the structure to be rigid. The resulting time history of forces is then applied to the structural model to determine its response. The assumption here is evident: feedback of structural deformations to the fluid is neglected. The uncoupled method is judged to be conservative for the following reason (11): it is widely held that the pressures computed on a rigid wall will be greater than if the wall is permitted to deform under the load.

To investigate the relative importance of the coupled interaction, Rivard and Torrey (12,13,14) performed three-dimensional calculations for the dynamics of the fluid and core support barrel of the HDR reactor (Fig. 3.2.1) vessel during blowdown. Besides investigating fluid-structure coupling, they also examined (a) the adequacy of a two-dimensional fluid modeling in place of the three-dimensional representation, and (b) the effect of a mass ring placed at the bottom of the core barrel to simulate the core mass and stiffness.

In their work, the fluid is represented by the two fluid, six equation model. These equations are solved by the code KFIX (15). The cold leg break is simulated by imposing the pressure history shown in Fig. 3.2 as a boundary condition. The core barrel is modeled as a linear elastic cylinder clamped rigidly at the top and unrestrained

at the bottom. The code FLX solves the corresponding structural
dynamics equations. A coupled calculation is obtained by passing the
fluid pressure as an external force to the structural code while pass-
ing the structure velocity as a differentiated boundary position to
the fluid code. In their uncoupled calculations the same algorithm
is used except that the structure velocity passed to the fluid code is
explicitly set to zero. In this way the fluid dynamics are calculated
for a rigid core barrel.

The first set of calculations performed were for the coupled and
uncoupled blowdown of the pressure vessel shown in Fig. 3.1. The
results indicate the relative importance of fluid structure-coupling.
Figures 3.3a-d show the radial deflection of the core support barrel
in the $\theta=0$ plane through the break. The inward deflection of the core
barrel at 10 and 20 ms accomodates the fluid displaced downward by the
bulging of the core barrel in the vicinity of the broken nozzle.
Figure 3.4 shows the response of the core barrel bottom directly
below the break. Note the frequency and amplitude are smaller for the
coupled case. Figures 3.5a-d compare the axial bending stresses at
the top of the core barrel. This was shown to be the most significant
stress acting at this location. Often it is also the location of the
maximum stress. Figure 3.6 shows the effect of coupling on the time
history of stress at the core barrel top next to the break.

A second set of calculations were performed to investigate the
adequacy of a coupled two-dimensional fluid modeling in place of the
coupled three-dimensional representation. A simple depressurization
model was substituted for the three-dimensional model of the lower

plenum and core regions. The two-dimensional representation of the downcomer region was retained, however. Figures 3.7a-d show the radial deflection of the core barrel in the plane θ=0 for the two- and three-dimensional calculation. Rivard and Torrey judge the two-dimensional calculation to be adequate for determining deflection profiles. Figures 3.8a-d give the axial bending stresses for the two- and three-dimensional coupled calculations. Differences of 25% to 40% occur. The two-dimensional case required 9 minutes of CDC 7600 time compared to 56 minutes for the three-dimensional case.

A third set of calculations were performed to investigate the effect of the core internal structures on the core barrel dynamics. The stiffness and inertia of the internal structures were simulated by a mass ring placed on the inside of the core barrel at its bottom boundary. Three-dimensional calculations were performed for this configuration. Figures 3.9a-d compare the radial deflection of the core barrel through the plane θ=0 with and without the mass ring. The ring is seen to reduce the deflection at the bottom boundary. Figure 3.10 compares the deflection history of the core barrel bottom in the plane θ=0. The mass ring reduces deflections by a factor of two. Figure 3.11 compares the axial bending stresses at the top of the core barrel. The stress magnitude is seen not to change significantly.

A parallel but independent line of investigation is being carried out by Diennes et al. (9,16,17,18). They have divided their study of fluid-structure interaction into three separate phases (18). The first phase involved the development of a coupled fluid-structure code to describe decompression in the axisymmetric apparatus shown in Fig. 3.12.

The results of experiments conducted with this device were used as the basis for code refinements. The second phase will simulate the asymmetric geometry of a PWR in blowdown, but without the complexities of internal structures. Experimental data for the HDR reactor will be compared against analytical predictions. In the third phase, the effects of internal structure will be included in the code.

Their study of blowdown in the axisymmetric structure shown in Fig. 3.12 is as follows: the fluid is modeled in two dimensions using the two phase drift flux approximation. The code SOLA-DF solves the corresponding fluid equations in cylindrical r,z coordinates using a finite difference scheme. The core barrel is modeled as a cylindrical shell using the classical shell equations. These equations are solved by the finite difference code FLX. Coupling is achieved in the same way as described for the Rivard and Torrey work. A set of blowdown experiments was conducted with the apparatus shown in Fig. 3.12. Blowdown was initiated by cutting the end cap (located at top of figure but not shown) with an explosive charge. The pretest calculations differed widely from the experimental results. However, analytical-experimental agreement improved when the code was modified to include (a) effects of wall velocity on adjacent fluid density that had been previously neglected, (b) a more accurate method for calculating the speed of sound in the fluid and (c) a heat conduction limited liquid to vapor production model. The pressure release mechanism is believed to be responsible for a shock wave that propagated down the apparatus causing spurious pressure peaks to appear. The experiments will be repeated with an improved mechanism.

3.3 Karlsruhe Laboratory Research

Full scale blowdown experiments are being planned by the
Karlsruhe Laboratory for the former HDR reactor vessel (19). Scheduled
for 1979, these experiments are intended to verify the fluid-structure
codes that have been under development at Los Alamos and Karlsruhe.
The HDR reactor vessel has been modified in several ways in preparation
for the experiments. The core barrel thickness has been reduced to
make blowdown induced deformations larger and hence fluid-structure
interaction more evident. The core barrel has been rigidly clamped
at its top since this assumption is made in the current set of codes.
A mass ring has been substituted for the core internals since the codes
do not as yet model details of the core structure. Figure 3.13 com-
pares the HDR vessel with a typical PWR.

Four fluid-structure interaction codes are under development in
Germany (20). We will describe two of these, STRUYA and FLUX, both
intended to be applied to the HDR experiments.

In their coupled code STRUYA, Katz et al. (21) have adapted the
two dimensional Los Alamos code YAQUI to describe fluid flow in the
unwrapped downcomer. Flow is parallel to the fluid-structure interface
and fluid thickness is determined by local structural displacements.
The core barrel is modeled with the code CYLDY2, a semi-analytical ap-
proach that represents displacements as a sum of modal shape functions.
Computer time for this structural code is considerably less than for
general purpose finite element codes. Coupling of the fluid and struc-
tural codes to give STRUYA is currently underway.

The second coupled code, FLUX, is in a more advanced state (22).
The fluid model is based on three dimensional potential flow and has

versions for both a compressible and incompressible fluid. The structure is modeled using the CYLDY2 code. Reference 22 describes in detail the analytical formulation. The three vessel geometries given in Table 3.1 were examined with the coupled and uncoupled versions of FLUX. In all three cases the decoupled calculation gave a conservative value for the maximum stress in the core barrel. The coupled results for the Battelle-Frankfurt vessel agree well with the data obtained from a blowdown experiment run with this vessel. The HDR uncoupled results are to be compared with experiment in the near future.

3.4 Structural Mechanics and Fluid Dynamics Methods

Appendix B contains a summary of available fluid mechanics, structural dynamics and fluid-structure interaction codes. The name, reference and source of each code is given, along with a short discussion of the code's intended use and numerical method. In addition, any known verification or applications of the codes are discussed.

32

Table 3.1 INPUT PARAMETERS FOR NSR, PWR AND RS16 SITUATIONS

Table a.   Geometric Data [m]

|		NSR	PWR	RS16
R_M	Radius of core barrel center plate	1.3185	2.145	0.3065
L_M	Length of annulus = dynamically effective length of core barrel	7.57	8.24	7.39
R_S	Vent radius	0.100	0.4025	0.0715
L_F	Distance of nozzle axis from flange support	0.72	1.12	1.34
H_R	Annulus width	0.150	0.315	0.077
H_M	Core barrel shell thickness	0.023	0.080	0.008
L_S	Length of blowdown nozzle (short/long)	1.10 /5.43	3.7 /6.0	0.35 / -
R_{RI}	Mass ring, inner radius	0.81	1.20	0.2
R_{R1}	Mass ring, outer radius	1.105	2.105	0.3065
B_{R1}	Height of mass ring	0.75	0.682	0.3065
B_{R2}	Height of intermediate ring	0.14	0	0.13
R_{RA}	Outer radius of intermediate ring	1.307	0	0.13
L_U	Effective height of upper plenum: so that $\pi R_V^2 L_U$ = volume of upper plenum	1.0	1.6	1.97
L_L	Effective height of lower plenum: so that $\pi R_V^2 L_L$ = volume of lower plenum	1.8	1.5	1.7
R_V	Pressure vessel inner radius = = $R_M + H_M/2 + H_R$	1.48	2.50	0.3875
f_{hole}	Component of hole area on flange relative to annulus cross-section = = Θ in § A3.2.4	0	0	0.039

Table b.   Core Barrel Physical Constants

		NSR	PWR	RS16
ρ_M	Barrel density at nominal dimensions [kg/m^3]	7800	7800	7800
E	Modulus of elasticity [N/m^2]	$1.7 \cdot 10^{11}$	$1.7 \cdot 10^{11}$	$2 \cdot 10^{11}$
ν	Transverse contraction number	0.3	0.3	0
ρ_R	Mass ring density [kg/m^3]	7800		
	or			
M_R	Mass ring mass $\approx$ 1/2 core mass, or mass of rigid barrel component [kg]	$12 \cdot 10^3$	$50 \cdot 10^3$	1400
I_{ZZ}	Rotational inertia of ring (if geometric dimensions and density are not fixed) [kg m^2]	6100	75000	9067
s_{damp}	Damping coefficient for structure according to equation (A4-10) [%]	0	1	1

Table c.   Characteristic Fluid and Input Data
(NSR for Test 3, RS16 for Test PWR5)

|		NSR	PWR	RS16
p_0	Initial pressure [MPa]	11	15.75	14.2
T_R	Initial temperature (averaged) in annulus [°C]	268	290	280
T_I	Initial temperature (averaged) in interior [°C]	305	320	280
ρ_0	Density at (p_0, T_R) [kg/m^3]	781.3	746.9	762.5
a	Velocity of sound at (p_0, T_R) [m/sec]	1088	948	1070
p_S	Saturated vapor pressure at T_R [MPa]	5.335	7.445	6.419
T_S	Saturated vapor temperature at p_0 [°C]	318	346	337.75
$\Delta t_{rupture}$	Pipe rupture time [msec]	0	3	1
f_{damp}	Damping for fluid according to equation (A1-37) [1]	0	0.1	0.25
η	Dynamic viscosity [10^{-5} kg/(msec)]	10.1	9.44	9.8
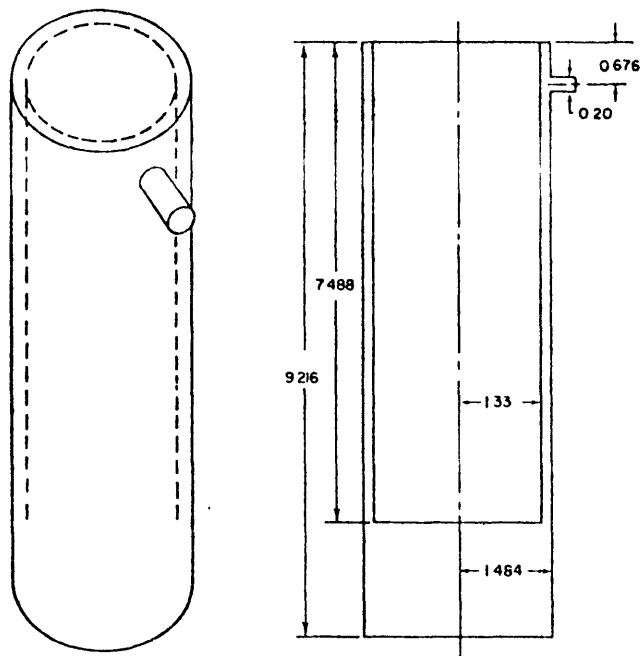
Fig. 3,1
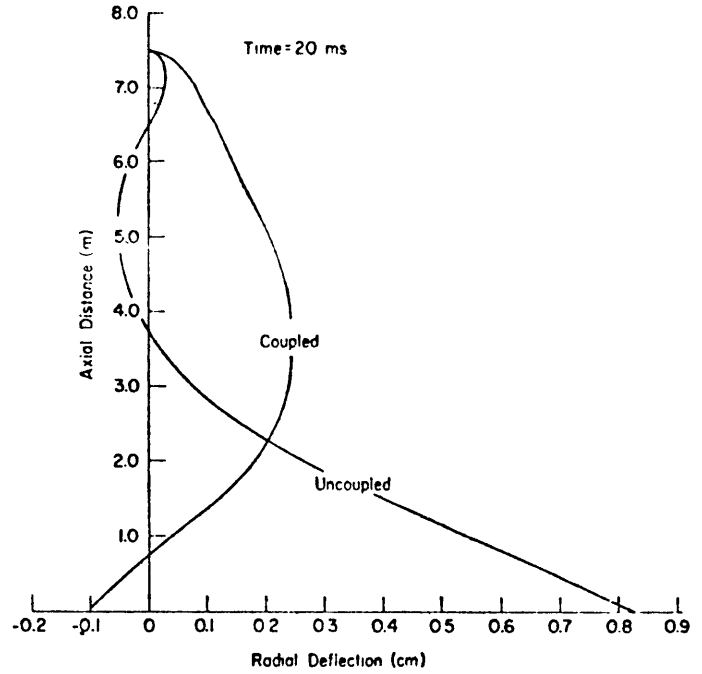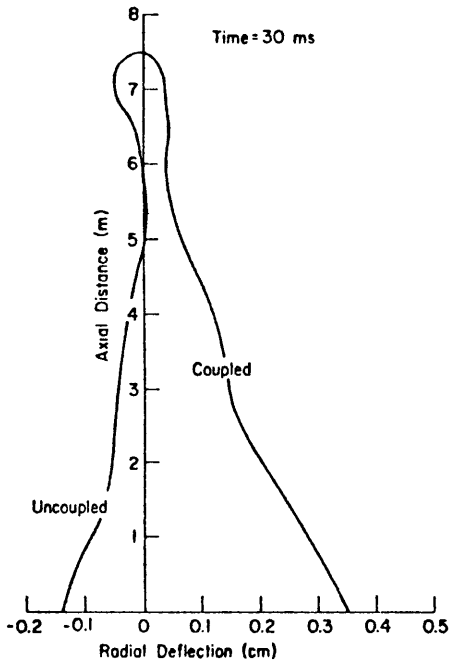*Geometry of HDR pressurized water reactor vessel. Dimensions are in meters.* (Ref. 13)
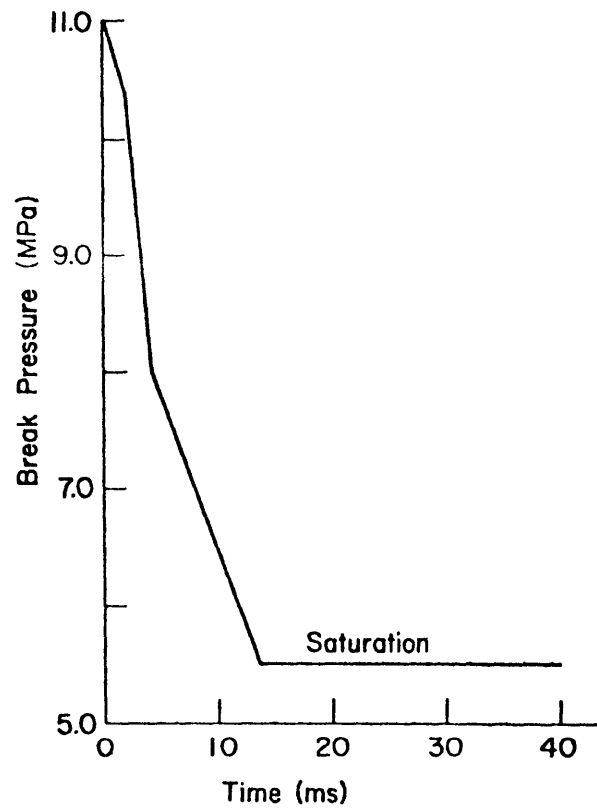
Fig. 3.2

Prescribed pressure history at the cold leg break that is used as a boundary condition for the calculations. (Ref. 13)
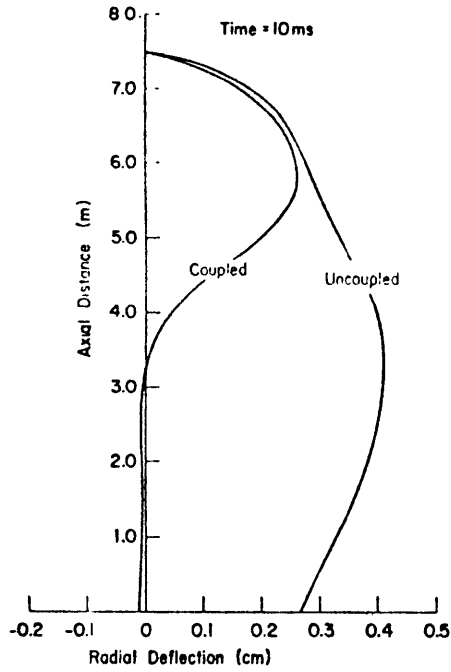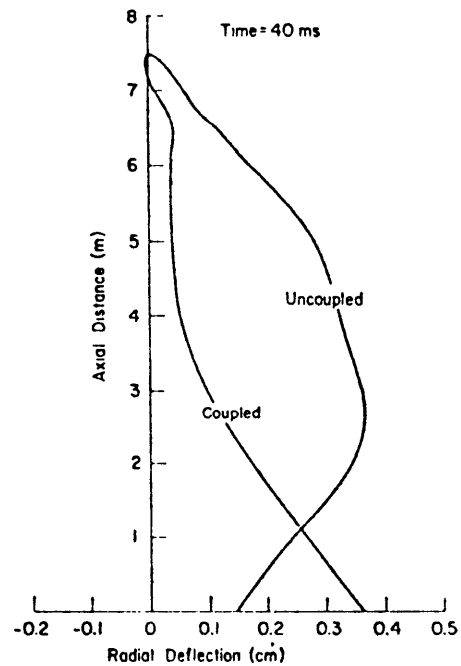
Fig. 3.3

Radial deflections of the core barrel in the plane φ = 0° through the break at 10, 20, 30, and 40 ms after the pipe break. The results were calculated in three dimensions with and without fluid-structure coupling. (Ref. 13)

Fig. 3.4

Radial deflections of the core barrel bottom directly below the break calculated in three dimensions with and without fluid-structure coupling. (Ref. 13)

Fig. 3.5

Axial bending stresses at the top, built-in boundary of the core barrel calculated in three dimensions with and without fluid-structure coupling at 10, 20, 30, and 40 ms after the pipe break. (Ref. 13)

Fig. 3.6

Axial bending stresses at the top of the core barrel in the plane $\phi = 0°$ through the break calculated in three dimensions with and without fluid-structure coupling. (Ref. 13)
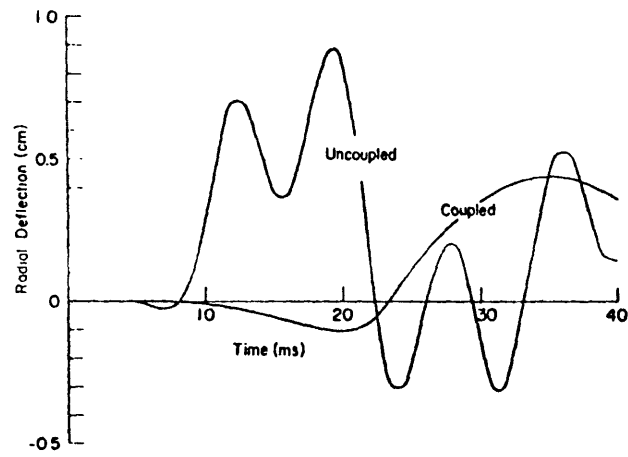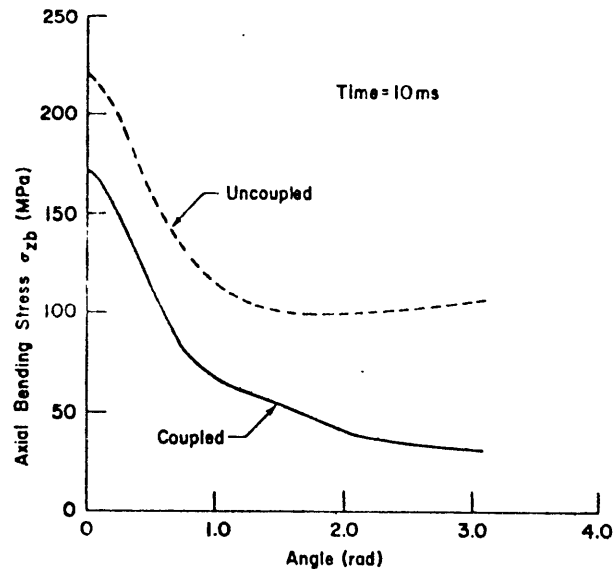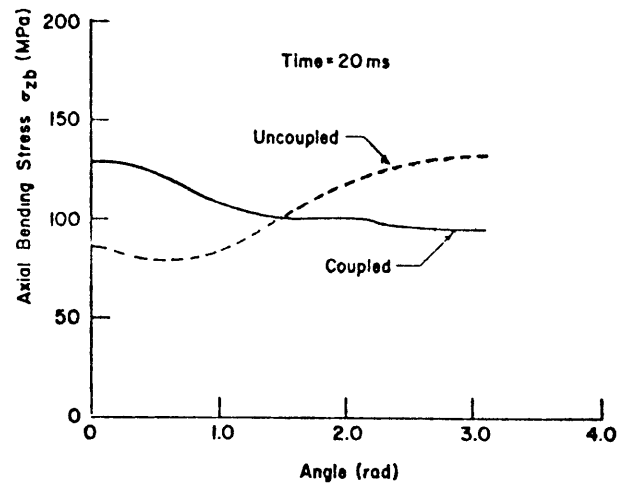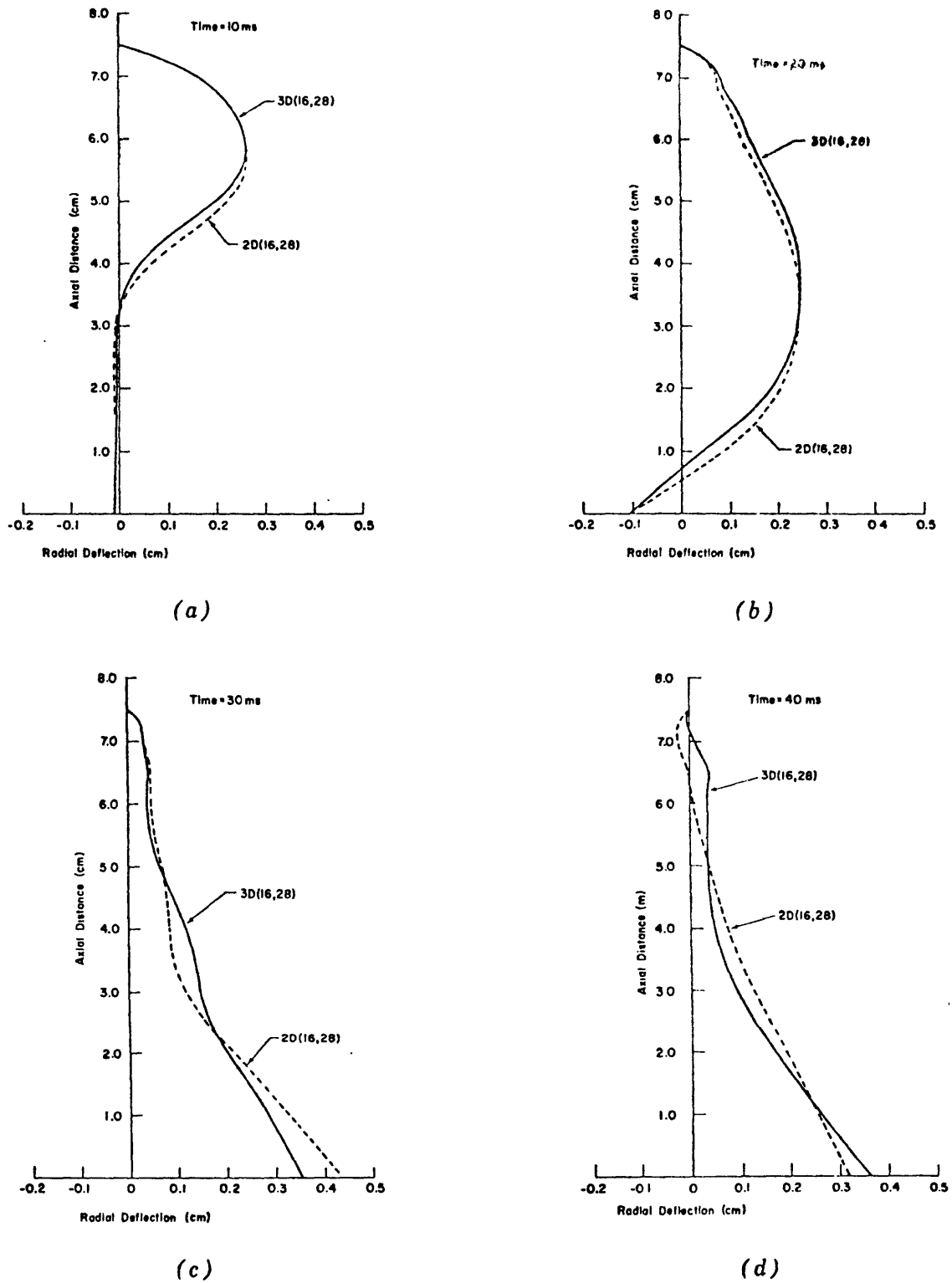
Fig. 3.7

Radial deflections of the core barrel in the plane $\phi = 0°$ *through the break at 10, 20, 30, and 40 ms after the pipe break. The results were calculated with two- and three-dimensional fluid descriptions and structural coupling.* (Ref. 13)
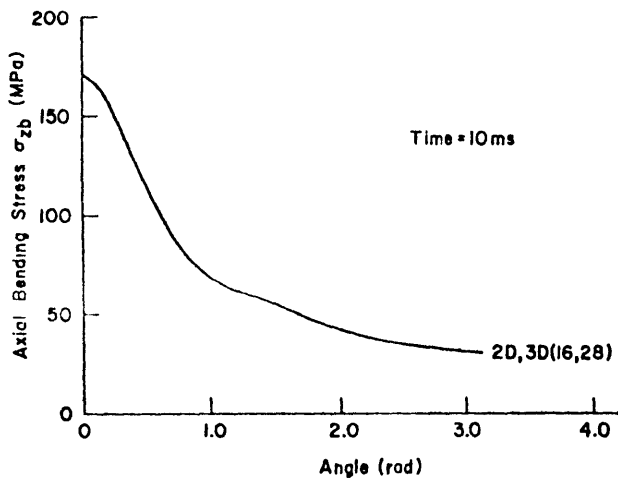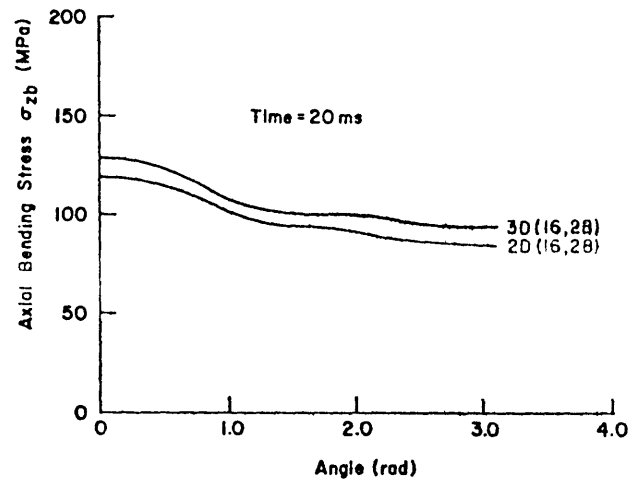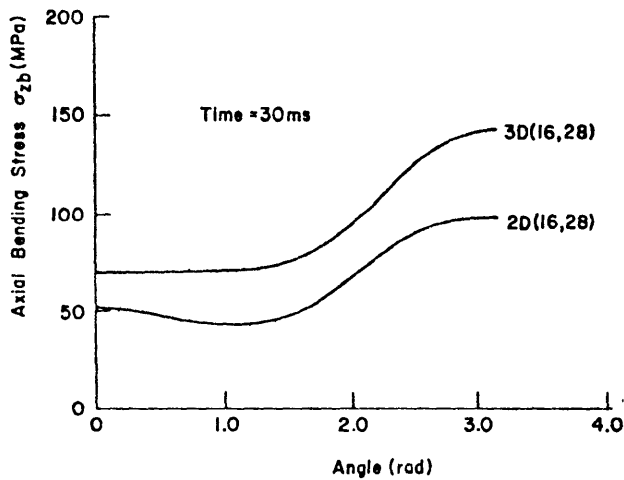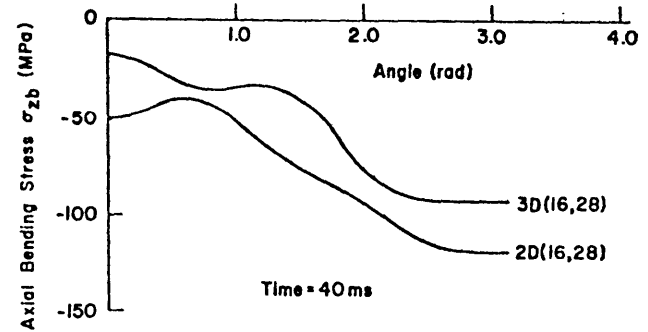
Fig. 3.8

Axial bending stresses at the top, built-in boundary of the core barrel calculated with two-and three-dimensional fluid descriptions and structural coupling at 10, 20, 30, and 40 ms after the pipe break. (Ref. 13)
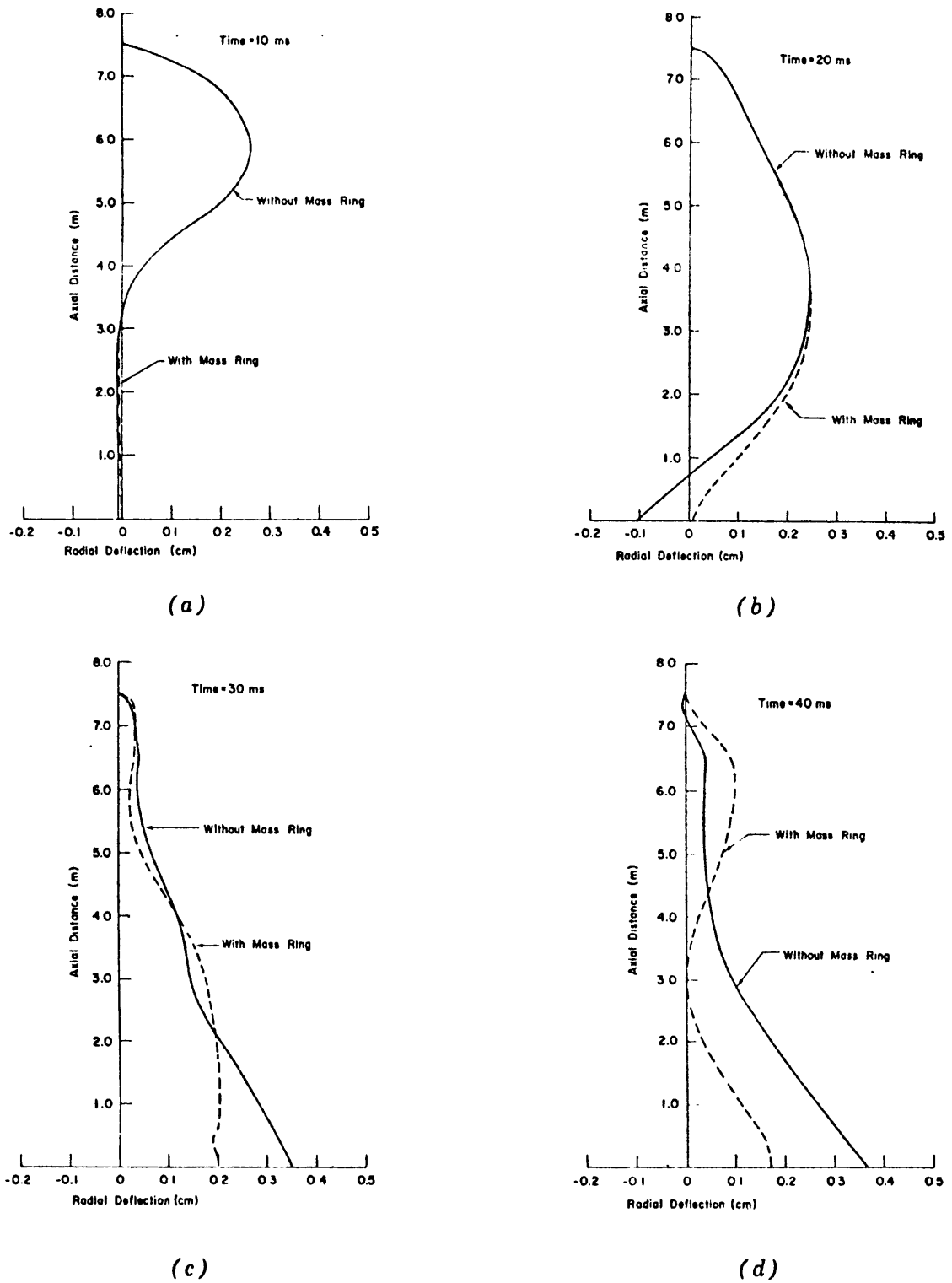
Fig. 3.9

Radial deflections of the core barrel in the plane $\phi = 0°$ through the break at 10, 20, 30, and 40 ms after the pipe break. The results were calculated in three dimensions with and without the bottom ring. (Ref. 13)
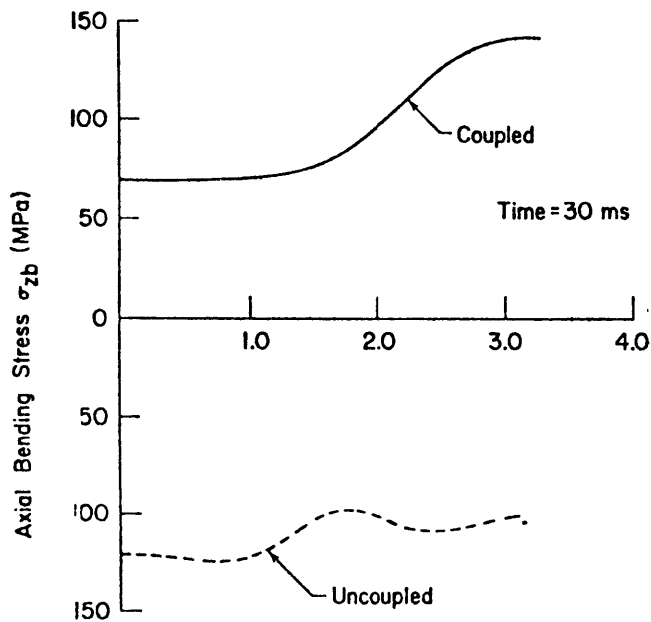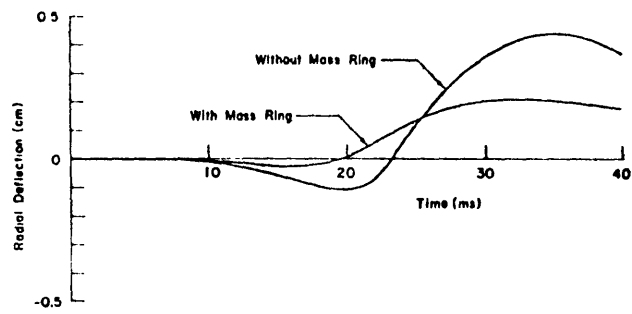
Fig. 3.10

Radial deflection of the core barrel bottom directly below the break calculated in three dimensions with and without the bottom ring. (Ref. 13)
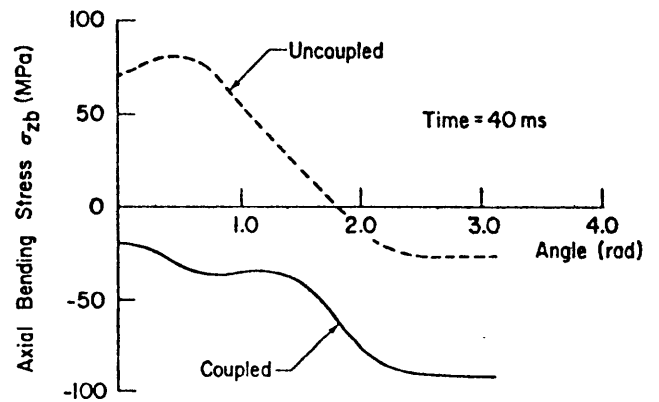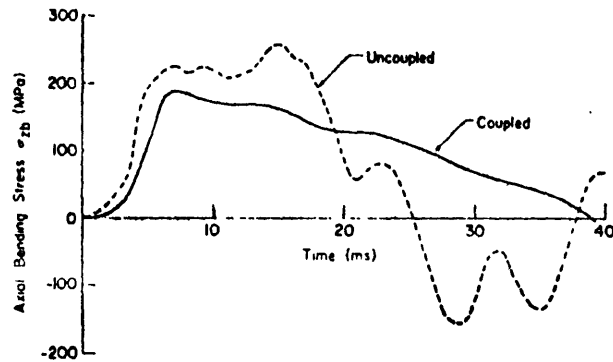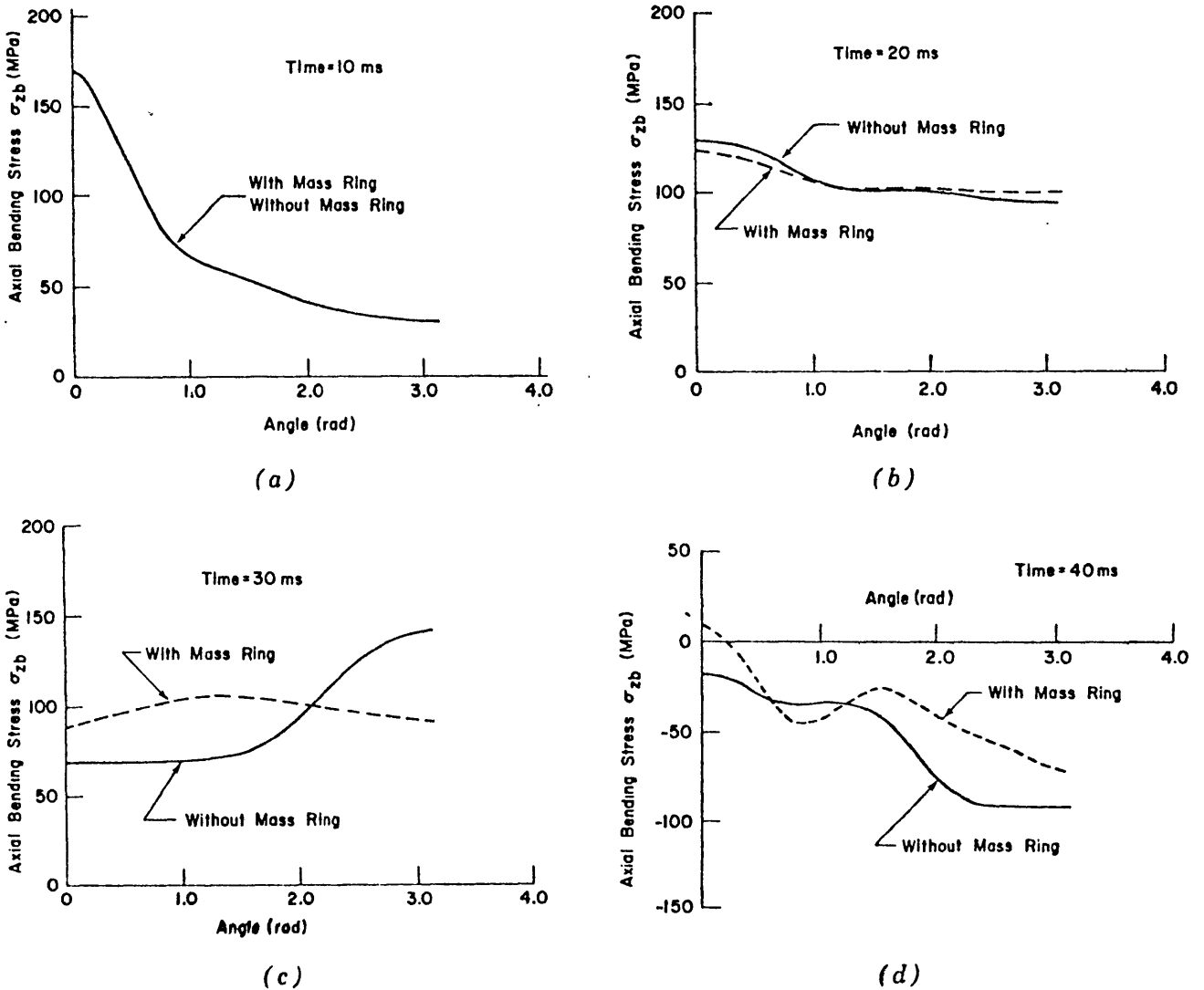
Fig. 3.11

Axial bending stresses at the top, built-in boundary of the core barrel calculated in three dimensions with and without the bottom ring at 10, 20, 30, and 40 ms after the pipe break.
(Ref. 13)

46
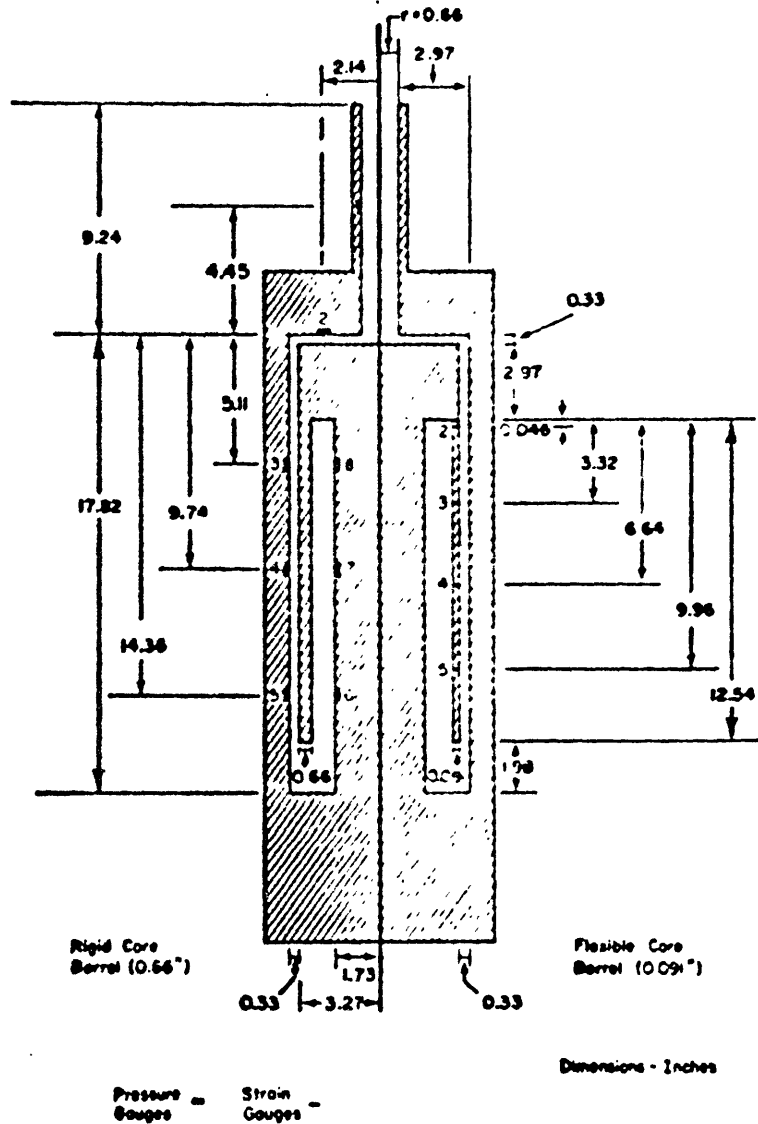
Geometry of the planned hydroelastic experiment showing the location of pressure and strain gauges. The geometry is in some respects that of a 1/25 scale PWR, modified to allow axisymmetric scoping calculations. The thick shell geometry is shown on the left and the thin shell on the right. Strain gauges will be located at several azimuthal locations to investigate the symmetry.

Fig. 3.12 Axisymmetric Blowdown Apparatus (Ref. 18)
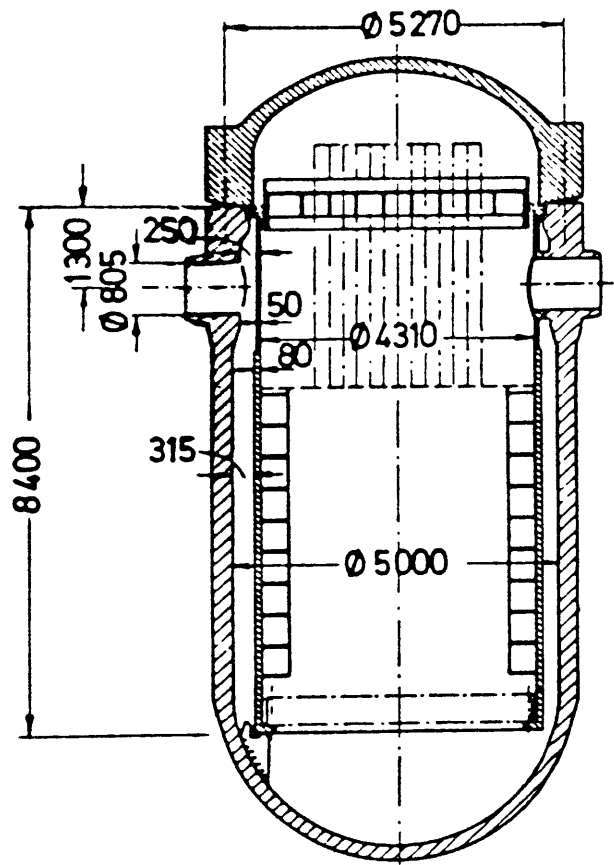
PWR of the
1200 MW-type
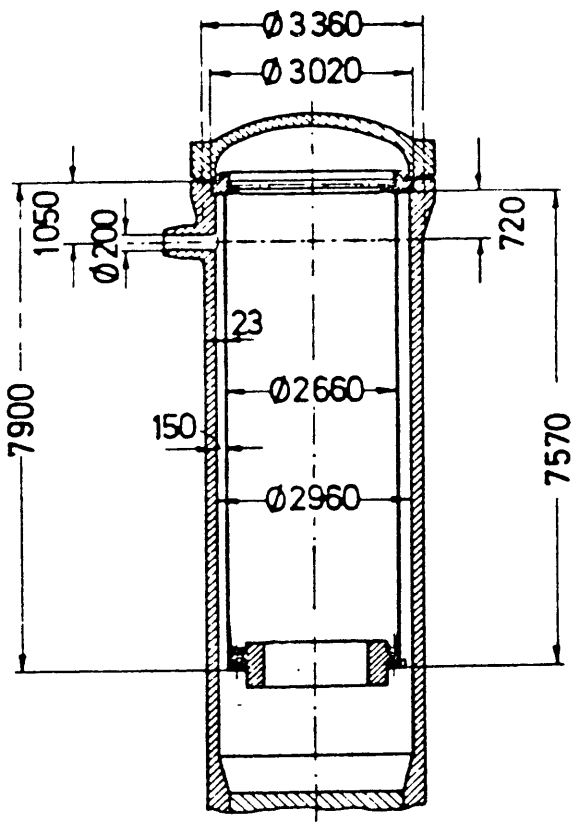
HDR experimental
facility
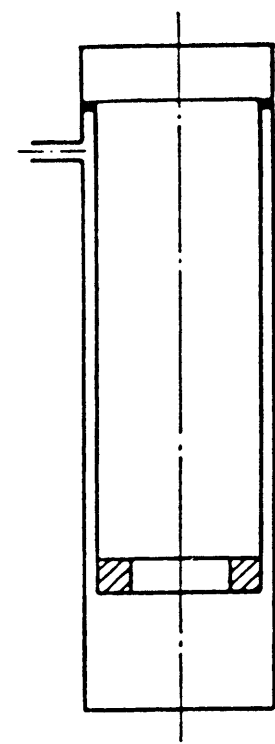
geometrical model
of the HDR used
in FLUX

Fig. 3.13 Geometry of PWR, HDR und FLUX model (Ref. 20)
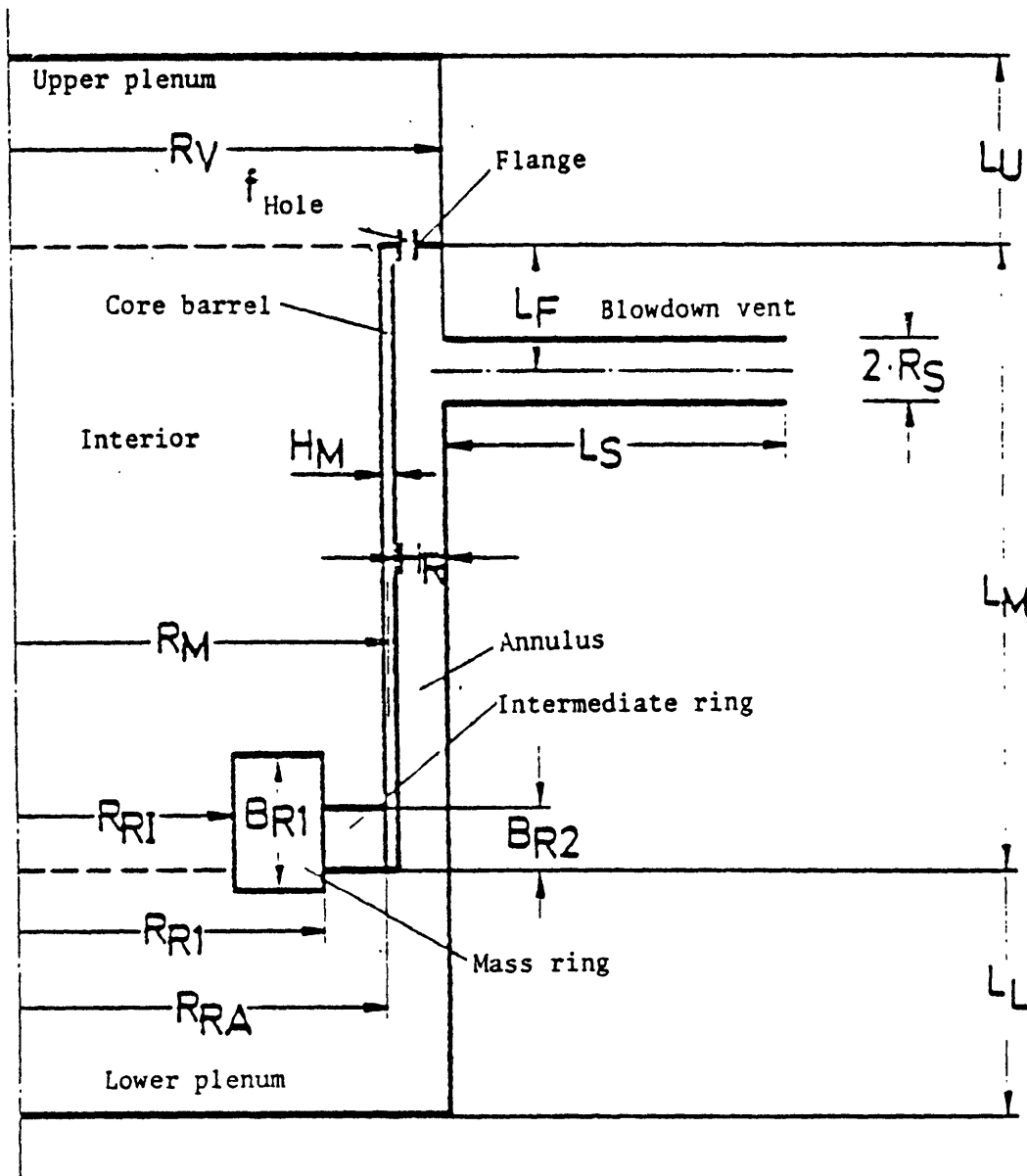
Figure 3.14   Geometry Parameters in FLUX Model.   (The Ring is divided
into two parts only with reference to computation of rotational inertia
in the structure model.   In the fluid dynamic component $R_{R1} = R_{RA} = R_M$.)
(Ref. 22)

4. EXAMINATION OF ASSUMPTIONS

The calculation of blowdown induced forces may involve a number

of assumptions and approximations which help to make the problem more

tractable. The appropriateness of such assumptions and their effect

on the calculated results must be assessed. To that end, this chapter

will highlight a number of these assumptions, including both qualitative

and quantitative assessments.

4.1 Sonic Velocities

The calculation of sonic velocities is important in determining

the propagation of pressure waves through the reactor flow paths during

a LOCA. In order to have a well-understood source for sonic velocities,

subcooled liquid tables were used to derive needed partial derivatives

by numerical differentiation. The sonic velocities were then calcu-

lated using the following equation:

$$C = \left[\frac{1}{R_p - R_T \left(\frac{S_p}{S_T} \right)} \right]^{\frac{1}{2}} \qquad (4.1.1)$$

where C = sonic velocity, evaluated for isentropic conditions;

   R_p = partial derivative of density with respect to pressure,
         holding temperature constant;

   R_T = partial derivative of density with respect to
         temperature, holding pressure constant; and

   S_p, S_T = corresponding partial derivatives of entropy.

Results indicated that, for the cold leg conditions of Table 2.2

(15.6 MPa, 290°C), C was approximately 1010 m/s. For the hot leg con-

ditions (15.5 MPa, 318°C), C was approximately 850 m/s. These velocities

can be compared to those employed in computer codes of interest.

4.2 Exact One Dimensional Solution

In order to examine the methods used to treat one-dimensional
pressure wave propagation, an "exact one-dimensional" treatment was
developed. In this technique, the decompression wave is considered to
advance through a sequence of one-dimensional pipes, each characterized
by a length and flow area. At each junction between pipes, a portion
of the wave is transmitted and a portion is reflected. Knowing the
sonic velocity, the pressure conditions in the pipes can be calculated
by adding the transmitted and reflected pressure waves. The pipes
were divided into equal length steps for the purpose of calculating
the progression of the wave fronts. The pipe lengths and the time
step size were selected such that a wave traveling at sonic velocity
would advance one length step each time step. The one-dimensional
equations are derived in Appendix C.1, while the reflection and trans-
mission coefficients are derived in Appendix C.2. The formulation of
the exact solution in the steady-state is given in Appendix C.3.

The model used for the one-dimensional solution was based on
the base case illustrative problem of Chapter 2. It consisted of nine
connected pipes with a flow boundary condition on the left hand side
and a pressure boundary condition on the right hand side. These nine
pipes represent the volumes in the calculational model shown in Fig. 2.1.
Table 4.1 gives the geometric configuration of the one-dimensional
model, with the corresponding volume numbers from Chapter 2. The left
hand side flow condition represents the net result of the flow out
of the broken pipe and the flow into the vessel from the unbroken legs,
while the right hand pressure condition represents the depressurization
of the upper plenum.

Five different combinations of pressure and flow boundary conditions were used. These boundary conditions are summarized in Table 4.2 and consist of combinations of step and ramp changes in pressure and velocity. The particular combinations of boundary conditions used were selected to investigate the importance of the break model to the calculation of forces on core internals. Boundary condition 1 consisted of a 60 ms ramp in flow with pressure held constant for 20 ms, then ramped for 40 ms. This was considered to be the most realistic case, since the depressurization of the upper plenum begins some time after the break. The holdup of pressure following the break represents the time required for depressurization to travel from the break to the upper plenum.

The results of these calculations are shown graphically in Figs. 4.1a-4.5a. The calculations were performed for a length increment of 0.5 m, a time step of 0.5 ms, and a sonic velocity of 1000 m/s. The figures show pressure differentials across the core barrel during the first 200 ms of the accident. Each figure shows the curves for the pressure differences between the downcomer (pipe 3) and the core volumes (pipes 6,7,8). Examination of these figures reveals that the three curves are nearly the same, making it difficult to distinguish between them. All five cases show large fluctuations in pressure difference with some degree of periodicity. The fluctuations are of the order of MPa and vary from positive to negative. Case 3 (Fig. 4.3) resulted in the largest pressure differences, having a positive peak of approximately 40 MPa and a negative peak of approximately 37 MPa. Some of the pressures involved in computing these differences are quite

negative and unattainable physically. They serve to indicate the magnitude of numerical differencing errors however, since results of the FLASH/RELAP techniques are also calculated on a no-flashing basis. A comparison of the graphs shows that the results were more sensitive to the flow boundary condition than to the pressure boundary condition. Figures 4.2 and 4.4 show very similar behavior, though the pressure boundary condition in the former was a step change while a constant pressure boundary condition was applied in the latter. However, the agreement between Figs. 4.4 and 4.5 was not very good, despite the same pressure boundary condition (constant pressure). The step change flow boundary condition of Fig. 4.4 gave lower peak pressure differences than did the 20 ms ramp of Fig. 4.5. In addition, the shape of the curves differed substantially. Based on these comparisons, it seems that the results are more sensitive to the flow boundary condition than the pressure boundary condition.

Another conclusion which may be drawn is that ramped boundary conditions result in higher pressure differences than step change boundary conditions. This indicates that the assumption of an instantaneous break may give non-conservative results for forces on core internals. However, the high pressure differences occur only very late in the transient (80 ms or later). At these times, waves would probably become blunted from friction, departure from one-dimensionality, etc. The questions of which boundary condition (ramped or step) is worst cannot be answered based on these calculations alone.

The periodicity displayed by the results lends credence to the possibility of dynamic effects being important in determining the

stresses and deflections during the accident. If these periodic loadings have frequencies which match natural frequencies of the structures, and if the spatial shape of the pressure wave corresponds to the mode shape, then a resonance effect could be the result. This feature is addressed further in section 4.4.2.

4.3 FLASH/RELAP Solutions

Having developed an exact treatment of one-dimensional pressure wave propagation, a solution technique based on that of the FLASH/RELAP codes was applied to the same problem. This solution provides a basis for comparison and gives insight into the computational errors associated with the methods most often used. The FLASH/RELAP method utilizes finite difference techniques to solve the equations of momentum and continuity. The formulation of these finite difference equations is given in Appendix D.1. Assumptions made in this Appendix are that the flow is isentropic and that density and sonic velocity are constant. These physical assumptions are completely equivalent to those employed in Section 4.2 for the "exact solution". The finite difference equations are solved as a tridiagonal matrix by a technique outlined in Appendix D.2.

As in the exact solution of Section 4.2, the FLASH/RELAP solution was applied to a nine pipe representation of the base case illustrative problem with left hand side flow and right hand side pressure boundary conditions. For details of the model, see Section 4.2. Each pipe in Table 4.1 is represented by one control volume. Time steps of 0.25 ms, 0.5 ms, and 1.0 ms were employed with very little difference in results (the plotted results are based on the time step of 0.5 ms).

The results of the analyses are presented graphically in
Figs. 4.1b through 4.5b. As in Section 4.2, the figures show the
pressure difference across the core barrel for 200 ms following the
break. Three curves on each graph show the differences in the down-
comer pressure (pipe 3) and the core pressures (pipes 6,7,8). As in
the exact one-dimensional case, these three curves were often so close
as to be indistinguishable. Examination of the figures shows that the
fluctuations in pressure differential are somewhat smooth and regular.
The maximum pressure differential was approximately -12.5 MPa on
Fig. 4.2b. Figure 4.1b shows that the most realistic boundary con-
ditions gave a very weakly varying pressure differential. Figures
4.2b and 4.4b show that two problems with the same flow boundary con-
dition but different pressure boundary conditions have very similar
results. This is consistent with the results of the previous section.
In the same way, Figs. 4.4b and 4.5b show that two problems with the
same pressure boundary condition and different flow boundary conditions
give rather different results. This result is also consistent with
the previous section. That is, if we consider both the exact solution
and the FLASH/RELAP solution, it seems that the results are more sensi-
tive to the flow boundary condition than to the pressure boundary
condition, independent of the solution technique. However, in this
case, the ramp flow condition gives less severe pressures than the
step, whereas the opposite conclusion was reached before.

Since the cases run with the FLASH/RELAP program were identical
to those done with the exact analytical solution, the results can be
compared directly. The FLASH/RELAP solutions gave significantly lower

pressure differentials and less fluctuations than did the exact solution. The shape of the curves in Figs. 4.2b through 4.5b mimic the corresponding curves from the previous section, as if some sort of numerical damping were applied by the FLASH/RELAP solution technique. In the case of the most realistic boundary condition, the agreement between the two techniques was quite poor. These results indicate that the FLASH/RELAP solution technique damps out some of the higher frequency pressure oscillations and under-predicts the pressure differentials across the core barrel. This effect was not due to time step size, as was shown by a time step size sensitivity study performed for boundary conditions 1, 2 and 3 of Table 4.2. The sensitivity of the FLASH/RELAP solution to time step selection was shown to be very small. See Appendix A for the results in graphical form. It is likely that using more control volumes in the FLASH/RELAP case would reduce the damping and give a more satisfactory numerical solution.

4.4 Comments on Other Effects

4.4.1 Multi-dimensional Effects. The wave propagation through the downcomer cannot easily be visualized as an approximate one-dimensional problem. Figure 4.6 shows the pressure in a PWR downcomer obtained by a multi-dimensional fluid-structure coupled calculation (20). This figure reveals two effects that are obscured in a one-dimensional calculation. First, at a given time, the depressurization has traveled further down the downcomer at 0° from the nozzle than at 180°. Second, the zone of least pressure is located in the vicinity of the nozzle. The consequences of these effects on the core barrel motion are illustrated in Fig. 4.7. Radial forces from the asymmetric pressure distribution cause a beam-like motion of the barrel while the reduced

pressure in the vicinity of the nozzle results in local bulging of the barrel.

It is also apparent that other multi-dimensional effects would be observed in a case with hot leg penetration and with other cold legs present (see also Fig. 2.5).

4.4.2 <u>Dynamic Structural Analysis</u>. The loads on the core barrel and other structures vary rapidly and at times are of the order of the natural periods of the structure so that resonances between the structure and fluid may occur. Therefore, the mechanical analyses of the structure are most properly done with dynamic techniques.

As a first step, the natural frequencies of the structure can be compared with the frequency of pressure oscillations in the fluid. Those structure modes with natural frequencies close to the frequency of pressure oscillations in the fluid may be preferentially excited. The rate of amplitude increase seen will depend on the structural damping and on the difference between the excitation frequency and the natural frequency of the mode.

A simple method for determining the lowest natural frequency of the core barrel follows. Kreig et al. (6) calculated the modal shape functions for the HDR core barrel rigidly clamped at the top and loaded with a mass ring at the bottom. The modal shapes corresponding to the first fifteen eigenfrequencies are given in Fig. 4.8. Note that the first shape function is the beam-bending mode for which the radius of the barrel is constant. An expression for the natural frequency of this mode is (23):

$$f^2 = \left(\frac{1}{2\pi}\right)^2 \left[\frac{4 \pi E H_m}{\frac{2}{\rho} \pi L_m R_m H_m \rho_m + M}\right] \left(\frac{R_m}{L_m}\right)^3 \qquad (4.1)$$

where the symbols are as defined in Table 3.1. Now if the core and support structures are simulated by a mass ring attached at the bottom of the core barrel, then Eq. (4.1) can be used to predict the frequency of the lowest mode. The ring will be dynamically equivalent to the core and core support structure if it is taken as 1/2 of the sum of their masses (22). Frequencies obtained in this way are always higher than the true value. Table 4.3 compares these with those obtained from the sophisticated structures code STRUDL/DYNAL (6,22) for three different core barrels.

Based on the above, we can estimate the frequency of the beam bending mode of the Maine Yankee core barrel. There are 217 fuel assemblies inside the barrel, each of mass 581 kg. Neglecting the core support structure mass, the barrel internals are then dynamically equivalent to a 63,000 kg mass ring attached to the barrel bottom. The variable thickness of the core barrel as seen in Fig. A.1 presents a difficulty as far as the application of (4.1) is concerned. We will assume the barrel to have a constant thickness equal to the average thickness of 50.4 mm. The barrel is Type 304 stainless steel. Its mass is obtained by computing its volume from Fig. A.1 and then multiplying by the density of Type 304 stainless steel. The values to be used in (4.1) are:

E (GPa)	H_m (m)	R_m (m)	L_m (m)	ρ_m (kg/m^3)	M (kg)
193.0	0.054	1.88	8.33	8027.0	44,200.0

The frequency of the beam-bending mode is then found to be 26.9 Hz. Based on Table 4.3, this value is 15% to 30% high so that the true frequency of the first mode is expected to be somewhere between 20.5 and 23.5 Hz.

Simple estimates for the frequency of pressure oscillations in the downcomer and core region can also be made. The one-dimensional water hammer results obtained from the representation of the Maine Yankee vessel as a series of half meter pipe lengths are useful in this respect. Although the core barrel pressure differentials given by this method are axisymmetric, the frequency of pressure oscillations should be similar to those found using a multi-dimensional fluid representation. Therefore the one-dimensional water hammer results provide a measure of the frequency of the forces acting on the core barrel during blowdown. Examination of the water hammer plots for step and ramp boundary conditions show core barrel differential pressure frequencies of 12-13, 19-20, 71-81 and 200-228 Hz.

These simple estimates indicate that for the Maine Yankee plant the natural frequency of the core barrel beam bending mode is close to one of the characteristic frequencies of the core barrel differential pressures. Whether the amplitude of this mode grows in time will depend on the degree of pressure relief due to the displacement of the core barrel wall under the pressure load. If it should grow, the core snubber block and core restraining lugs may be damaged.

4.4.3 <u>Interaction of Motions and Loads</u>. The above discussion is based on decompression wave propagation into regions of fixed geometry. Normally, however, the vessel internals deform (either elastically or plastically) under the loads imposed by the fluid. This is accompanied by a corresponding change in flow region geometry. In this section, conservative estimates are given for the circumferential strain experienced by the core barrel, shroud and thermal shield during blowdown. These numbers help characterize the relative change in flow area of key coolant regions and indicate how close components are to yielding.

Conservative estimates for the circumferential strain experienced by the core barrel, core shroud and thermal shield are obtained as follows. Consider a thin metal annulus of infinite length bounded on both the inside and outside by annular regions of fluid whose inside and outside boundaries, respectively, are rigid. Suppose a pressure differential is applied to the thin annulus via the fluid on either side. The annulus then strains, reducing the fluid pressure differential until the hoop stress balances the pressure differential. A conservative estimate for this strain can be obtained by assuming the thick annulus has zero stiffness in which case it will deform further until the pressure differential across it is zero. Appendix E gives an expression for this total strain as a function of the initial fluid pressures. This expression was used to compute the strain and radius change necessary to relieve representative blowdown pressure loads acting on the core shroud, core barrel and thermal shield. These figures give orders of magnitude for the amount of component deformation

that can occur. In reality, the stiffness of these components and their finite length (fluid vented through the ends) should limit deformations to less than what we calculate from the expression given in Appendix E. Hence these calculations yield upper bounds on the deformations.

Five "worst case" component loadings are defined in Table 4.4. The corresponding circumferential strains necessary to relieve these loads were computed using the expression of Appendix E and are given in Table 4.5. Note that the radius used for the core shroud was obtained by fitting a 6 m^3 (bypass region volume) annulus inside the core barrel such that the outside radius equalled that of the bypass region. The core shroud radius was then taken as the inside radius of the annulus (1.74 m).

The numbers given in Table 4.5 involve several assumptions. First, the pressure changes due to structural deformation occur isentropically. Second, the region of lowest pressure is assumed to be at saturation while the region of higher pressure corresponds to the state reached by following an isentropic path from the state of lower pressure.

In light of the assumption of zero component stiffness, the values for strain given in Table 4.5 indicate the core shroud, core barrel and thermal shield deform elastically (in the breathing mode) since the strain is roughly no greater than 0.2%. Note the breathing mode deformation of these components affects coolant flow area negligibly.

Table 4.1

Geometric Parameters for One-Dimensional Model

Pipe No.	Base Case Volumes	Volume m^3	Flow Path m	Length m	Area m^2	Volume m^3
1	26 & 14	2.5	4.38	4.5	1.7058	7.676
2	27	10.0	1.7	2.0	5.89	11.780
3	28	14.0	5.58	5.5	2.51	13.805
4	29	7.8	2.3	3.0	2.59	7.770
5	47	10.4	2.43	1.0	8.12	8.120
6	30 ⎫			1.0	4.9	4.9
7	31 ⎬	17.1	3.48	1.0	4.9	4.9
8	32 ⎭			1.0	4.9	4.9
9	2	3.4	.44	0.5	7.79	3.895

Note: In pipe No. 1, three loops were combined.

Table 4.2

Boundary Conditions for One-Dimensional Model

Case	Left Hand Side Velocity	Right Hand Side Pressure
1	Ramp of 60ms to -11.7m/s	Ramp to 10.7 MPa after 20ms hold
2	Step change to -11.7m/s	Step change to 10.7 MPa
3	Ramp of 20ms to -11.7m/s	Ramp of 20ms to 10.7 MPa
4	Step change to -11.7m/s	Constant at 15.5 MPa
5	Ramp of 20ms to -11.7m/s	Constant at 15.5 MPa

Note: (a) Pretransient velocity at left hand side is + 14.6m/s in all cases.

             (b) Pretransient pressure at right hand side is 15.5 MPa in all cases.

Table 4.3   Error in Computed Frequency of Lowest Mode
             Compared to Results.

Core Barrel	Computed (Hz)	STRUDL/DYNAL (Hz)	Error
NSR	21.5	18.9	14%
PWR	34.5	29.7	16%
HDR	23.4	17.95	30%

Table 4.4   Differential Pressure Relief Through Component Circumferential Strain: Case Definitions

Component	Case	Definition
Core Shroud	1	- core shroud stiffness zero - all other structures rigid - no depressurization in bypass, region b - depressurization throughout core, region a
	2	- core shroud and core barrel stiffness zero - all other structures rigid - no depressurization in bypass and between thermal shield and core barrel, region b - depressurization in core, region a
Core Barrel	3	- core barrel and thermal shield stiffness zero - all other structures rigid - no depressurization in bypass, region a - depressurization through downcomer, region b
Thermal Shield	4	- thermal shield stiffness zero - all other structures rigid - no depressurization between thermal shield and barrel, region a - depressurization between thermal shield and pressure vessel, region b
	5	- thermal shield and core barrel stiffness zero - all other structures rigid - no depressurization in bypass and between core barrel and thermal shield, region a - depressurization between thermal shield and core vessel wall, region b

Table 4.5 Differential Pressure Relief Through Component Circumferential Strain: Case Parameters

Component	Case	$Pa°, Pb°$ (MPa)	$\rho_a°$ (kg/m³)	$\rho_b°$ (kg/m³)	$\frac{\partial P}{\partial \rho}\vert a$ ($\frac{MPa}{kg/m^3}$)	$\frac{\partial P}{\partial \rho}\vert b$ ($\frac{MPa}{kg/m^3}$)	R_o (m)	R_1 (m)	R_2 (m)	ε	$\frac{\Delta d}{(mm)}$
Core Shroud	1	8,15	722	722	0.50	0.50	1.88	1.74	0	-0.15%	-2.6
	2	8,15	722	722	0.50	0.50	1.99	1.74	0	-0.25%	-4.4
Core Barrel	3	15,8	722	722	0.50	0.50	2.18	1.88	1.74	+0.1%	1.9
Thermal Shield	4	15,8	722	722	0.50	0.50	2.18	1.99	1.92	+0.05%	1.0
	5	15,8	722	722	0.50	0.50	2.18	1.99	1.74	0.1%	2.0

a. Exact Solution

b. FLASH/RELAP Solution
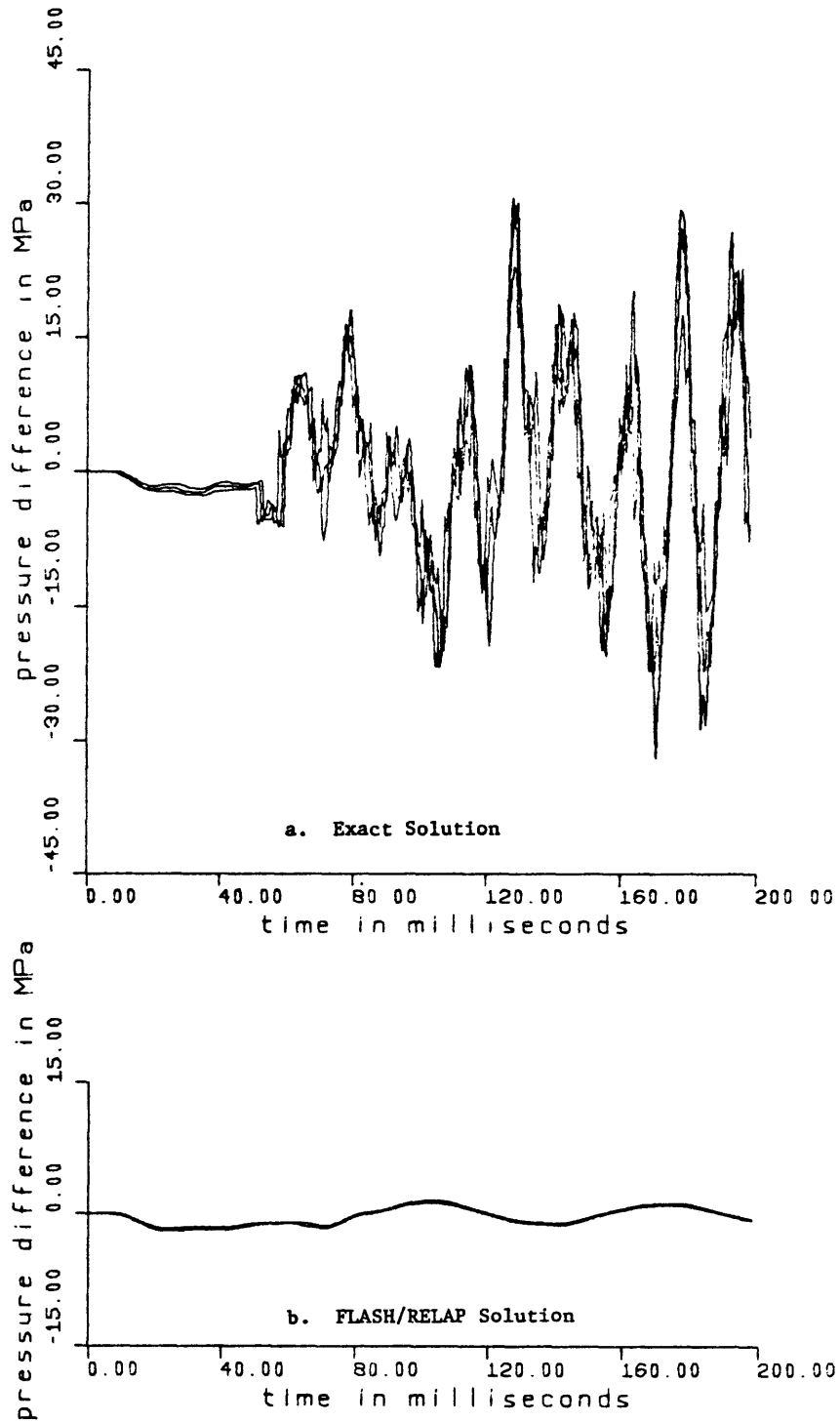
Fig. 4.1 Core Barrel Pressure Differential, Case 1

a. Exact Solution

b. FLASH/RELAP Solution

Fig. 4.2 Core Barrel Pressure Differential, Case 2

a. Exact Solution

b. FLASH/RELAP Solution

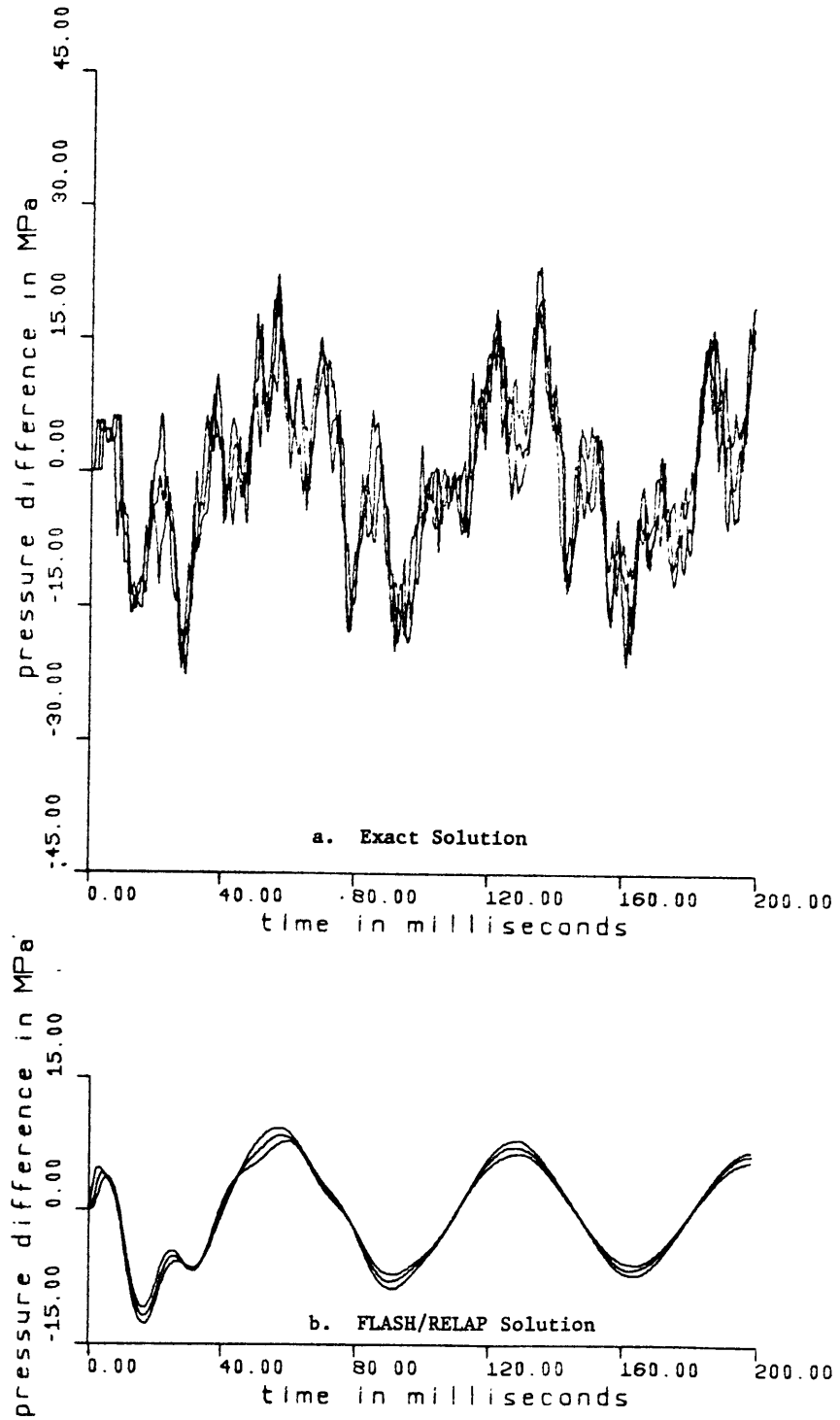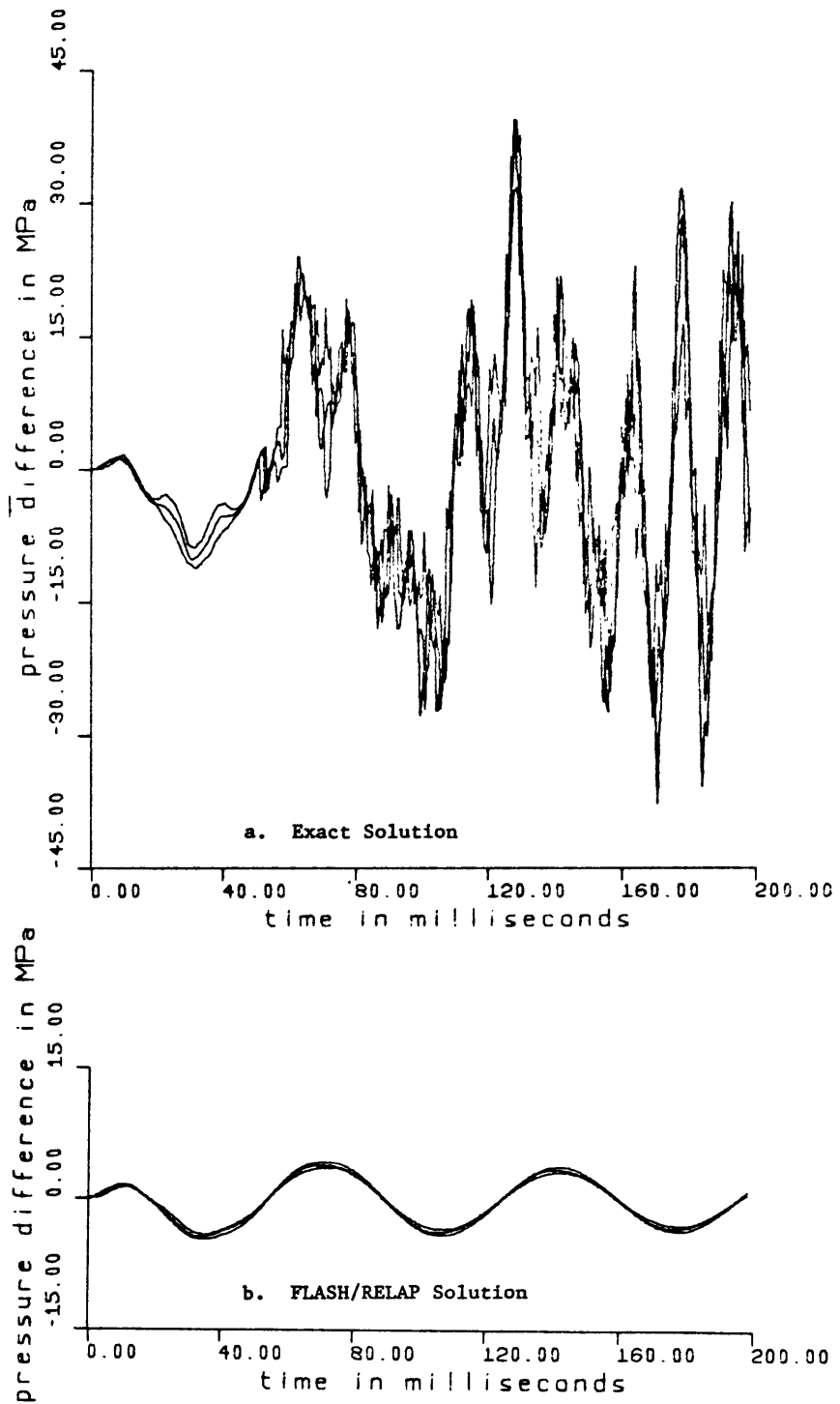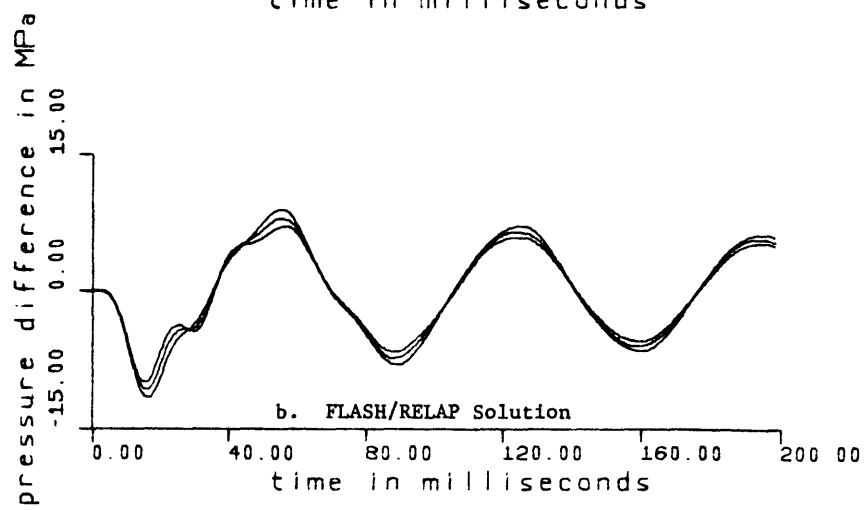Fig. 4.3 Core Barrel Pressure Differential, Case 3
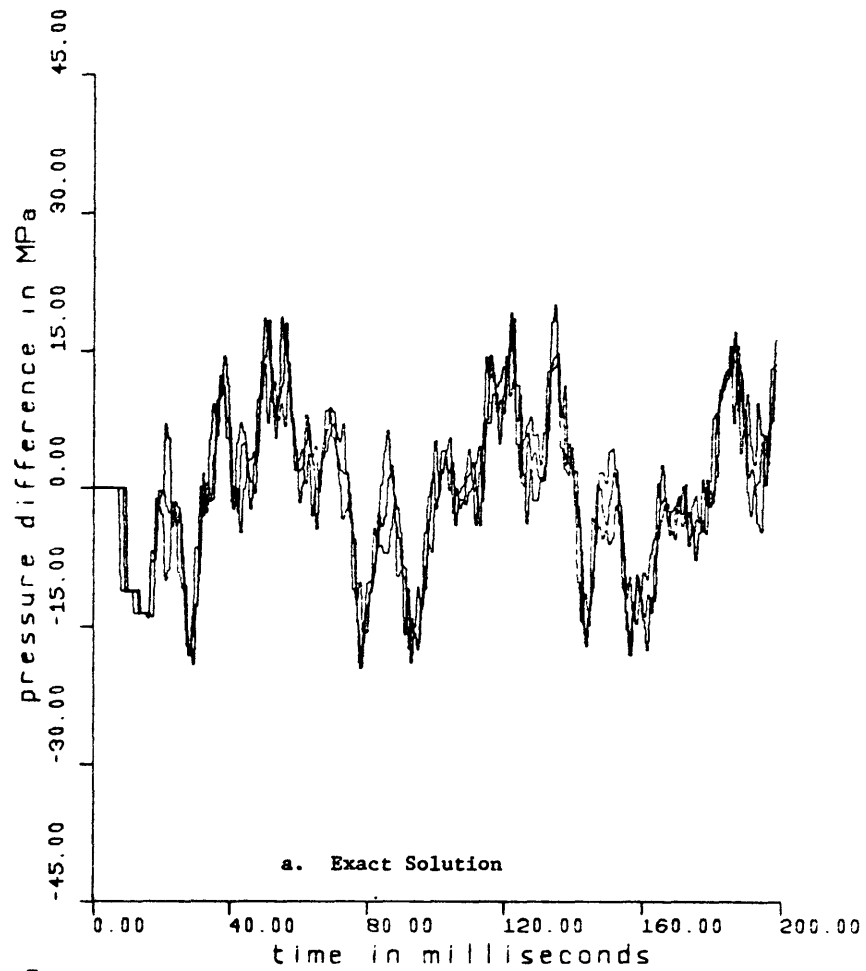
Fig. 4.4 Core Barrel Pressure Differential, Case 4

a. Exact Solution

b. FLASH/RELAP Solution

Fig. 4.5 Core Barrel Pressure Differential, Case 5

centerline nozzle outlet

top

128,8

135,7

132,3

125,3

139,2 bar

142,6

146,1

149,5 bar

153

156,4

bottom

160 bar
pressure

0 mm

no displacement

0,25

0,25

0,5 mm

0,75

0,5 mm

0,75

1 mm

-1 mm

1,25 mm

-125mm
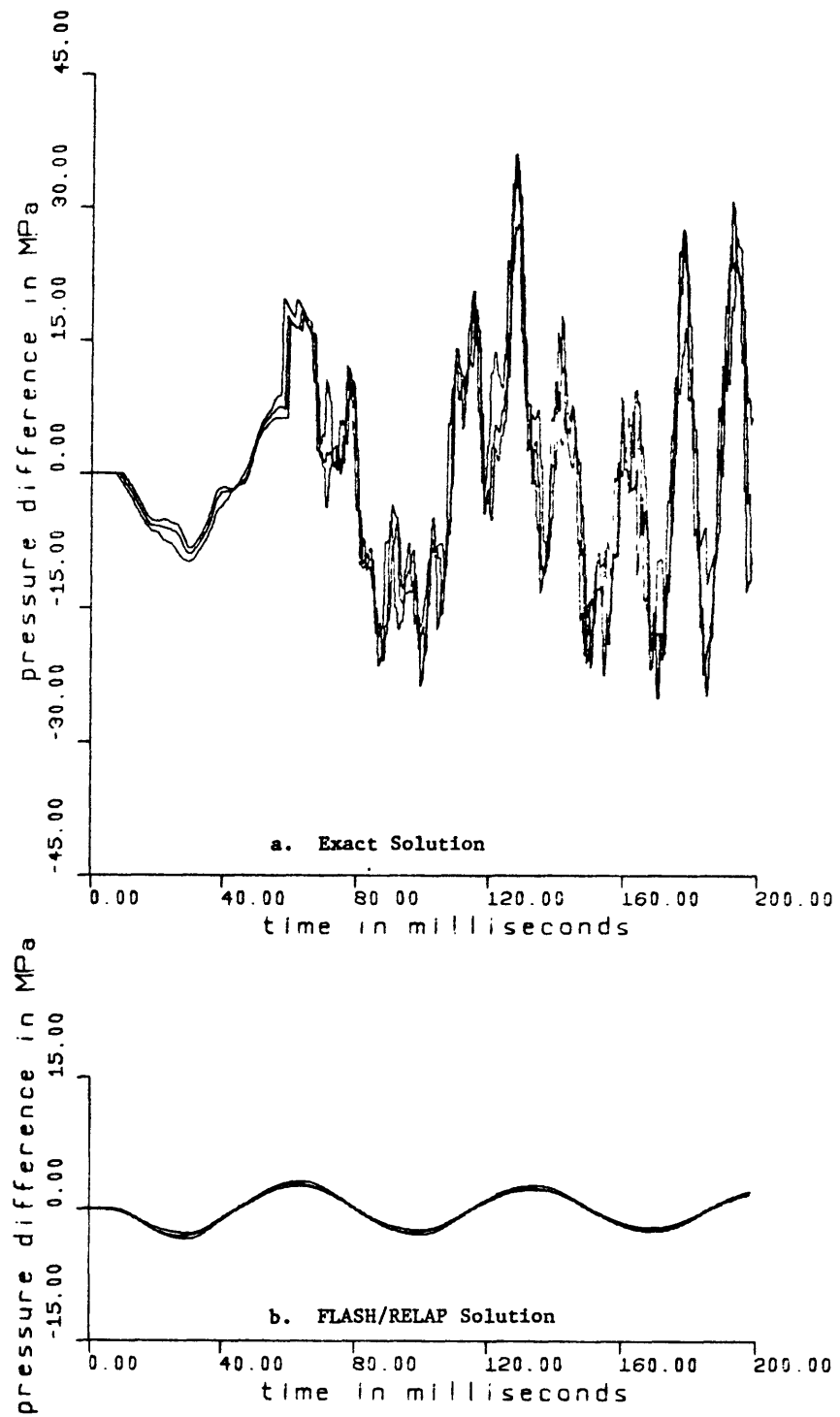
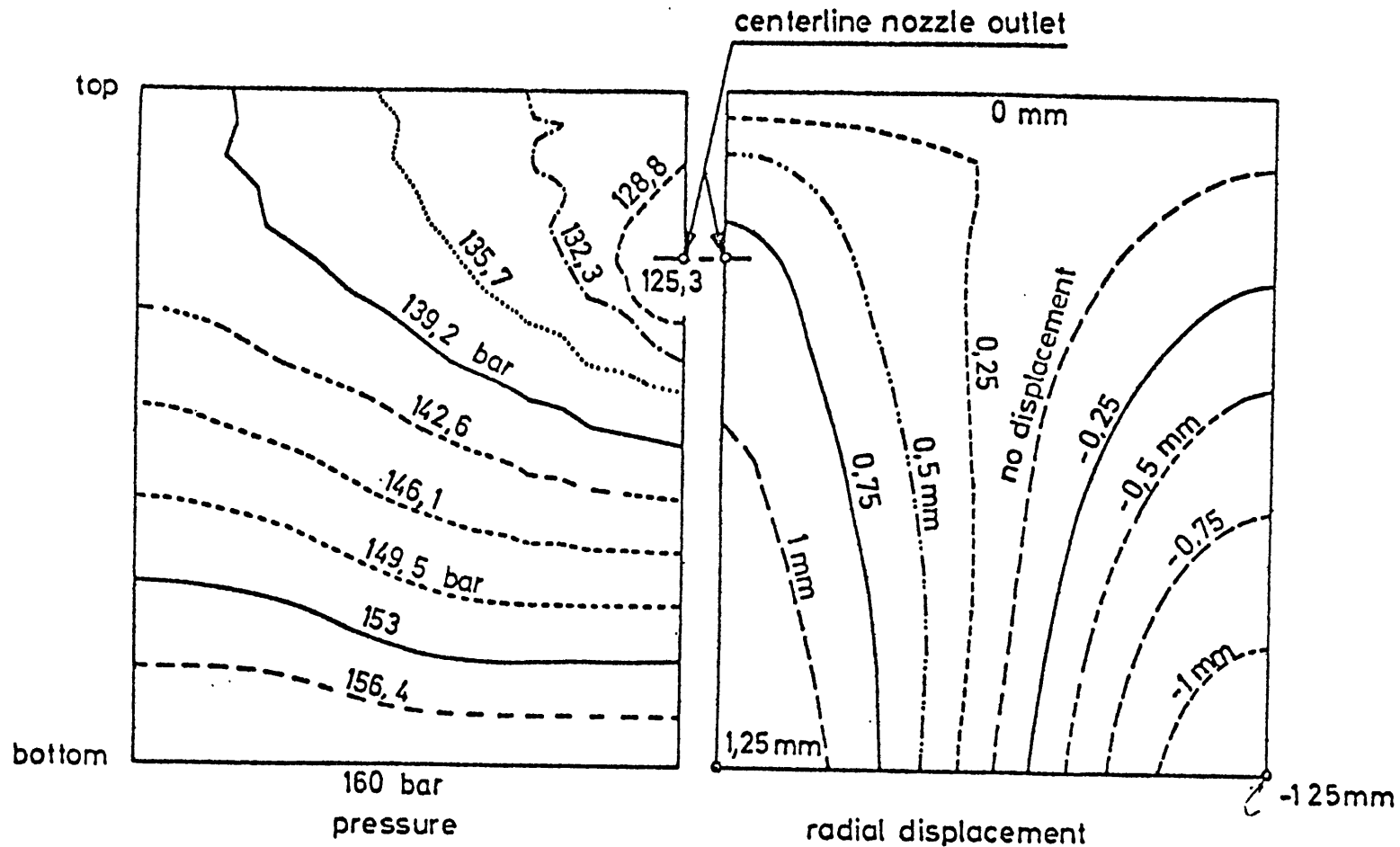radial displacement

Fig. 4.6   Pressure Field in the Downcomer and Corresponding Radial
Displacement of the Core Barrel (12ms after Start of Blowdown)
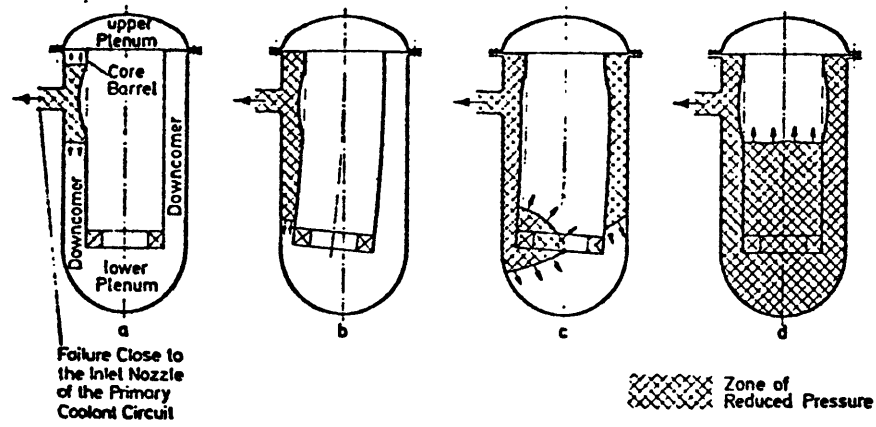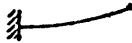Results from FLEXWALL (KWU) (Ref. 20)

Fig. 4.7   Expansion wave propagation and growth of core barrel deformations. (Ref. 20)

No.	Eigenfrequency (Hz)	Circumferential mode (periodicity n)	Axial mode (total number of waves m)
1	17,95	$n = 1$	$m = 1/4$
2	49,0	$n = 3$	$m = 1$
3	55,6	$n = 4$	$m = 1$
4	69,0	$n = 2$	$m = 1$
5	79,5	$n = 5$	$m = 1$
6	86,2	$n = 4$	$m = 3/2$
7	92,9 *	$n = 0$	$m = 1$
8	96,1	$n = 5$	$m = 3/2$
9	102,6	$n = 3$	$m = 3/2$
10	111,0	$n = 1$	$m = 3/4$
11	112,8	$n = 6$	$m = 1$
12	123,1	$n = 6$	$m = 3/2$
13	127,3	$n = 5$	$m = 2$
14	132,7	$n = 4$	$m = 2$
15	145,0	$n = 6$	$m = 2$

* Since in STRUDL/DYNAL curved finite elements are not available the circular cross-sections are approximated by polygons which reduce the frequency of the breathing mode considerably. The true value is roughly five times larger.

Fig. 4.8 Eigenfrequencies and corresponding mode shapes for the HDR-core barrel (Ref. 6)

5. CONCLUSIONS

The calculation of blowdown-induced forces is important for assessing the response of a PWR to a loss-of-coolant accident. Techniques for performing these calculations are being developed and experimental verification is underway. Thus, the state-of-the-art is in the process of being revised and refined. In particular:

(A) The blowdown is usually calculated with structures assumed static and most core components modeled in one dimension. The downcomer and the broken inlet leg are often modeled in two dimensions. Thermal equilibrium is usually assumed throughout the fluid dynamic calculation. In some cases, a nonequilibrium critical flow model is used for the break. A coupled fluid-structural calculation in three dimensions has been performed by Los Alamos Scientific Laboratory, as well as a coupled calculation with a two-dimensional downcomer and one-dimensional modeling elsewhere. Experiments for the verification of these advanced techniques are being prepared, but little verification has yet been done. Therefore, it is not yet known which treatment gives the best results. A comparison of the different techniques indicates that the uncoupled calculation gives results for maximum stresses and deflections which are conservative with respect to a coupled calculation. The results are quite different functions of time, however, and the uncoupled calculation is only marginally conservative in a time-history sense. Though the coupled technique is physically more correct, the technique has not yet been verified experimentally.

(B)   A comparison of results for different levels of dimensionality

showed that a strictly one-dimensional representation is unacceptable

since it masks pressure differences across the core barrel which

arise because of the asymmetric depressurization and flow in the

downcomer. Very little difference was seen between two- and three-

dimensional modeling, suggesting that two-dimensional modeling is

probably adequate.

(C)   The effect of modeling core internals (admittedly by a single

mass ring) proved to be a reduction in deflections and some reduction

in stresses over time. The maximum stress appeared to be independent

of the modeling of core internals. Thus a model for the core barrel

which does not take the core internals into account is probably con-

servative with respect to core barrel stresses. Effects on structures

which transmit forces to the core apparently have not been assessed.

(D)   A comparison of the techniques for calculating one-dimensional

pressure wave propagation was performed. An exact one-dimensional

solution was developed and compared with a FLASH/RELAP type solution.

The exact solution gave much larger pressure differences across the

core barrel than did the FLASH/RELAP solution. The FLASH/RELAP solu-

tion gave much smaller pressure fluctuations with longer peiods than

did the exact solution. This indicates that the FLASH/RELAP solution

may mask the higher frequency pressure variations or somehow damp the

calculated pressure differences. Thus, the FLASH/RELAP solution tech-

nique as used herein may not be conservative for this type of problem.

Other conclusions made from this analysis were that the flow boundary

condition was more important than the pressure boundary condition

and that ramp boundary conditions may give large pressure differen-
tials than do the step change boundary conditions.

(E)   The importance of dynamic structural effects was also investi-
gated. A simple calculation for the frequency of the beam-bending
deflection mode of the core barrel was performed. When compared with
the results of the exact one-dimensional solution, it was seen that
the bending-mode frequency was near to some of the characteristic
frequencies of the core barrel pressure differences. Thus, a resonance
effect is possible in which the frequency of the core barrel loadings
excites the natural bending mode frequency, leading to larger stresses
and deflections.

(F)   The importance of the interaction of motion and loads was in-
vestigated by means of a simple calculation for the circumferential
strain experienced by the core barrel during a blowdown. An upper
bound for the "breathing mode" strains was calculated by assuming a
thin annulus of zero stiffness. The results were that the circum-
ferential strain experienced by core barrel, shroud and thermal shield
during blowdown was not greater than .2%.

(G)   A review of the various available computer codes for the analysis
was completed and the results given in an appendix.

(H)   It appears that further development, refinement and verification
of techniques for blowdown-induced forces on core internals is called
for. Experimental verification and the development of benchmark prob-
lems is needed for assessing the advanced techniques. Modeling of
core internals other than the core barrel should be considered. Core

support structures should be considered as part of these models. In addition, forces which may be generated on exterior supports need to be assessed. Improvements in the coupling techniques and in the calculation of pressure wave propagation should be pursued.

APPENDIX A

ADDITIONAL FIGURES

Dimensions (cm)			
A	358.1	I	24.8
B	308.0	J	188.0
C	166.4	K	218.4
D	386.1	L	6.35
E	24.1	M	7.62
F	11.7	N	4.45
G	6.7	O	5.72
H	5.4		

Table of Materials
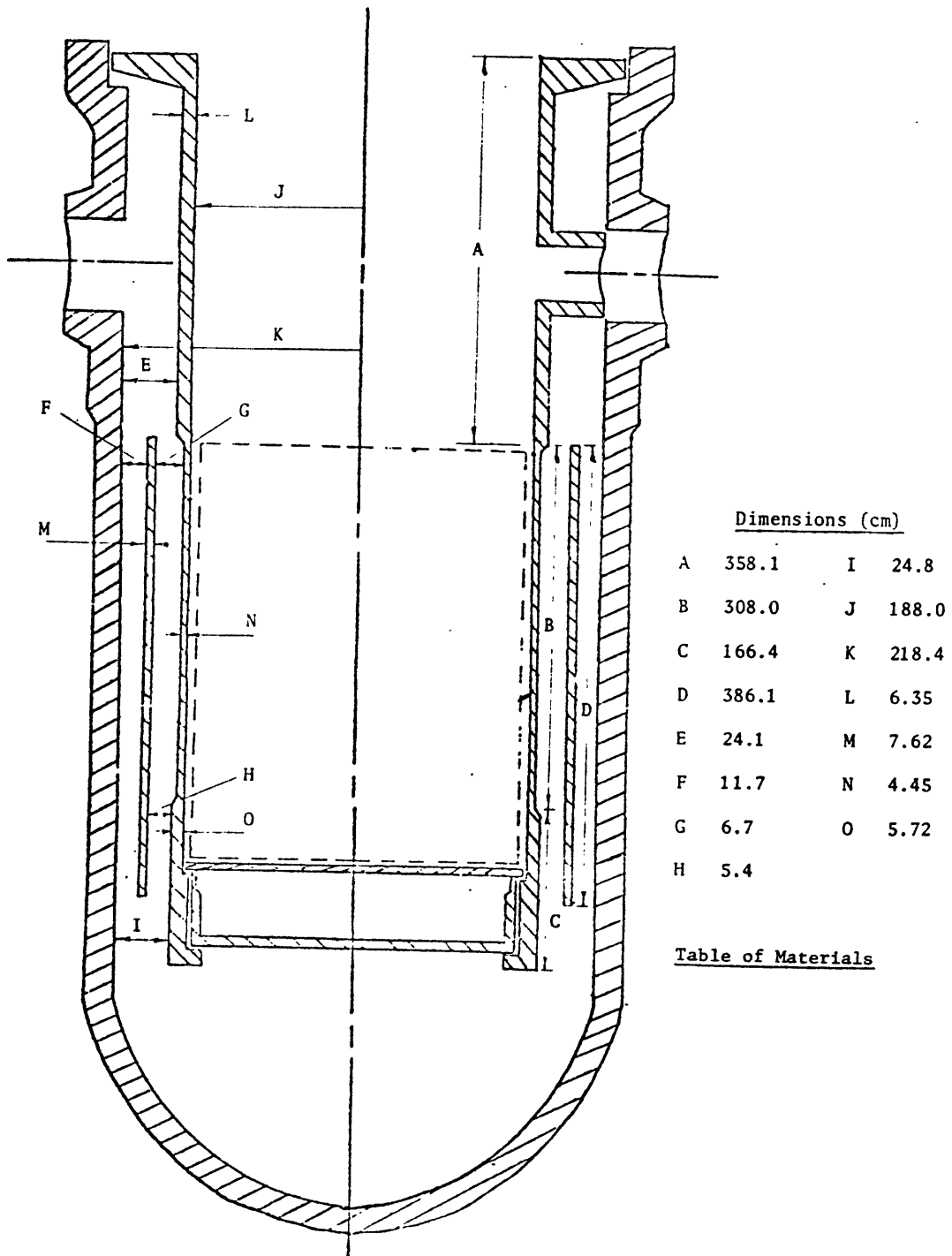
Fig. A.1 Dimensions of Major Core Structures
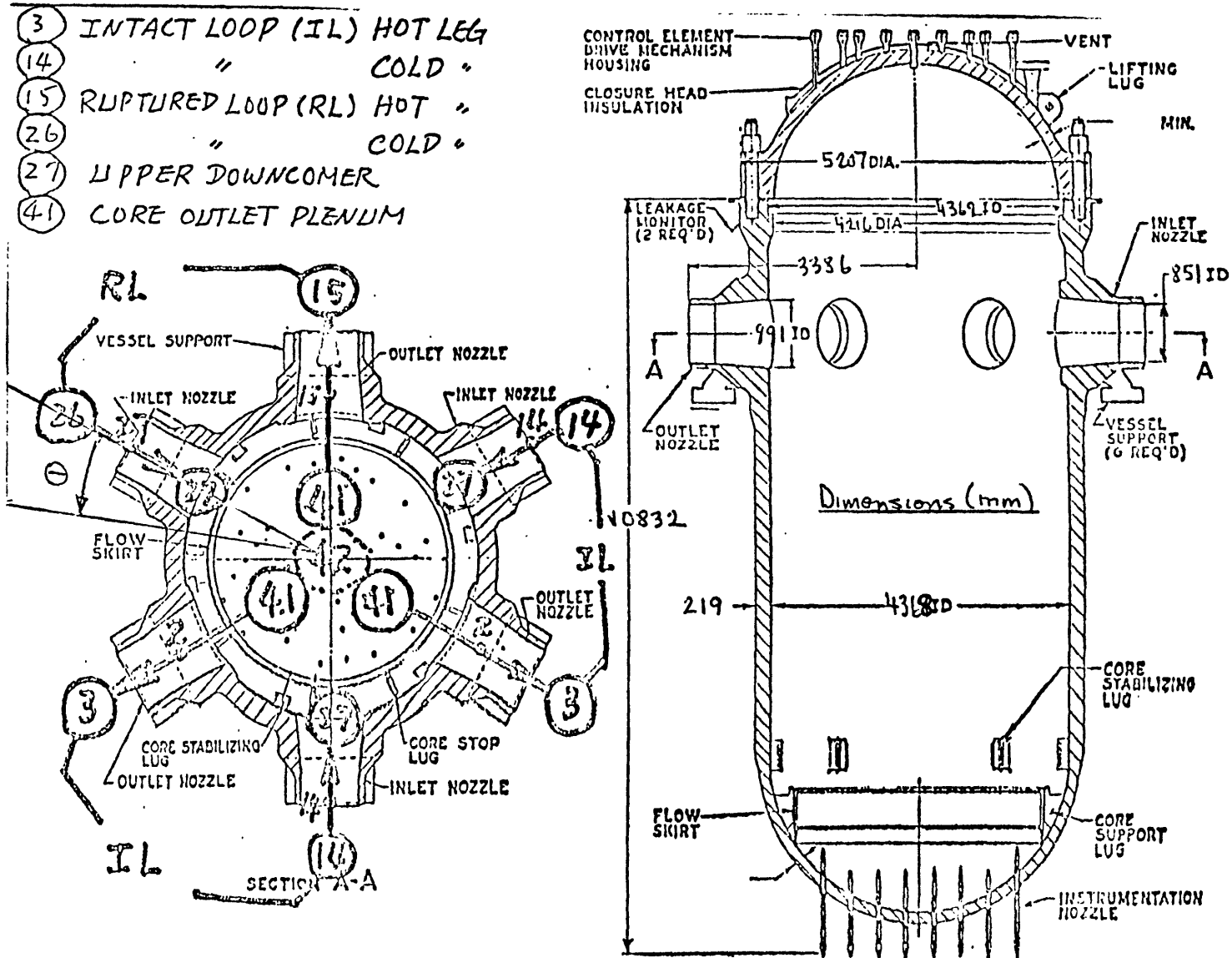
Figure A.2   Reactor Details.

Fig. A.3 Core Bypass Region and Core Shroud
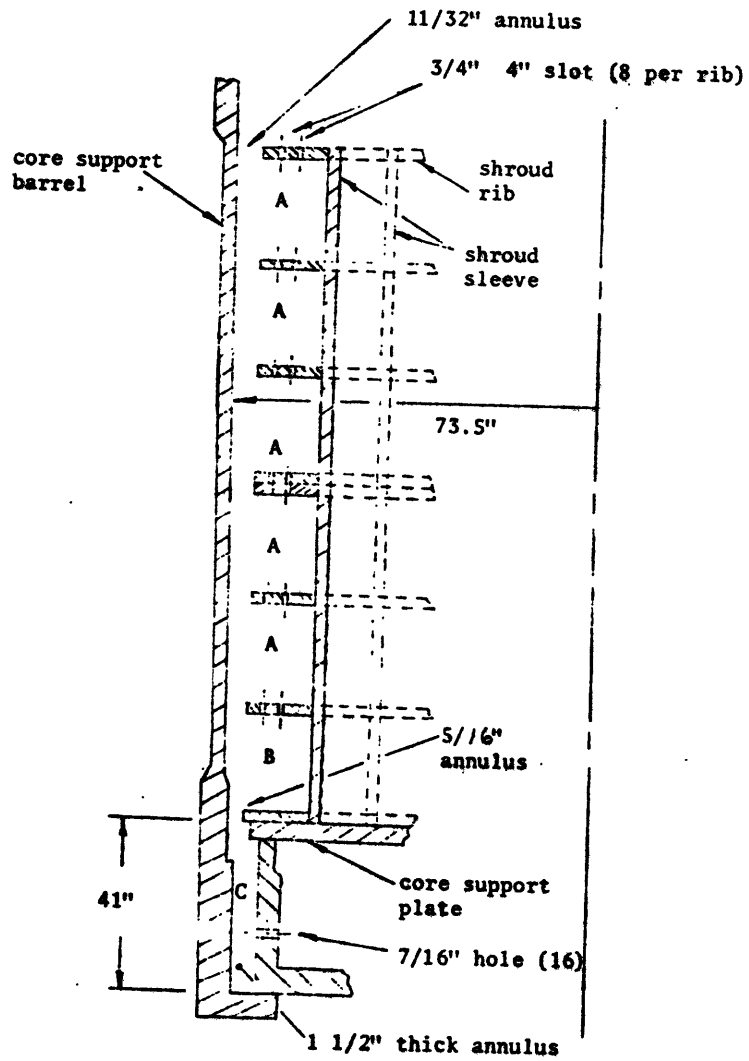
	Volume (m^3)	Inlet Flow Area (m^2)	Outlet Flow Area (m^2)
A	1.0	0.1	0.1
B	1.0	0.05	0.1
C	0.9	0.028	0.05

Time Step = .25 ms

Time step = 1.0 ms
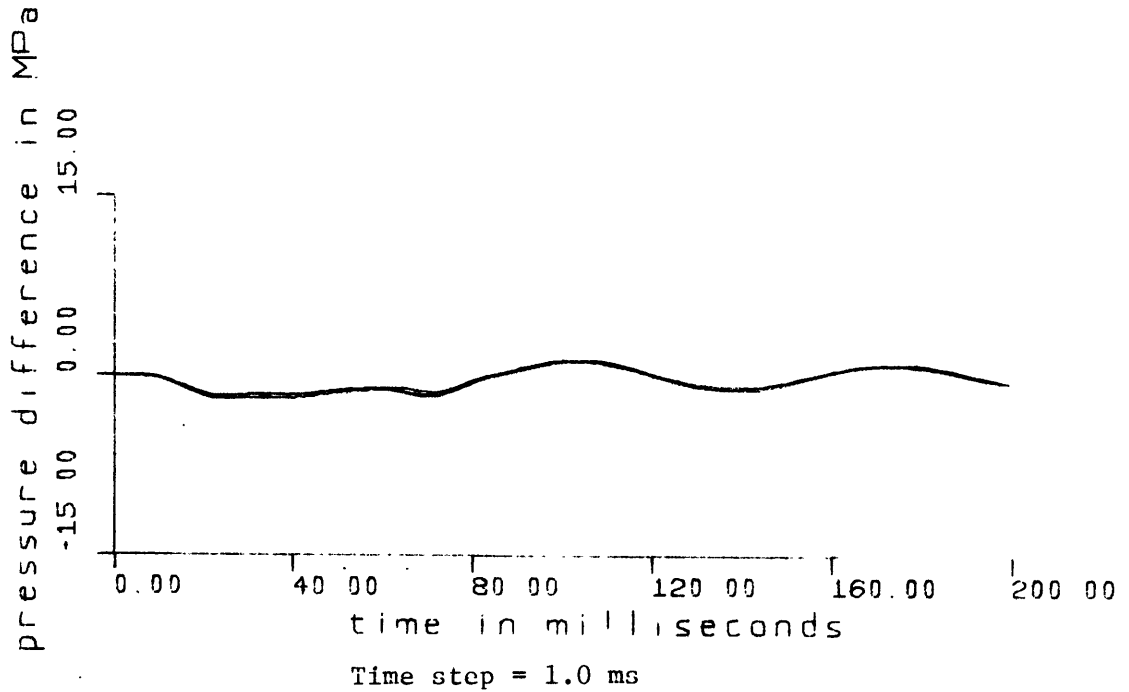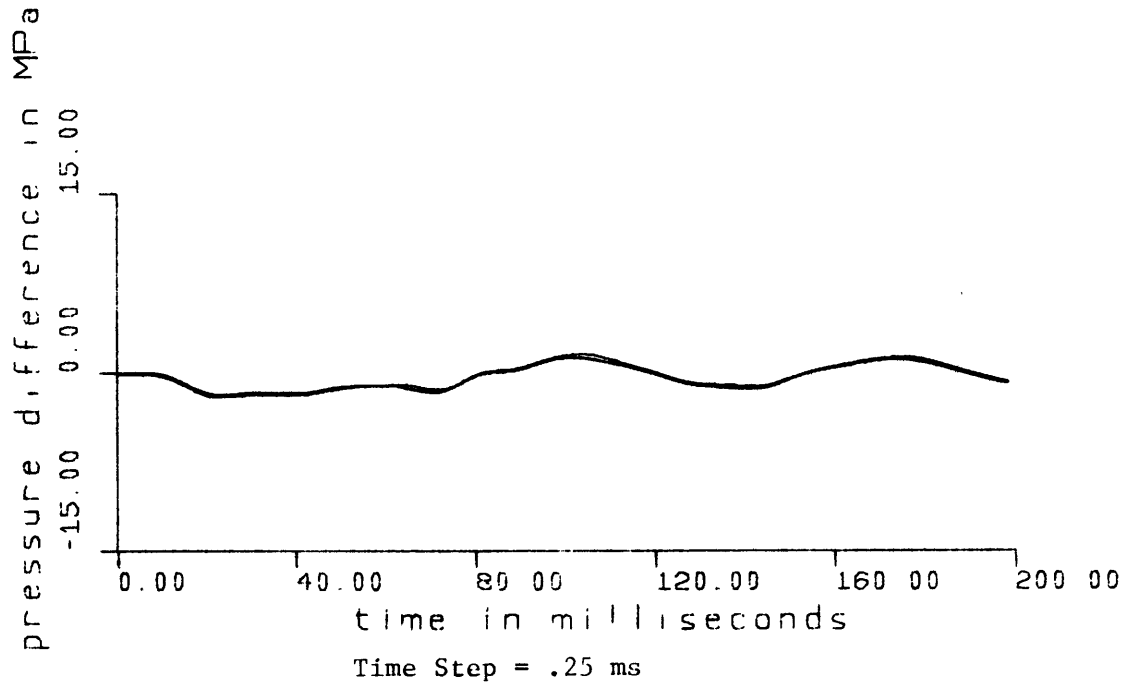
Fig. A.4 Core Barrel Pressure Differential, FLASH/RELAP

Fig. A.5 Core Barrel Pressure Differential, FLASH/RELAP

Time step = .25 ms

Time step = 1.0 ms
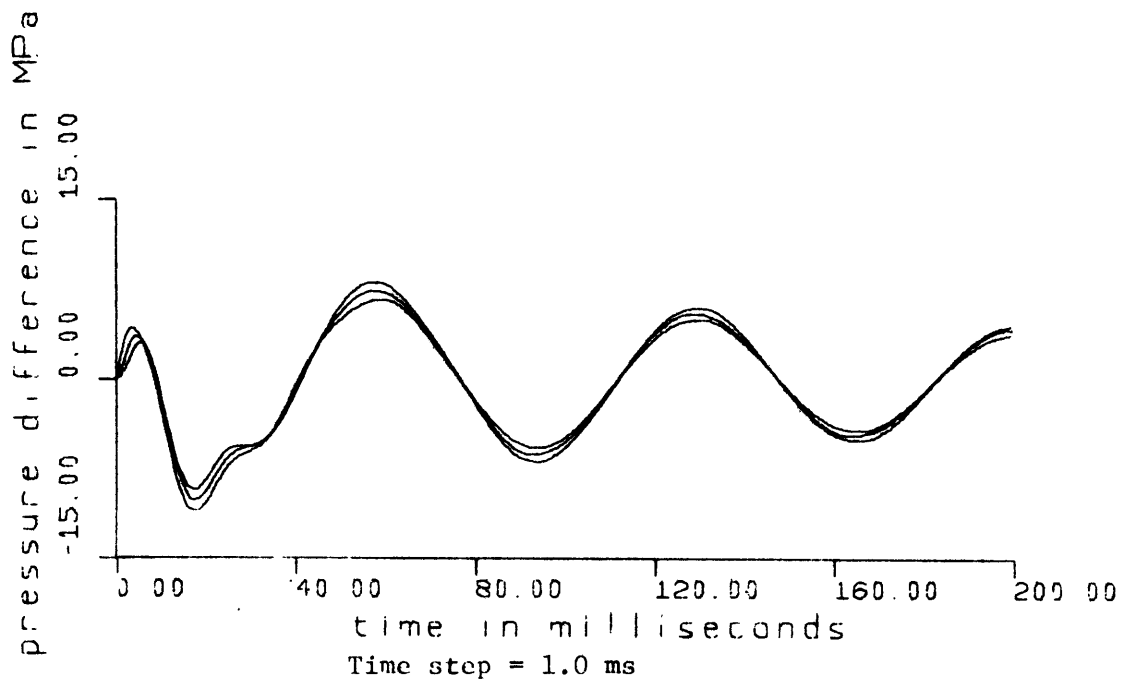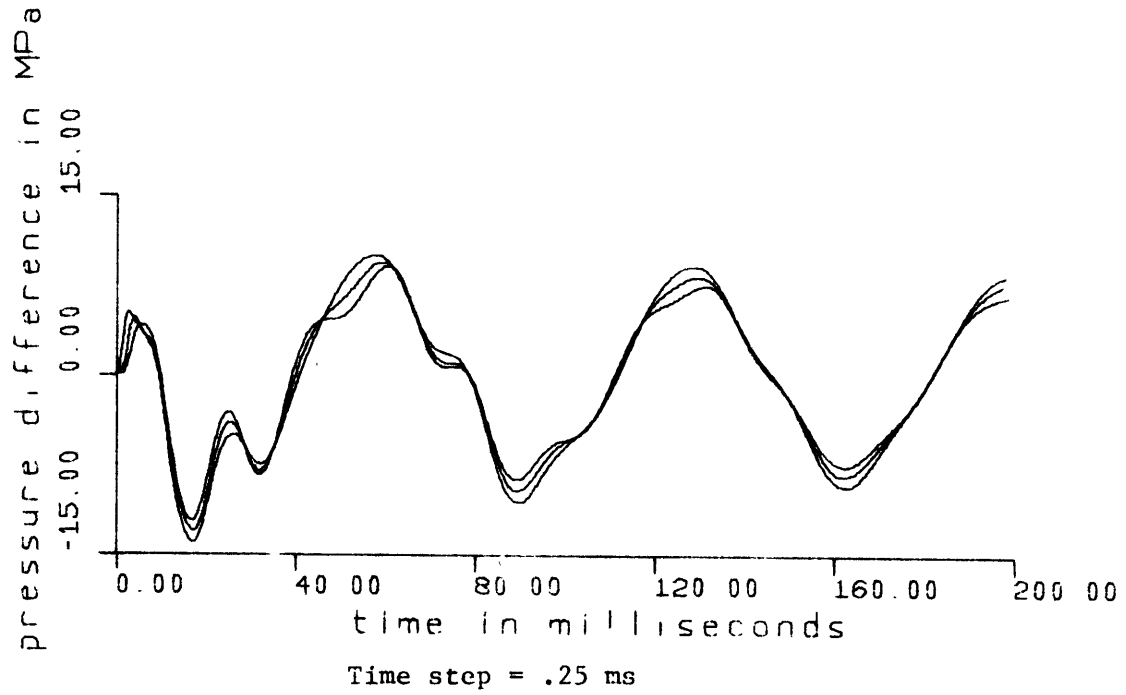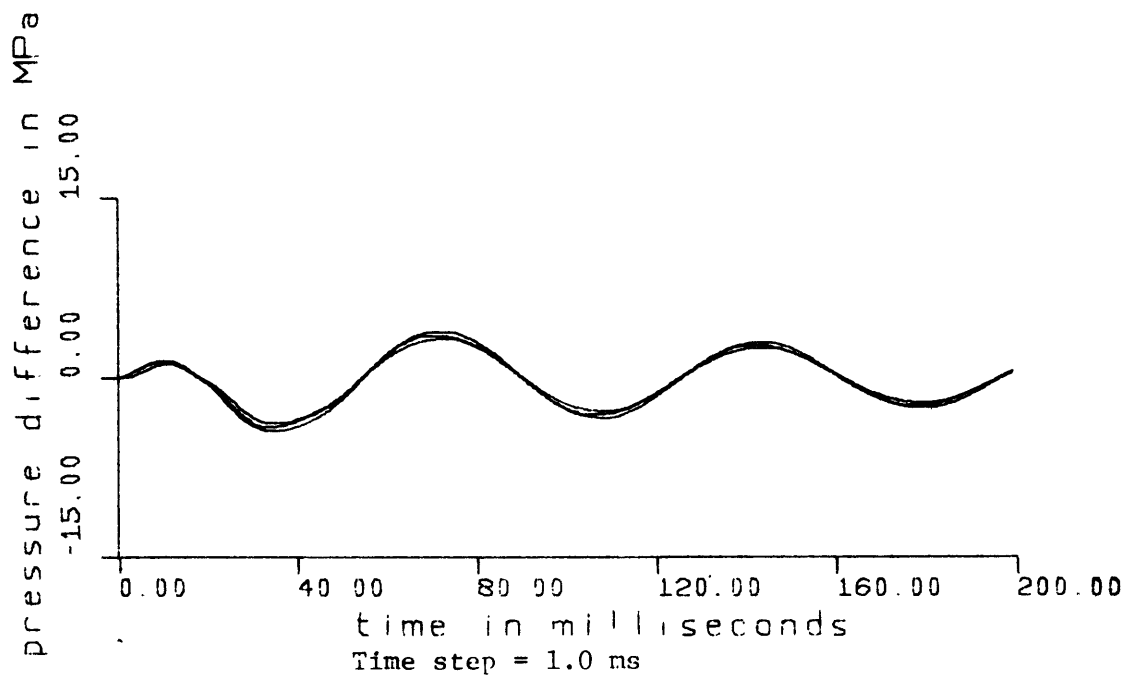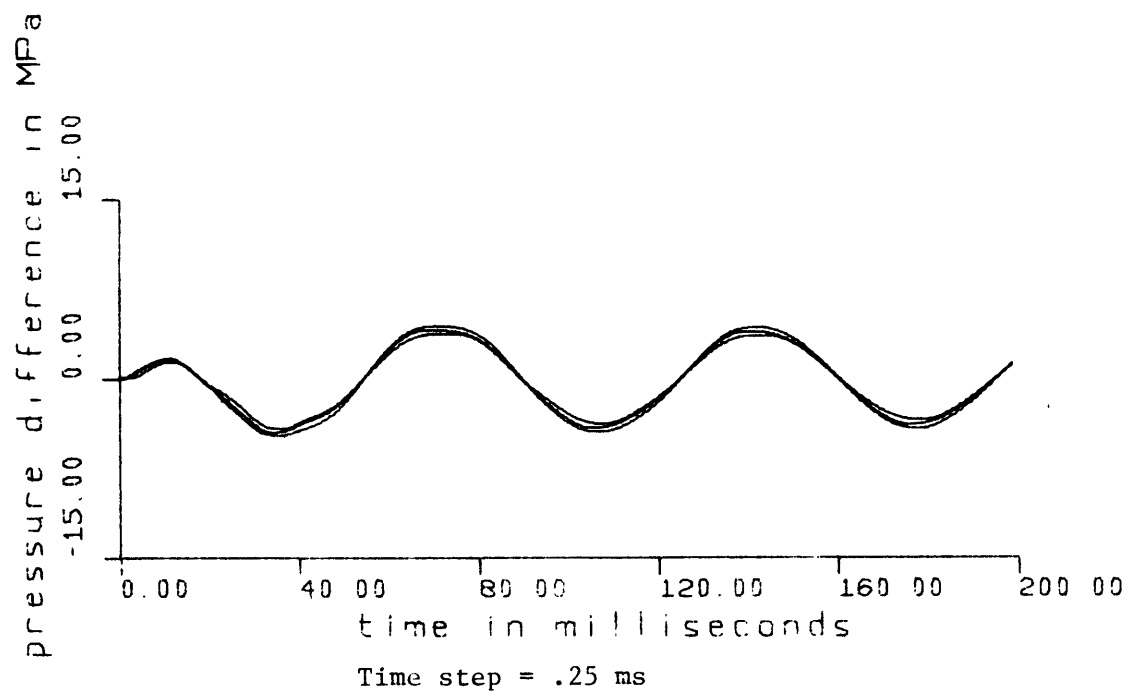
Fig. A.6 Core Barrel Pressure Differential, FLASH/RELAP

APPENDIX B

COMPUTER CODES - STATE OF THE ART

FLUID MECHANICS CODES

Code	SOLA-PLOOP (Ref. 24)
Source	Los Alamos Scientific Laboratory
Intended Use	Developed for use in nuclear reactor safety analysis. Describes transient, nonequilibrium, two phase flow in networks.
Method	Each network component has a one dimensional axial representation with variable flow area. The flow dynamics are governed by a set of nonlinear conservation laws based on a generalized drift-flux model for two phase mixtures. Code is claimed to be compatible with multidimensional codes. This permits modeling of systems with single and multidimensional components.
Verification	Calculations performed to simulate blowdown of a straight pipe initially filled with hot wate- under pressure. Results compared with experiment (Ref. 24).
Applications	Code applied to hypothetical single loop PWR (Ref. 24).

Code	SOLA-DF (Refs. 17, 18, 25)
Source	Los Alamos Scientific Laboratory
Intended Use	Provides finite-difference solutions to the equations of motion of a two phase fluid in two dimensions.
Method	Eulerian fluid description. Drift flux approximation. Equations of motion for a two-phase fluid in two dimensions are written in a partially implicit finite-difference form and solved by a variant of the "ICE" method. The partially implicit method is a "hybrid" of the explicit characteristic method and the strict implicit method which bridges any gap between the stability criteria of the two methods. Stable solutions are obtained when the time step size exceeds the value prescribed by the Courant condition.
Verification	References 17, 18, 25 do not cite any attempt to verify code by experiment.

Applications	References 17, 18, 25 describe coupling of SOLA-DF to the structural code "FLX". Resultant code is used to analyze the dynamic response of a PWR core barrel and coolant during blowdown (Ref. 18).

Code	YAQUIR (Refs. 6, 11, 26)
Source	Institut fur Reaktorentwicklung, Karlsruhe, Germany.
Intended Use	To describe the fluid dynamics in the downcomer of a PWR.
Method	Significantly modified version of the Los Alamos code "YAQUI". Uses a finite difference scheme to solve fluid dynamics equations in two dimensions.
Verification	References 6, 11, 26 do not cite any attempt to verify code by experiment.
Applications	Reference 26 describes coupling of YAQUIR to a structural code "CYLDY2". Resultant code is to be used to analyze the dynamic response of a PWR core barrel during blowdown.

Code	TRAC (Ref. 27)
Source	Los Alamos Scientific Laboratory
Intended Use	Analysis of accidents in Light Water Reactors.
Method	Finite difference, three dimensional treatment of fluid dynamics equations. Nonhomogeneous, non-equilibrium two phase models. Flow-regime-dependent constitutive equation package.
Verification	Code is being applied to a broad range of reduced-scale water reactor safety experiments. TRAC predictions are to be compared with the experimental results to verify the thermal-hydraulic models in the code.
Applications	Code has been used to simulate in sequence the blow-down, refill and reflood stages of a PWR LOCA (Ref. 27).

Code   KFIX (Refs. 12, 13, 15)

Source   Los Alamos Scientific Laboratory.

Intended Use   To provide finite-difference solutions to the
                    equations of motion of a two phase fluid in three
                    dimensions.

STRUCTURAL DYNAMICS CODES

Code	SAP IV (Ref. 8)
Source	Earthquake Engineering Research Center, University of California.
Intended Use	To perform linear, elastic dynamic and static analyses of three dimensional structural systems.

Code	FLX (Refs. 12, 13, 16, 17, 18, 25)
Source	Los Alamos Scientific Laboratory
Intended Use	To solve Timoshenko equations of elastic shell motion for an annulus.
Method	Equations of motions are solved by a finite difference scheme.
Verification	Approximate verification obtained by comparing code results with beam and membrane theory.
Applications	References 12, 13, 16, 17, 18 describe coupling of FLX to two different fluid codes "SOLA-DF" and "K-FIX". Resultant codes are used to analyze the dynamic response of PWR core barrel and coolant during blowdown.

Code	CYLDY2 (Refs. 6, 26)
Source	Institut fur Reaktorentwicklung, Karlsruhe, Germany.
Intended Use	To model the dynamic behavior of a PWR core barrel during blowdown.
Method	Deformations are described as a superposition of appropriate modal functions satisfying the kinematic boundary conditions. Hamilton's principle is applied leading to a system of eigenvalue problems. Approach reduces computer effort considerably in comparison to usual finite element codes.
Verification	References 6, 26 do not cite any attempt to verify code by experiment.

Applications   References 6, 26 describe coupling of CYLDY2 to the fluid code "YAQUIR". Resultant code is used to analyze the dynamic response of PWR core barrel and coolant during blowdown.

COUPLED FLUID STRUCTURE CODES

Code	SOLA-FLX (Refs. 9, 16, 17, 18, 25)
Source	Los Alamos Scientific Laboratory
Intended Use	To analyze the dynamic response of a PWR core barrel and coolant during blowdown.
Method	The fluid code "SOLA-DF" is coupled to the structure code "FLX". The coupling algorithm uses a staggered solution scheme. The pressure computed from the fluid solution at the end of a time step is applied to the cylindrical shell as a loading function, while the shell velocities are imposed as kinematic boundary conditions for the fluid solution.
Verification	An experiment was run to verify the code. However, various difficulties in the experimental and computational techniques prevented good agreement. A modified version of the experiment is being planned (Ref. 9).
Applications	Code used to simulate blowdown of a simplified version of the HDR reactor (Ref. 18).

Code	K-FIX-FLX (Refs. 12, 13)
Source	Los Alamos Scientific Laboratory
Intended Use	To investigate the relative importance of fluid structure interaction during PWR blowdown.
Method	The fluid code "K-FIX" is coupled to the structure code "FLX". Coupling is explicit.
Verification	Several full-scale blowdown experiments will be performed in the former HDR reactor (Ref. 12).
Applications	Calculations were performed for the dynamics of the core support barrel in a reactor vessel during blowdown (Ref. 13).

Code	STRUYA (Refs. 19, 20, 26)
Source	Institut fur Reaktorentwicklung, Karlsruhe, Germany
Intended Use	To investigate the relative importance of fluid structure interaction during PWR blowdown.
Method	The fluid code "YAQUIR" is coupled to the structure code "CYLDY2".
Verification	Several full-scale blowdown experiments will be performed in the former HDR reactor (Ref. 19).
Applications	Calculations were performed for the dynamics of the HDR core barrel during blowdown (Ref. 20).

Code	FLUX1 (Refs. 19, 20)
Source	Institut fur Reaktorentwicklung, Karlsruhe, Germany
Intended Use	To provide a "Best Estimate" analysis of the stresses in PWR vessel internals during blowdown.
Method	The structure code "CYLDY2" is coupled to a three dimensional finite difference fluid code.
Verification	Full-scale experiments carried out at Battelle Frankfurt simulated PWR blowdown conditions. Pressures measured in the downcomer and upper plenum regions were in good agreement with those predicted by FLUX.

Code	PELE-IC (Refs. 25, 28)
Source	Lawrence Livermore Laboratory
Intended Use	A coupled fluid structures code for the analysis of BWR pool dynamics.
Method	A fluid module and structure module are coupled using a staggered solution scheme. The fluid module solves the two dimensional incompressible fluid mechanics equations by a finite difference method. The structure module is a finite element representation.
Verification	Reference 28 sketches several experiments used for code verification.

Code	STEALTH (Refs. 11, 21)
Source	Electric Power Research Institute
Intended Use	Intended for use in design situations such as water hammer, soil-structure interaction, missile impact, mixed fluid impact and fluid-structure interaction.
Method	Coupled fluid-structure code; fluid mesh and structural mesh are both Lagrangian; explicit finite difference technique; two dimensional.
Verification	Reference 21 lists verification cases the code has been run against. Results were good enough to permit distribution of the code.

Code	WHAMS (Ref. 29)
Source	Department of Civil Engineering Northwestern University, Chicago, Illinois
Intended Use	Program for nonlinear, transient analysis of two dimensional and axisymmetric three dimensional structures and continua. Most appropriate for problems where time frame of interest is short, such as several of the lowest periods of the structure.
Method	Finite element format; elements subdivided into three groups: 1. Flexural elements, which are used for modeling thin walled structures; 2. continuum elements, which are used for modeling solids; and 3. Hydrodynamic elements, which are used for modeling fluids.
Verification	Reference 29 compares the results of several experiments with the results predicted by WHAMS.
Applications	Examples of types of problems program is intended for: 1. Clamped ring loaded impulsively over a section. This is an elastic-plastic problem with large changes in geometry. 2. Model of a primary containment enclosing a fluid.

Code	STRAW (Refs. 11, 25)
Source	Argonne National Laboratory
Intended Use	Energy source and fluid representation in structural response.
Method	Two dimensional coupled fluid-structure code.

Code	SING-S (REfs. 6, 20)
Source	Institut fur Reaktorentwicklung, Karlsruhe, Germany
Intended Use	Detailed analysis of fluid-structure interaction in the BWR pressure suppression system during Brunsbutter blowdown experiments.
Method	Fluid module coupled to a structural module.
Applications	Code used to successfully predict occurrence of oscillations in Brunsbutter blowdown experiments resulting from fluid-structure interaction (Ref. 20).

APPENDIX C

EXACT ONE-DIMENSIONAL SOLUTION

C.1 Equations for a Single Pipe

This section derives the necessary equations for the exact

analytical solution of the one-dimensional conservation equations,

as described in Section 4.2.

Conservation of Mass

$$\frac{\partial \rho}{\partial t} + u \frac{\partial \rho}{\partial z} + \rho \frac{\partial u}{\partial z} = 0 \qquad\qquad (C.1)$$

Conservation of Momentum

$$\rho \left[\frac{\partial u}{\partial t} + u \frac{\partial u}{\partial z} \right] + \frac{\partial p}{\partial z} = - \left[\frac{4\tau}{De} + \rho\, g \right] \qquad\qquad (C.2)$$

Conservation of Energy

$$\rho \left[\frac{\partial e}{\partial t} + u \frac{\partial e}{\partial z} \right] + p \frac{\partial u}{\partial z} = \left[\frac{4\tau u}{De} + Q \right] \qquad\qquad (C.3)$$

where   u = fluid velocity
         ρ = fluid density
         p = pressure
         s = fluid entropy

Equation of State

$$\rho = R(p,e) \qquad\qquad (C.4)$$

define:

$$R_p \equiv \frac{\partial R}{\partial p}\bigg| \quad e = \text{constant}$$

$$P_e \equiv \frac{\partial R}{\partial e}\bigg| \quad p = \text{constant}$$

Development:

The four equations given contain four unknowns:

$$\rho, \ u, \ p, \ e$$

Equations (C.1), (C.2), and (C.3) may be written in the following form:

$$A_1 \vec{X}_t + A_2 \vec{X}_z = \vec{\psi} \qquad\qquad\qquad (C.5)$$

where

$$\vec{X} = \begin{vmatrix} u \\ \hline p \\ \hline e \end{vmatrix} \qquad \text{and} \quad \vec{\psi} = \begin{vmatrix} 0 \\ \hline -\dfrac{4\tau}{De} + \rho\, g \\ \hline \dfrac{4\tau u}{De} + Q \end{vmatrix}$$

and the subscripts t and z indicate differentiation with respect to time and position, respectively.

Utilizing (C.4) to eliminate derivatives of density in (C.1), the matrices A_1 and A_2 are as follows:

$$A_1 = \begin{vmatrix} 0 & R_p & R_e \\ \hline \rho & 0 & 0 \\ \hline 0 & 0 & \rho \end{vmatrix} \qquad\qquad A_2 = \begin{vmatrix} \rho & uR_p & uR_e \\ \hline \rho u & 1 & 0 \\ \hline p & 0 & \rho u \end{vmatrix}$$

We desire to transform (C.5) into the following form:

$$(\vec{m}_i)^T \; [\vec{X}_t = \lambda_i \; \vec{X}_z] = (\vec{\psi}_i')^T \qquad\qquad i=1,2,3 \qquad\qquad (C.6)$$

This transformation may be accomplished by defining a pair of fectors $\vec{\ell}$ and $\vec{m}$ which satisfy the following relations:

$$(\vec{\ell})^T \; A_1 = (\vec{m})^T \; \alpha$$

$$(\vec{\ell})^T \; A_2 = (\vec{m})^T \; \beta \qquad\qquad\qquad (C.7)$$

where α, β are scalars.

Rearranging (C.7) gives: $(\vec{\ell})^T \; [\frac{\beta}{\alpha} \; A_1 - A_2] = 0$

Let $\frac{\beta}{\alpha} = \lambda$: $\qquad\qquad (\vec{\ell})^T \; [\lambda \; A_1 - A_2] = 0 \qquad\qquad (C.8)$

In order for (C.8) to have non-trivial solutions for $(\vec{\ell})$, the following relation must be satisfied:

$$| \; \lambda \; A_1 - A_2 \; | = 0 \qquad\qquad\qquad (C.9)$$

Solving (C.9) yields three roots (eigenvalues):

$$\lambda_1 = u + c$$

$$\lambda_2 = u - c$$

$$\lambda_3 = u$$

where

$$c^2 = \frac{1 - pR_e/\rho^2}{R_p}$$

(C.10)

For each eigenvalue λ_i, there is a corresponding "left-handed" eigenvector $(\vec{\ell}_i)$ which must satisfy (C.8).

i	λ_i	$(\vec{\ell}_i)^T$		
1	$u + c$	1	cR_p	$-\dfrac{R_e}{\rho}$
2	$u - c$	1	$-cR_p$	$-\dfrac{R_e}{\rho}$
3	u	1	0	$-\rho/p$

Operating on (C.5) with $(\vec{\ell}_i)^T$:

$$(\vec{\ell}_i)^T A_1 \vec{X}_t + (\vec{\ell}_i)^T A_2 \vec{X}_z = (\vec{\ell}_i)^T \vec{\psi}$$

By (C.7), (C.5) becomes:

$$(\vec{m}_i)^T \alpha \vec{X}_t + (\vec{m}_i)^T \beta \vec{X}_z = (\vec{\ell}_i)^T \vec{\psi}$$

or:

$$(\vec{m}_i)^T [\vec{X}_T + \lambda_i \vec{X}_z] = \frac{1}{\alpha} (\vec{\ell}_i)^T \vec{\psi}$$

This is the desired form. Performing the indicated operations yields three transformed equations:

$$\left[\frac{\partial p}{\partial t} + (u+c)\ \frac{\partial p}{\partial z}\right] + \rho c \left[\frac{\partial u}{\partial t} + (u+c)\ \frac{\partial u}{\partial z}\right] = c\psi_2 - \frac{R_e}{\rho R_p}\ \psi_3 \qquad (C.11)$$

$$\left[\frac{\partial p}{\partial t} + (u-c)\ \frac{\partial p}{\partial z}\right] - \rho c \left[\frac{\partial u}{\partial t} + (u-c)\ \frac{\partial u}{\partial z}\right] = -c\psi_2 - \frac{R_e}{\rho R_p}\ \psi_3 \qquad (C.12)$$

$$\left[\frac{\partial p}{\partial t} + u\ \frac{\partial p}{\partial z}\right] - \frac{\rho^2 c^2}{p} \left[\frac{\partial e}{\partial t} + u\ \frac{\partial e}{\partial z}\right] = - \frac{\rho}{pR_p}\ \psi_3 \qquad (C.13)$$

Equations (C.11), (C.12), and (C.13) will be solved subject to the
following assumptions:

$$\rho = \rho* = \text{constant}$$

$$c = c* = \text{constant}$$

$$u \ll c$$

$$\psi_2 = \psi_3 = 0$$

Rewriting (C.11) and (C.12)

$$\frac{\partial}{\partial t}\ [p + \rho*c*u] + c* \frac{\partial}{\partial z}\ [p + \rho*c*u] = 0 \qquad (C.14)$$

$$\frac{\partial}{\partial t}\ [p - \rho*c*u] - c* \frac{\partial}{\partial z}\ [p - \rho*c*u] = 0 \qquad (C.15)$$

Let $\qquad Y_1 = p + \rho*c*u$

$$Y_2 = p - \rho*c*u \qquad (C.16)$$

Substituting:

$$\frac{\partial Y_1}{\partial t} + c* \frac{\partial Y_1}{\partial z} = 0 \qquad\qquad (C.17)$$

$$\frac{\partial Y_2}{\partial t} - c* \frac{\partial Y_2}{\partial z} = 0 \qquad\qquad (C.18)$$

Thus we can obtain a solution by having a Y_1 wave moving with velocity $+c*$, a Y_2 wave with velocity $-c*$, and retrieve the pressures and velocities when required

$$p = \frac{1}{2} (Y_1 + Y_2)$$

$$u = \frac{1}{2} \rho * c* (Y_1 - Y_2)$$

APPENDIX D

FLASH/RELAP SOLUTION

D.1 Formulation

In this appendix, the solution technique used in FLASH/RELAP is applied to the same situation as the exact analytical solution of Appendix C. This involves the derivation of tridiagonal coefficients for the pressure calculation from finite difference forms of the equations of momentum and energy.

As in the analytical solution, the problem to be solved involves a series of connected pipes of different cross sections. Consider two pipes as shown:
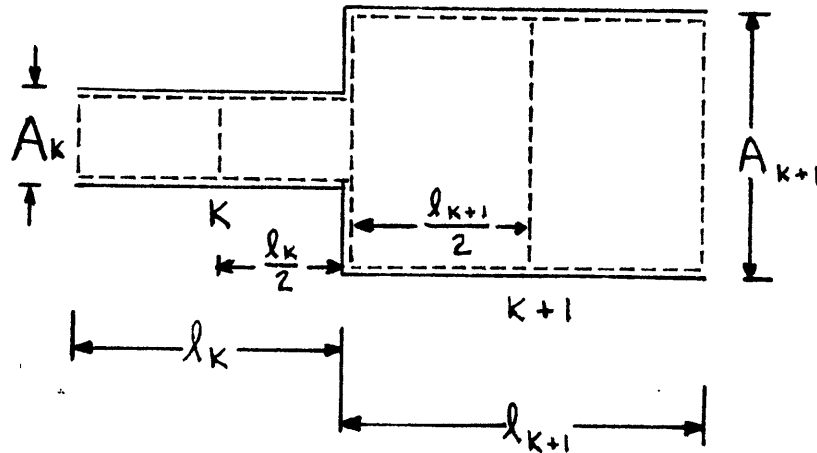
where ℓ_K, ℓ_{K+1} = lengths of pipes K and K+1

A_K, A_{K+1} = area of pipes K and K+1

Define the interface flow rate:

$$W_{K+\frac{1}{2}} \equiv \rho A_K U^-_{K+\frac{1}{2}} = \rho A_{K+1} U^+_{K+\frac{1}{2}}$$

where ρ = density

$U^-_{K+\frac{1}{2}}, U^+_{K+\frac{1}{2}}$ = fluid velocities at interface of pipes K and K+1.

Applying conservation of momentum to control volumes inside the two pipes:

$$P_K - P_{K+\frac{1}{2}}^{-} = \frac{\ell_K}{2A_K} \left[\frac{d}{dt} (W_{K+\frac{1}{2}}) \right] \qquad (D.1)$$

$$P_{K+\frac{1}{2}}^{+} - P_{K+1} = \frac{\ell_{K+1}}{2A_{K+1}} \left[\frac{d}{dt} (W_{K+\frac{1}{2}}) \right] \qquad (D.2)$$

where $P_{K+\frac{1}{2}}^{-}, P_{K+\frac{1}{2}}^{+}$ = pressures of pipe K and K+1 at the interface (which will be taken to be the same, to the order to accuracy of Appendix C.1).

Combining Eqs. (D.1) and (D.2):

$$P_K - P_{K+1} = I_{K+\frac{1}{2}} \left[\frac{d}{dt} (W_{K+\frac{1}{2}}) \right] \qquad (D.3)$$

where $I_{K+\frac{1}{2}} = \left(\frac{\ell_K}{2A_K} + \frac{\ell_{K+1}}{2A_{K+1}} \right)$.

For an isentropic process, the following relation is true:

$$\frac{dp}{d\rho} = c^2 \qquad (D.4)$$

or

$$\frac{dp}{dt} = c^2 \frac{d\rho}{dt} \qquad (D.5)$$

In the notation of this appendix:

$$\frac{\ell_K A_K}{c^2} \frac{dp_K}{dt} = \frac{dm_K}{dt} \qquad (D.6)$$

where m_K is the total fluid mass in pipe K.

Conservation of mass applied to pipe K gives:

$$\frac{dm_K}{dt} = W_{K-\frac{1}{2}} - W_{K+\frac{1}{2}} \tag{D.7}$$

Combining Eqs. (D.6) and (D.7) and writing in finite difference form gives:

$$\frac{P_K^{N+1} - P_K^N}{\Delta t^N} = c^2 \left[\frac{W_{K-\frac{1}{2}}^{N+1} - W_{K+\frac{1}{2}}^{N+1}}{\ell_K A_K} \right] \tag{D.8}$$

where superscripts n,n+1 refer to times n and n+1.

Equation (D.3) may also be written in finite difference form:

$$P_K^{N+1} - P_{K+1}^{N+1} = I_{K+\frac{1}{2}} \left[\frac{W_{K+\frac{1}{2}}^{N+1} - W_{K+\frac{1}{2}}^N}{\Delta t^N} \right] \tag{D.9}$$

Equations (D.8) and (D.9) are the basis for the FLASH/RELAP solution. In the program, the following variables are used:

$$c\ \text{node}(K) \equiv \frac{\ell_K A_K}{(c^2)(\Delta t)}$$

$$c\ \text{jct}(K) \equiv \frac{I_{K+\frac{1}{2}}}{\Delta t} = \frac{\dfrac{\ell_K}{2A_K} + \dfrac{\ell_{K+1}}{2A_{K+1}}}{\Delta t}$$

where K is the pipe number, as before.

The boundary conditions give:

$$cjct(kmax) \equiv \frac{\ell_{kmax}}{2[A_{kmax}][\Delta t]}$$

$$W_{\frac{1}{2}}^{N} \equiv bclw(n)$$

where kmax is the maximum of the K pipes and bclw is the flow rate boundary condition at the left hand side.

Rewriting Eq. (D.9):

$$W_{K+\frac{1}{2}}^{N+1} = W_{K+\frac{1}{2}}^{N} + \frac{P_{K}^{N+1} - P_{K+1}^{N+1}}{cjct(K)} \qquad (D.10)$$

Transposing subscripts and defining Kd = K-1:

$$W_{K-\frac{1}{2}}^{N+1} = W_{K-\frac{1}{2}}^{N} + \frac{P_{K-1}^{N+1} - P_{K}^{N+1}}{cjct(Kd)} \qquad (D.11)$$

Substituting Eqs. (D.10) and D.11) into (D.8) gives:

$$P_{K}^{N+1} - P_{K}^{N} = \frac{\left[W_{K-\frac{1}{2}}^{N} - W_{K+\frac{1}{2}}^{N} \right] - \left[\frac{1}{cjct(Kd)} + \frac{1}{cjct(K)} \right] P_{K}^{N+1} + \frac{1}{cjct(Kd)} P_{K-1}^{N+1} + \frac{1}{cjct(K)} P_{K+1}^{N+1}}{cnode(K)}$$

$$(D.12)$$

Equation (D.12) may be rearranged to yield:

$$- \frac{1}{\text{cnode}(K)\ \text{cjct}(Kd)}\ P_{K-1}^{N+1} - \frac{1}{\text{cnode}(K)\ \text{cjct}(K)}\ P_{K+1}^{N+1} + \left[1 + \frac{\frac{1}{\text{cjct}(Kd)} + \frac{1}{\text{cjct}(K)}}{\text{cnode}(K)} \right] P_K^{N+1} =$$

$$P_K^N + \frac{W_{K-\frac{1}{2}}^N - W_{K+\frac{1}{2}}^N}{\text{cnode}(K)} \qquad (D.13)$$

Notice that in this form, the pressures at the new time step are written in terms of the pressures and flow rates from the current time step. In order to simplify the equation for further treatment, the following definitions were used:

$$A_K \equiv \frac{1}{[\text{cnode}(K)][\text{cjct}(K)]}$$

$$B_K \equiv 1 + \frac{\frac{1}{\text{cjct}(Kd)} + \frac{1}{\text{cjct}(K)}}{\text{cnode}(K)}$$

$$C_K \equiv \frac{1}{[\text{cnode}(K)][\text{cjct}(Kd)]}$$

$$D_K^N \equiv P_K^N + \frac{W_{K-\frac{1}{2}}^N - W_{K+\frac{1}{2}}^N}{\text{cnode}(K)}$$

These definitions hold for $K = 2, 3, \ldots, K_{\text{max}-1}$. Equation (D.13) may thus be written:

$$-A_K P_{K+1}^{N+1} - C_K P_{K-1}^{N+1} + B_K P_K^{N+1} = D_K \qquad , K = 2, 3, \ldots, K_{\text{max}-1}. \qquad (D.14)$$

The boundary conditions at the left hand side (pipe 1, flow rate

condition) and at the right hand side (pipe 9, pressure condition)

must be combined with Eq. (D.14) to give a solution. This is done as

follows:

By Eqs. (D.10) and (D.8)

$$W_{3/2}^{N+1} = W_{3/2}^{N} + \frac{P_1^{N+1} - P_2^{N+1}}{cjct(1)} \tag{D.15}$$

$$P_1^{N+1} - P_1^{N} = \frac{W_{1/2}^{N+1} - W_{3/2}^{N+1}}{cnode(1)} = \frac{bclw(n+1) - W_{3/2}^{N+1}}{cnode(1)} \tag{D.16}$$

Substituting Eq. (D.15) into (D.16) gives:

$$P_1^{N+1} + \frac{P_1^{N+1} - P_2^{N+1}}{cjct(1) \, cnode(1)} = P_{.}^{N} + \frac{bclw(N+1)}{cnode(1)} - \frac{W_{3/2}^{N}}{cnode(1)} \tag{D.17}$$

The following definitions were made for K = 1:

$$A_1 = \frac{1}{cnode(1) \, cjct(1)}$$

$$B_1 = 1 + \frac{1}{cjct(1) \, cnode(1)} = 1 + A_1$$

$$D_1^{N} = P_1^{N} + \frac{bclw(N+1) - W_{3/2}^{N}}{cnode(1)}$$

Similarly, for the right hand side:

$$P_9^{N+1} - P_9^{N} = \frac{W_{8 1/2}^{N+1} + W_{9 1/2}^{N+1}}{cnode(9)} \tag{D.18}$$

$$W_{9\frac{1}{2}}^{N+1} = W_{9\frac{1}{2}}^{N} + \frac{P_9^{N+1} - P_{10}^{N+1}}{CJCT(9)}$$

$$= W_{9\frac{1}{2}}^{N} + \frac{P_9^{N+1} - bcpr(N+1)}{cjct(9)} \tag{D.19}$$

$$W_{8\frac{1}{2}}^{N+1} = W_{8\frac{1}{2}}^{N} + \frac{P_8^{N+1} - P_9^{N+1}}{cjct(8)} \tag{D.20}$$

Combining Eqs. (D.18) − (D.20):

$$\left[1 + \frac{\frac{1}{cjct(8)} + \frac{1}{cjct(9)}}{cnode(9)} \right] P_9^{N+1} - \frac{1}{cjct(8)\ cnode(9)}\ P_8^{N+1} = P_9^N$$

$$+ \frac{W_{8\frac{1}{2}}^{N} - W_{9\frac{1}{2}}^{N} + \frac{1}{cjct(9)}\ bcrp(N+1)}{cnode(9)} \tag{D.21}$$

By analogy with Eq. (D.14), the constants for $K = K_{max} = 9$ are:

$$B_9 \equiv 1 + \frac{\frac{1}{cjct(8)} + \frac{1}{cjct(9)}}{cnode(9)}$$

$$C_9 \equiv \frac{1}{cjct(8)\ cnode(9)}$$

$$D_9^N \equiv P_9^N + \frac{W_{8\frac{1}{2}}^N - W_{9\frac{1}{2}}^N + \frac{1}{cjct(9)}\, bcrp(N+1)}{cnode(9)}$$

A complete set of equations and constants have now been developed.

To summarize:

$$- A_1 P_2^{N+1} + B_1 P_1^{N+1} = D_1^N$$

$$- A_K P_{K+1}^{N+1} + B_K P_K^{N+1} - C_K P_{K-1}^{N+1} = D_K^N \qquad\qquad K = 2,\ 3,\ \ldots\ K_{max-1}$$

$$B_9 P_9^{N+1} - C_9 P_8^{N+1} = D_9^N$$

These equations may be written in matrix form:

$$
\begin{bmatrix}
B_1 & -A_1 & 0 & 0 & 0 & 0 & 0 & 0 & 0 \\
-C_2 & B_2 & -A_2 & 0 & 0 & 0 & 0 & 0 & 0 \\
0 & -C_3 & B_3 & -A_3 & 0 & 0 & 0 & 0 & 0 \\
0 & 0 & -C_4 & B_4 & -A_4 & 0 & 0 & 0 & 0 \\
0 & 0 & 0 & -C_5 & B_5 & -A_5 & 0 & 0 & 0 \\
0 & 0 & 0 & 0 & -C_6 & B_6 & -A_6 & 0 & 0 \\
0 & 0 & 0 & 0 & 0 & -C_7 & B_7 & -A_7 & 0 \\
0 & 0 & 0 & 0 & 0 & 0 & -C_8 & B_8 & A_8 \\
0 & 0 & 0 & 0 & 0 & 0 & 0 & -C_9 & B_9
\end{bmatrix}
\begin{bmatrix}
P_1^{N+1} \\ P_2^{N+1} \\ P_3^{N+1} \\ P_4^{N+1} \\ P_5^{N+1} \\ P_6^{N+1} \\ P_7^{N+1} \\ P_8^{N+1} \\ P_9^{N+1}
\end{bmatrix}
=
\begin{bmatrix}
D_1^N \\ D_2^N \\ D_3^N \\ D_4^N \\ D_5^N \\ D_6^N \\ D_7^N \\ D_8^N \\ D_9^N
\end{bmatrix}
$$

This sytem of equations is solved in the manner given in Section

D.2.

D.2 Formulation of Tridiagonal Solution

In Section D.1, a set of linear equations with a tridiagonal coefficient matrix was derived. An efficient and accurate means of solving such a set of equations is described below, where P is pressure and all other constants are as given in D.1.

$$B_1P_1 - A_1P_2 = D_1$$

$$- C_2P_1 + B_2P_2 - A_2P_3 = D_2$$

$$\vdots$$

$$- C_KP_{K-1} + B_KP_K - A_KP_K = D_K$$

$$\vdots$$

$$- C_9P_8 + B_9P_9 = D_9$$

Define variables E_K and F_K such that:

$$E_1 = \frac{A_1}{B_1}$$

$$\vdots$$

$$E_K = \frac{A_K}{B_K - C_K E_{K-1}}$$

and

$$F_1 = \frac{D_1}{B_1}$$

$$\vdots$$

$$F_K = \frac{D_K + C_K F_{K-1}}{B_K - C_K E_{K-1}}$$

The unknown pressures may then be calculated in the order of decreasing subscript K as follows:

$$P_9 = F_9 \qquad (K_{max} = 9)$$
$$\vdots$$
$$P_K = E_K P_{K+1} + F_K$$

Thus the pressure coefficients E_K and F_K are first generated by starting with K=1 and moving consecutively to $K=K_{max}$. The pressures are then calculated starting with P_{Kmax} and moving "backwards" through the system to K=1. This procedure is often referred to as forward elimination - back substitution. It is highly desirable for the proper operation of this procedure that the following conditions be met:

$$A_K > 0, \quad B_K > 0, \quad \text{and} \quad C_K > 0$$
$$B_K \geq A_K + C_K$$

All the A_K's, B_K's, and C_K's are strictly greater than zero, as defined in D.1. It is easily shown that:

$$B_1 = A_1 + 1 \quad (C_1 \text{ is not defined})$$
$$B_K = A_K + C_K + 1 \quad , \quad K = 2, \ldots, K_{max-1}$$
$$B_9 = 1 + C_9 + \frac{1}{cjct(9) \ cnode(9)} \quad (A_9 \text{ is not defined})$$

Thus, the problem is well suited to this solution scheme. Having calculated the pressures at the new time step in this way, the interface

flow rates can be calculated with Eq. (D.10). The constants D_K can then be calculated and a new pressure calculation can be performed.

D.3   Code Description

As written, the code contains no "read" statements. All necessary data is given in "data" statements within the program. The left hand flow boundary condition and the right hand pressure boundary condition are given as simple functions of time, with values for each time step set in do-loops. A number of variable arrays are dimensioned by the number of time steps or the number of "pipes" in the problem. The required data are presented in Table D.1, along with the variable names and a sample value. The calculations are performed as described in Sections D.1 and D.2 and the pressure differences between pipe 3, representing the downcomer, and pipes 6, 7 and 8, representing core volumes, are printed out in MPa for each time step.

D.4   FLASH/RELAP Program Listing

```
      dimension bclw(401),bclv(401),bcrp(401)
      dimension area(9),slength(9)
      dimension w(9,401),p(9,401)
      dimension dpt(401),dpm(401),dpb(401)
      dimension cjct(9),cnode(9)
      dimension ca(9),cb(9),cc(9),cd(9),ce(9),cf(9)
      data dt/0.0005/
      data ds,c,dx/690.,1000.,0.5/
      data area/1.7058,5.89,2.51,2.59,5.13,4.9,4.9,4.9,7.79/
      data slength/4.5,2.0,5.5,3.0,1.0,1.0,1.0,1.0,0.5/
      data kmax/9/
      data kkmax/1/
      data psteady/15500000./
ccccc set boundary conditions
      do 3001 l=1,41
 3001 bcrp(l)=15500000.
      do 3002 l=42,121
 3002 bcrp(l)=15500000.-57500.*float(l-41)
      do 3003 l=122,401
 3003 bcrp(l)=10900000.-554.1*float(l-121)
      do 3004 l=1,121
 3004 bclv(l)=14.6-0.219*float(l-1)
      do 3005 l=122,401
 3005 bclv(l)=bclv(121)
      do 3006 l=1,401
 3006 bclw(l)=ds*area(1)*bclv(l)
ccccc set initial conditions
      do 10 k=1,kmax
      w(k,1)=bclw(1)
   10 p(k,1)=psteady
ccccc coefficients calculation
      kmaxd=kmax-1
      do 11 k=1,kmaxd
      ki=k+1
   11 cjct(k)=0.5*(slength(k)/area(k)+slength(ki)/area(ki))/dt
      cjct(kmax)=0.5*slength(kmax)/(area(kmax)*dt)
      do 12 k=1,kmax
   12 cnode(k)=slength(k)*area(k)/(dt*c**2)
ccccc solution of linear equations with a tridiagonal coefficient matrix
      ca(1)=1.0/(cjct(1)*cnode(1))
      cb(1)=ca(1)+1.0
      cc(kmax)=1.0/(cjct(kmaxd)*cnode(kmax))
      cb(kmax)=1.0+(cjct(kmaxd)+cjct(kmax))/(cjct(kmax)*cnode(kmax)*cjct(kmax))
      do 13 k=2,kmaxd
      kd=k-1
      cc(k)=1.0/(cjct(kd)*cnode(k))
      cb(k)=1.0+(cjct(kd)+cjct(k))/(cjct(kd)*cnode(k)*cjct(k))
   13 ca(k)=1.0/(cnode(k)*cjct(k))
      ce(1)=ca(1)/cb(1)
      do 100 n=1,400
      ni=n+1
      cd(1)=p(1,n)+(bclw(ni)-w(1,n))/cnode(1)
      cd(kmax)=p(kmax,n)+(w(kmaxd,n)-w(kmax,n)+bcrp(ni)/cjct(kmax))/cnode(kmax)
      do 101 k=2,kmaxd
      kd=k-1
  101 cd(k)=p(k,n)+(w(kd,n)-w(k,n))/cnode(k)
      cf(1)=cd(1)/cb(1)
      do 102 k=2,kmax
      kd=k-1
      ce(k)=ca(k)/(cb(k)-cc(k)*ce(kd))
  102 cf(k)=(cd(k)+cc(k)*cf(kd))/(cb(k)-cc(k)*ce(kd))
      k=kmax
      p(k,ni)=cf(k)
  103 kd=k-1
      p(kd,ni)=ce(kd)*p(k,ni)+cf(kd)
      k=k-1
      if(k-1)104,104,103
  104 do 105 k=1,kmaxd
      ki=k+1
  105 w(k,ni)=w(k,n)+(p(k,ni)-p(ki,ni))/cjct(k)
  100 w(kmax,ni)=w(kmax,n)+(p(kmax,ni)-bcrp(ni))/cjct(kmax)
ccccc print out
      do 2000 n=1,401
      dpt(n)=(p(3,n)-p(9,n))*0.000001
      dpm(n)=(p(3,n)-p(7,n))*0.000001
      dpb(n)=(p(3,n)-p(6,n))*0.000001
      time=float(n-1)*dt*1000.
 2000 write(21,17)time,dpt(n),dpm(n),dpb(n)
   17 format(11x,'time= ',f6.1,' ms',5x,e13.6,5x,e13.6,5x,e13.6)
      stop
```

Table D.1

Data for FLASH/RELAP Solution Program

Description	Units	Variable Name	Sample Value
Time step size	seconds	dt	0.0005
Fluid density	kg/m^3	ds	680
Sonic velocity	M/S	c	1000
Length step size	m	dx	0.5
Pipe flow area	m^2	area(1)	1.7058
Pipe length	m	slength(1)	4.5
Number of pipes		kmax	9
Steady-state pressure	Pa	psteady	15500000

APPENDIX E

This appendix derives an expression for the circumferential
strain of a thin-walled annulus of infinite length and zero stiffness
subjected to an initial pressure differential $P_a^o - P_b^o$.
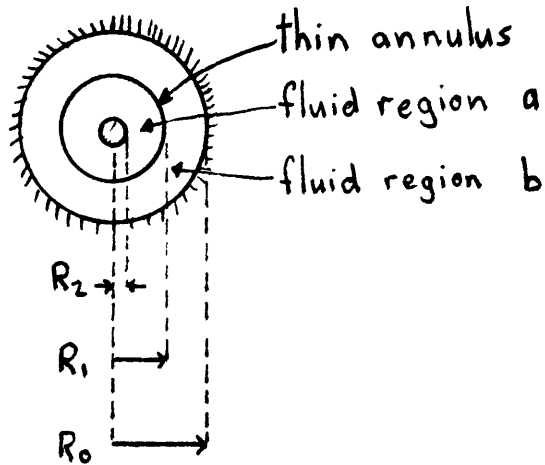
Let P_f be the pressure in the fluid after the annulus has strained to
relieve the initial pressure differential, $P_a^o - P_b^o$.

$$P_a^o + \Delta P_a = P_f \qquad\qquad P_b^o + \Delta P_b = P_f$$

$$\therefore \quad P_a^o - P_b^o = \Delta P_b - \Delta P_a$$

$$P_a^o - P_b^o = \frac{\partial P}{\partial \rho} \, \Delta \rho \,\Big|_b - \frac{\partial P}{\partial \rho} \, \Delta \rho \,\Big|_a$$

If R is the initial radius of the annulus and Δd is the change in radius, then circumferential strain is:

$$\varepsilon = \frac{2\pi(R_1 + \Delta d) - 2\pi R_1}{2\pi R_1}$$

$$\therefore \quad \varepsilon = \frac{\Delta d}{R_1}$$

Letting a prime denote the final state, the density change in region a is:

$$\Delta\rho_a = \rho_a' - \rho_a^\circ$$

$$\Delta\rho_a = \frac{m}{\ell}\left(\frac{1}{\pi(R_1 + \Delta d)^2 - \pi R_2^2} - \frac{1}{\pi R_1^2 - \pi R_2^2}\right)$$

$$= \frac{\rho_a^\circ \, \pi\ell(R_1^2 - R_2^2)}{\pi\ell R_1^2}\left[\frac{1}{(1 + \frac{\Delta d}{R_1})^2 - (\frac{R_2}{R_1})^2} - \frac{1}{1 - (\frac{R_2}{R_1})^2}\right]$$

$$= \rho_a^\circ\left[1 - (\frac{R_2}{R_1})^2\right]\left[\frac{1}{(1 + \frac{\Delta d}{R_1})^2 - (\frac{R_2}{R_1})^2} - \frac{1}{1 - (\frac{R_2}{R_1})^2}\right]$$

$$= \rho_a^\circ\left[\frac{1 - (\frac{R_2}{R_1})^2}{(1 + \varepsilon)^2 - (\frac{R_2}{R_1})^2} - 1\right]$$

Now if $\varepsilon \ll 1$, $(1 + \varepsilon)^2 \sim 1 + 2\varepsilon$

$$\therefore \quad \Delta\rho_a = \rho_a^{\,o} \left[\frac{1 - (R_2/R_1)^2}{1+2\varepsilon - (R_2/R_1)^2} - 1 \right]$$

$$= \rho_a^{\,o} \left[\frac{-2\varepsilon}{1+2\varepsilon - (R_2/R_1)^2} \right] = -\rho_a^{\,o} \left[\frac{2\varepsilon}{1+2\varepsilon - (R_2/R_1)^2} \right]$$

Similarly, for region b

$$\Delta\rho_b = \rho_b^{\,\prime} \quad \rho_b^{\,o}$$

$$= \frac{m}{\ell} \left[\frac{1}{\pi[R_o^2 - (R_1+\Delta d)^2]} - \frac{1}{\pi(R_o^2 - R_1^2)} \right]$$

$$= \frac{\rho_b^{\,o} \pi\ell(R_o^2 - R_1^2)}{\pi\ell R_1^2} \left[\frac{1}{(R_o/R_1)^2 - (1+\varepsilon)^2} - \frac{1}{(R_o/R_1)^2 - 1} \right]$$

$$= \rho_b^{\,o} \left[(\frac{R_o}{R_1})^2 - 1 \right] \left[\frac{1}{(R_o/R_1)^2 - (1+\varepsilon)^2} - \frac{1}{(R_o/R_1)^2 - 1} \right]$$

$$= \rho_b^{\,o} \left[\frac{(R_o/R_1)^2 - 1}{(R_o/R_1)^2 - (1+\varepsilon)^2} - 1 \right]$$

$$\sim \rho_b^{\,o} \left[\frac{(R_o/R_1)^2 - 1}{(R_o/R_1)^2 - (1+2\varepsilon)} - 1 \right]$$

$$= \rho_b^{\,o} \frac{2\varepsilon}{(R_o/R_1)^2 - (1+2\varepsilon)}$$

Therefore,

$$P^\circ_a - P^\circ_b = - \left.\frac{\partial p}{\partial \rho}\right|_b \left[\rho^\circ_b \frac{2\varepsilon}{(1+2\varepsilon) - (R_o/R_1)^2}\right] + \left.\frac{\partial p}{\partial \rho}\right|_a \left[\rho^\circ_a \frac{2\varepsilon}{(1+2\varepsilon) - (R_o/R_1)^2}\right]$$

This expression includes only initial conditions and may be rearranged

to give a quadratic in ε, which may then be solved for ε. Then

$\Delta d = \varepsilon R_1$.

REFERENCES

1. A. Husain et al., "Application of Yankee-WREM-Based Generic PWR ECCS Evaluation Model to Maine Yankee 3-Loop Sample Problem", YAEC-1160, July 1978.

2. "Final Safety Analysis Report, Maine Yankee Atomic Power Station", Docket No. 50-309.

3. Not Used.

4. R.L. Cloud, "Primary System Design and Analysis", lecture notes from Structural Engineering in Nuclear Reactors Lecture Series, MIT, 1973.

5. "Method for the Analysis of Blowdown Induced Forces in a Reactor Vessel", CENPD-252-NP, December 1977.

6. R. Kreig, E.G. Schlechtendahl, and K.H. Scholl, "Design of the HDR Experimental Program on Blowdown Loading and Dynamic Response of PWR-Vessel Internals", Nucl Eng Des 43, 419-435(1977).

7. See Ref. 1.

8. R.E. Mathews, R.K. Mattu, and B.F. Saffell, Jr., "Dynamic Analysis of a Pressurized Water Reactor Primary Coolant System Subjected to Postulated Loss-of-Coolant Accident Transient Loads", ASME paper 77-WA/DE-23.

9. J.K. Dienes, "Comparison of SOLA-FLX Calculations with Experiments at Systems, Science and Software", LA-NUREG-6752-MS.

10. J.R. Travis and W.C. Rivard, "Nuclear Reactor Safety Quarterly Progress Report, July 1 - September 30, 1978", LA-7567-PR, December 1978, pp. 55-59.

11. T. Belytschko, "Methods and Programs for Analysis of Fluid-Structure Systems", Nucl Eng Des 42, 1-180(1977).

12. W.C. Rivard and M.D. Torrey, "Numerical Simulation of Three Dimensional Fluid-Structure Response", in Proceedings of a Topical Meeting on Computational Methods in Nuclear Engineering, 1979, pp. 1-15 to 1-31.

13. W.C. Rivard, M.D. Torrey, "Fluid-Structure Response of a Pressurized Water Reactor Core Barrel During Blowdown", NUREG/CR-0264, September 1978.

14. W.C. Rivard, "Nonequilibrium Phenomena and Structural Inter-
actions in LWR Blowdown Studies", LA-UR-78-2565, November 1978.

15. W.C. Rivard and M.D. Torrey, "K-FIX: A Computer Program for
Transient, Two Dimensional, Two-Fluid Flow", LA-NUREG-6623,
November 1976.

16. J.K. Dienes, C.W. Hirt, and L.R. Stein, "Hydro-Elastic
Calculations of the Dynamic Response of a Reactor to a
Sudden Loss of Coolant", LA-UR-77-1135, August 1977.

17. J.K. Dienes, C.W. Hirt, and L.R. Stein, "Computer Simulation
of the Hydroelastic Response of a Pressurized Water Reactor
to a Sudden Depressurization", LA-NUREG-6772-MS, April 1977.

18. J.K. Dienes, C.W. Hirt, and L.R. Stein, "Multi-Dimensional
Fluid-Structure Interactions in a Pressurized Water Reactor",
LA-UR-77-1599, November 1977.

19. R. Kreig, E.G. Schlechtendahl, K.H. Scholl and U. Schumann,
"Full-Scale HDR Blowdown Experiments as a Tool for Investigating
Dynamic Fluid-Structural Coupling", in Transactions of the 4th
International Conference on Structural Mechanics in Reactor
Technology, San Francisco, August 1977.

20. E.G. Schlechtendahl, "Status of Code Development in the
Federal Republic of Germany Concerning Fluid-Structural Dynamic
Coupling During Reactor Transients", Sixth Water Reactor Safety
Research Information Meeting, Gaithersburg, Maryland,
November 1978.

21. R. Hofmann, "STEALTH: A Lagrange Explicit Finite-Difference
Code for Solids, Structural and Thermohydraulic Analysis",
EPRI-NP-176, June 1976.

22. U. Schumann, "Efficient Computation of Three-Dimensional Fluid
Structure Interaction in LOCA of a Pressure Water Reactor-FLUX",
Karlsruhe Nuclear Research Center, KfK 2645, 1978.

23. J.F. Jackson and M. Stevenson, "Nuclear Reactor Safety:
Quarterly Progress Report, April 1 - June 30, 1978", NUREG/CR-
0385, pp. 31-32.

24. C.W. Hirt and T.A. Oliphant, "SOLA-PLOOP: A Nonequilibrium,
Drift-Flux Code for Two Phase Flow in Networks", LA-UR-76-1200,
August 1976.

25. R.E. Nickell, "Interaction of Structural Mechanics and Thermal-
Hydraulic-Neutronics Codes", in Proceedings of the Topical
Meeting on Computational Methods in Nuclear Engineering, 1979,
pp. 6-15 through 6-33.

26. F. Katz, R. Kreig, A. Ludwig, E.G. Schlechtendahl, and R. Stolting, "2D Fluid Flow in the Downcomer and Dynamic Response of the Core Barrel During PWR Blowdown", in Transactions of the 4th International Conference on Structural Mechanics in Reactor Technology, San Francisco, August 1977.

27. J.C. Vigil and R.J. Pryor, "Nuclear Reactor Safety Quarterly Progress Report, January 1 - March 31, 1978", LA-7278-PR, June 1978, p. 2.

28. W.H. McMaster, "Calculation Method for Fluid-Structure Interactions in the Pressure Suppression Pool Using a Coupling Eulerian-Finite Element Computer Program", presented at Sixth Water Reactor Safety Research Information Meeting, Gaithersburg, Maryland, November 1978.

29. T. Belytschko and R. Muller, "WHAMS - A Program for Transient Analysis of Structures and Continua", Department of Civil Engineering, Northwestern University, 1979.